

NRL Report 6195

UNCLASSIFIED

An Exploratory Study of Radiant Energy Transport in BeO

E. J. CHAPIN AND D. G. HOWE

Metallurgy Division

March 22, 1965



U.S. NAVAL RESEARCH LABORATORY
Washington, D.C.

Permission has been granted to use copyrighted material appearing in this report.

Figure 34 from "Annalen Der Physik," V. Folge 19, 1934.

Figure 35 from "Infrared Radiation," by Hackforth, H.L. Copyright 1960, McGraw-Hill, by permission of McGraw-Hill Book Co., Inc.

Figure B-1 from "Infrared Methods," by Conn and Avery, 1960 edition.

CONTENTS

| | |
|--|--------|
| Abstract | ii |
| Problem Status | ii |
| Authorization | ii |
| INTRODUCTION | 1 |
| REVIEW OF PROPERTIES OF BeO | 1 |
| REVIEW OF EXISTING HYPOTHESES FOR HIGH-TEMPERATURE EXCITATION PROCESSES | 6 |
| Phonon Conduction Parameter | 6 |
| Photon Conduction Parameter | 7 |
| Exciton Conduction Parameter | 10 |
| Effects of Vaporization or Sublimation | 11 |
| EXPERIMENTAL | 11 |
| Approach | 11 |
| Description of Apparatus | 12 |
| Experimental Procedure | 19 |
| RESULTS AND DISCUSSION | 22 |
| SUMMARY | 50 |
| CONCLUSIONS | 52 |
| ACKNOWLEDGMENTS | 53 |
| REFERENCES | 54 |
| APPENDIX A - Calibration of Gauge Section of Tungsten Wire Source | 57 |
| APPENDIX B - Thermocouple Detectors and Calibration Data | 59 |
| APPENDIX C - Miscellaneous Properties | 62 |

LIST OF FIGURES

| | |
|--|----|
| Fig. 1 - Thermal conductivity of BeO as a function of temperature (from Ref. 1) | 2 |
| Fig. 2 - q_r/q_k vs temperature for thermal conductivity of BeO | 9 |
| Fig. 3 - Schematic of the high-temperature vacuum furnace for the study of radiant energy transmission in BeO. The numbered components are described in the text on the preceding page (Page 12). | 13 |
| Fig. 4 - Cold-wall furnace assembly mounted on a vacuum bell-jar baseplate | 14 |
| Fig. 5 - View of the top of the furnace showing the top heater and the side radiation shields | 15 |
| Fig. 6 - View of the top of the furnace showing the arrangement of the crucible, thermal detectors on planar cross section, BeO sample tube in the center, BeO sleeve, side shields, and water-cooled furnace jacket | 18 |
| Fig. 7 - Arrangement of the vacuum bell jar containing the cold-wall furnace assembly and of the vacuum pumping system and instrumentation | 18 |
| Fig. 8 - Translucency of the protection tube | 20 |
| Fig. 9 - Radiation exchange between two cylindrical surfaces | 21 |
| Fig. 10 - Alternatives for radiation impinging on a body | 22 |
| Fig. 11 - Total emissivity and radiation intensity of tungsten and BeO as a function of temperature | 26 |
| Fig. 12 - Temperature rise of 40°C at the center detector for item 8, series 2 trials (baseline temperature, 1102°C; heater maximum temperature, 2271°C; 10-second pulse) | 28 |
| Fig. 13 - Temperature rise of 33°C at the center detector for item 11 (baseline temperature, 1498°C; heater maximum temperature, 2343°C; 10-second pulse) | 29 |
| Fig. 14 - Another trace showing a temperature rise of 33°C for the conditions as given in Fig. 13 | 29 |
| Fig. 15 - Temperature rise of 4°C at the middle detector for item 11 (baseline temperature, 1498°C; heater maximum temperature, 2343°C; 10-second pulse) | 30 |
| Fig. 16 - Temperature rise of 3°C at the middle detector for item 15 (baseline temperature, 1730°C; maximum heater temperature, 2335°C; 10-second pulse) | 31 |
| Fig. 17 - Temperature rise of 8°C at the middle detector for item 17 (baseline temperature, 1923°C; maximum heater temperature, 2471°C; 10-second pulse) | 31 |

| | |
|---|----|
| Fig. 18 - Temperature rise of 40°C at the center detector for item 20 (baseline temperature, 1482°C; maximum heater temperature, 1979°C; 10-second pulse) | 32 |
| Fig. 19 - Temperature rise of 42°C for the same conditions as in Fig. 18 | 32 |
| Fig. 20 - Temperature rise of 3°C at the middle detector for item 20 (baseline temperature, 1482°C; maximum heater temperature, 1979°C; 10-second pulse) | 33 |
| Fig. 21 - Temperature rise of 3°C at the middle detector for the same conditions as in Fig. 20 | 33 |
| Fig. 22 - Temperature rise of 3°C at the middle detector for the same conditions as in Fig. 20 | 33 |
| Fig. 23 - Temperature rise of 286°C at the center detector for item 21 (baseline temperature, 1477°C; maximum heater temperature, 1967°C; 300-second pulse) | 33 |
| Fig. 24 - Temperature rise of 33°C at the middle detector for item 21 (baseline temperature, 1477°C; maximum heater temperature, 1967°C; 300-second pulse). The three curve segments go from left to right in sequence. | 35 |
| Fig. 25 - Temperature rise of 341°C at the center detector for item 28 (baseline temperature, 1756°C; maximum heater temperature, 2101°C; 300-second pulse) | 36 |
| Fig. 26 - Temperature rise of 75°C at the middle detector for item 28 (baseline temperature, 1756°C; maximum heater temperature, 2101°C; 300-second pulse) | 37 |
| Fig. 27 - Radiant heating of a solid in the ideal case. Curve AE indicates the heating of the solid when the source is at the temperature indicated by BD. Line AC indicates the heating when the temperature rise is constant. | 38 |
| Fig. 28 - Values of the exponent t/j in Eq. (9) | 40 |
| Fig. 29 - Temperature-vs-time curve for the trial of Fig. 12 | 41 |
| Fig. 30 - Temperature-vs-time curve for the trials of Figs. 13 and 14 | 42 |
| Fig. 31 - Temperature-vs-time curve for the trials of Figs. 18 and 19 | 42 |
| Fig. 32 - Temperature-vs-time curve for the trial of Fig. 23. Curve (a) is the calculated curve, while curve (b) is the observed measurement at the center detector. | 43 |
| Fig. 33 - Temperature-vs-time curve for the trial of Fig. 25 | 44 |
| Fig. 34 - Spectral emissivity of BeO vs wavelength (from Ref. 38) | 45 |

| | |
|---|----|
| Fig. 35 - Blackbody radiant emittance vs wavelength (from Ref. 39) | 46 |
| Fig. 36 - Spectral radiancy distribution curves for (a) tungsten and (b) a blackbody at 2450°K (2177°C) (from Ref. 40) | 46 |
| Fig. A1 - Calibration of tungsten radiant energy source | 58 |
| Fig. B1 - The infrared spectrum, and the origin of spectra | 59 |
| Fig. B2 - Cutaway sketch showing the hot junction tungsten/iridium thermocouple welded to the flat tip of the tantalum sheath making a pressure-tight closure | 60 |
| Fig. B3 - Calibration curve for W/Ir thermocouples | 61 |
| Fig. C1 - Vapor pressure of BeO, iridium, tantalum, and tungsten | 64 |
| Fig. C2 - Specific heat of BeO | 66 |

Copies available from
Clearinghouse for Federal Scientific and
Technical Information (CFSTI)
Sills Building, 5285 Port Royal Road
Springfield, Virginia 22151
\$2.00

CONFIDENTIAL

ABSTRACT

Current hypotheses on the contribution of radiant energy to heat transfer in BeO were reviewed. The problem of radiant energy transmission in BeO was explored in high vacuum by exposing simultaneously, two types of BeO sample materials heated at temperatures from 1000° to 2000°C, to pulses of radiant energy of known intensity emitted from a tungsten wire source. The effects were monitored with potentiometers and oscilloscopes from emf signals generated by thermocouple detectors.

Thin-walled translucent BeO tube material exhibited no major transmission of radiant energy at temperatures of 1000° to 2000°C when exposed to pulses of high-intensity radiant energy. Oscilloscope data showed, however, an initial effect from incident radiant energy intensity. This effect was interpreted as being due to the exposed BeO surface being raised to a high temperature so rapidly that little heat was generated in the mass of the material, momentarily, with no immediate rise in BeO temperature. During this short interval it was postulated that incident radiant energy was transferred in the BeO by a process involving simultaneous emission and absorption of the radiant energy in depth. As soon as the BeO temperature began to rise, this process of radiant energy transfer appeared to be superseded by the normal process of radiant energy transfer which involved absorption of the radiant energy and reradiation. A comparison was made of calculated temperature-time heating curves based on initial rates of temperature rise detected from the experimental data. This comparison indicated that the temperature rise per unit of time was actually less than that calculated, showing that the initial rate and, therefore, the initial process of radiant energy transfer was not sustained. At temperatures above 1800°C, hot BeO exhibited no tendency toward a rapid transfer of radiant energy under the experimental conditions. The net radiant energy intensities incident upon the BeO at the higher temperatures were less than those at the lower temperatures. The lack of positive results was attributed to the inability of experimentally developing sufficient intensity.

The radiant energy transfer in granular fused BeO was explored simultaneously with that in the BeO tube material. Both materials were at the same baseline temperature at the beginning of a radiant energy pulse. The effects produced in the granular material by the pulse were very minor and could not be attributed to direct transfer of radiant energy from the tungsten source. Since the BeO tube surrounded the tungsten source, it intercepted most of the incident radiant energy before it reached the granular BeO. There were no detectable effects observed in the granular material from the brief initial transfer of radiant energy observed in the BeO tube. The actual effects produced in the granular BeO material were considered to result from radiant energy emitted by the BeO tube, heating the granular material by a process of absorption, reradiation, and conduction at contact points.

The overall results obtained indicated that hot BeO did not become progressively diathermanous as its temperature increased but rather it displayed a stronger opaque behavior toward radiant energy.

PROBLEM STATUS

This report completes the study of radiant energy transport in BeO. This problem was closed July 1, 1964.

AUTHORIZATION

NRL Problem M01-15
Special Projects Task No. 72404

Manuscript submitted October 5, 1964.

AN EXPLORATORY STUDY OF RADIANT ENERGY TRANSPORT IN BeO

INTRODUCTION

The unusual physical and chemical properties of BeO and its capability for withstanding oxidizing or other chemical environments at high temperatures make it a valuable candidate material for high-temperature, high-performance applications. Among the many requirements imposed on a candidate heat sink material for withstanding high thermal fluxes, the problem of total heat transfer is of prime importance. The physical properties which are of greatest significance in BeO are its exceptional high thermal conductivity (the highest of any known refractory oxide or ceramic substance), its specific heat, and its high electrical resistivity and dielectric strength. These characteristics make BeO a potentially useful material for specialized high-temperature heat sink applications.

The thermal conductivity of BeO up to about 2000°C is depicted in Fig. 1 (1). It will be noted that thermal conductivity drops with increasing temperature to an apparent minimum and then tends to rise slightly again at the higher temperatures. This increase in conductivity at high temperatures has been attributed to a radiative transport component operative at high temperatures (2) which contributes to the total heat transfer. This indicates that BeO may develop a degree of transparency to thermal radiation at high temperatures which could permit transmission of radiant energy through the material. If BeO transmits significant amounts of thermal energy at high temperatures, its value as a heat sink to syphon off thermal energy at the high temperatures would be somewhat questionable. It is therefore important to recognize this as a possible service limit of BeO and to attempt to understand the reasons for such limit. An exploratory investigation was therefore conducted for the purpose of examining the high-temperature thermal behavior of BeO in an attempt to determine if significant transmission of radiant energy occurs in BeO.

REVIEW OF PROPERTIES OF BeO

It is desirable to review some of the characteristics of BeO which may possibly have some relation to the phenomenon of radiant energy transmission.

BeO crystallizes in a crystalline zincite type structure (3) with Be and O possessing a coordination number four in the lattice. The low-temperature structure of BeO is an ordered hexagonal structure with no center of symmetry and the atomic arrangement is such that a disordered structure (required for a vitreous state) cannot form (4), although it has a small radius ratio 0.25 ($r_{\text{cation}}:r_{\text{anion}}$). Therefore, BeO does not form a glass even though it possesses some of the requirements necessary for a vitreous condition.

In a lattice of composition MO such as BeO, two electrons supplied by the metal atom can be fixed pairwise in homopolar or covalent bonding (5) with the electrons of the oxygen, in the way the zincite type lattice is arranged. Oxides with homopolar or covalent electron pair bonding or a transition to this type of bonding are electrical insulators, are hard, and are generally transparent as a consequence of the firm binding of the electrons.

From lattice structure data the theoretical density of BeO is 3.008 (cgs units) at room temperature. Based on this value the molar volume of BeO is 8.33 (cgs units) (taking the atomic weight of Be to be 9.013). Compared to other refractory oxides this is of small magnitude and reveals the compact structure of BeO, with nearly two-thirds of its atomic weight consisting of oxygen.

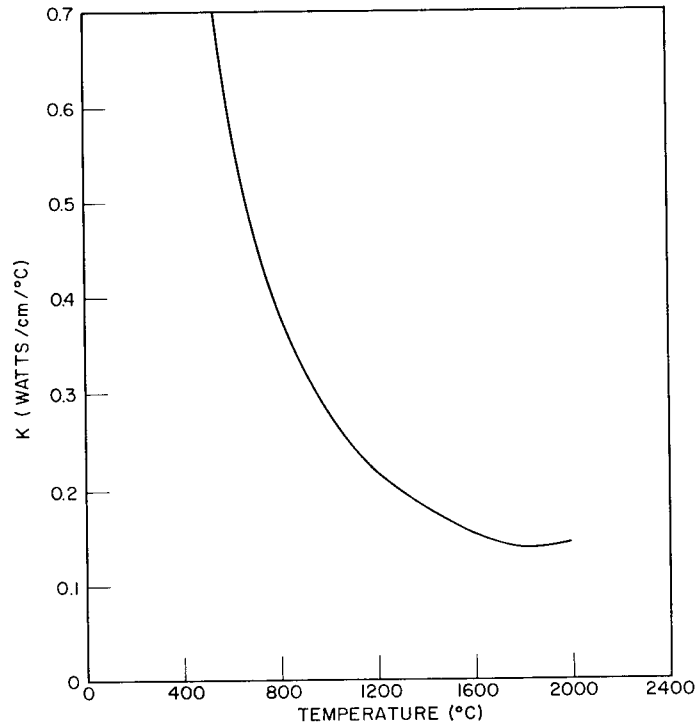


Fig. 1 - Thermal conductivity of BeO as a function of temperature (from Ref. 1)

From crystallographic property data BeO is considered to be a uniaxial substance displaying positive birefringence. The difference in the refractive indices of the extraordinary and ordinary rays is $\epsilon - w = 1.733 - 1.719 = +0.014$. This positive value although small is 1.5 times greater than the negative value for corundum. Birefringence, however, is a characteristic unfavorable for infrared transmission. The refractive index gives an approximate indication of the closeness of packing of the oxygen ions. All substances containing oxygen as ions in equally close packing must possess approximately the same refractive index, since all other atoms occur as cations and are consequently deprived of their valence electrons, so that relative to oxygen they contribute practically nothing to the refraction of light. Substances with the same closeness of oxygen packing as in BeO, such as corundum, spinel, cyanite (disthene) Al_2SiO_5 , and olivine, have approximately the same refractive index of 1.7.

BeO undergoes a high-temperature phase change at about 2050°C (6-8), which reaction is rapidly reversible. The polymorph is reported to be cubic with $a_0 = 4.76 \text{ \AA}$ and not of simple structure, the nature of which has not been determined. In the temperature range 2000° to 2050°C an extensive grain growth occurs in BeO which appears to be a conventional phenomenon and which does not appear to produce any evident degradation effect. The phase change at 2050°C , however, is accompanied by very large thermal expansion which has been reported to produce severe cracking (9) and disintegration as the result of an estimated 15% bulk volume change. It is not known if fused BeO would exhibit similar characteristics.

High-density hot pressed BeO (above 99.5% of theoretical) exhibits translucency (10), with the regions of translucency appearing grey in color. Fused BeO likewise exhibits a grey color and a high density. The grey color is attributed to internal scattering of incident

visible radiation and subsequent absorption within the mass of the translucent material. The lack of reflected light causes the BeO to appear grey in color. Translucent BeO exhibits a relative lack of porosity, and in hot pressed material the porosity is intergranular. High-density BeO is opaque to infrared radiation at wavelengths greater than 5 microns (9), and the high-density translucent material exhibits a 25% greater thermal conductivity at 1500°C and above than that of 99% density opaque BeO. This increase in thermal conductivity suggests that there may be some relation between the translucent condition of the BeO and its heat transport. For high translucency, radiant energy needs to be scattered (so that transmission is diffuse); however, a large fraction of the incident radiant energy should then be transmitted rather than diffusely reflected.

Another factor which may have some relationship to the transmission of radiant energy in BeO involves its vapor pressure and degree of dissociation (if significant) at high temperatures. The phase change which occurs at 2050°C indicates that the vapor pressure is significantly high at the high temperatures. From the theory of polymorphic transformations it is known that for any given crystalline substance only one structure is thermodynamically stable over a range of temperature and pressure. In this range all modifications of this structure will eventually transform to this structure. The rate at which this transformation occurs depends upon the structural change necessary. Such transformation either may be rapid (high-low type), occurring almost instantaneously, and reversible, involving only a slight structural change, or may be sluggish, proceeding slowly and involving a large structural change. Disregarding temperature, at normal pressures, only that modification having the lowest lattice energy will be stable. When temperature is considered, however, the most stable form will be that which has the least free energy at that temperature, namely, the form which has the least lattice energy combined with the ability to accommodate the thermal agitations. As temperature is increased, the ability to resist breaking of the bonds by thermal agitation (that is, the lowest vapor pressure) becomes increasingly important. From this, it is possible to explain the reason for polymorphic transformation and the existence of a definite transformation temperature. As temperature increases in a crystal in a stable form, the atoms and groups of atoms vibrate and by this vibration the crystal bonds are placed under strain. As the temperature increases further, there results a greater strain in the crystal bonds, giving rise to a higher vapor pressure. In some cases this leads to disruption of the bonds throughout the crystal and it melts. If at some temperature, however, there is an alternate structure which is capable of resisting the thermal agitation and which therefore has a lower vapor pressure, the original structure will transform to it. The new structure will now be stable and will continue so until another transformation occurs or it melts. Therefore, the transformation temperature may be considered as the temperature at which the vapor pressure curves of the polymorphic modifications cross, the high-temperature form having the lower vapor pressure above that point and the higher vapor pressure below it. Therefore, in the high-low type transformation (which BeO appears to follow) a distortion of the bonds occur in such a manner that the symmetry is altered into a structure having a lower bond-disrupting tendency. The vapor pressure of the new form should therefore be lower than that of the original. According to the literature data on the vapor pressure of BeO (11) there is no evidence reported that the vapor pressure changes at the temperature where the phase change occurs. The corrected experimental vapor pressure equation

$$\log_{10} P_{mm} = (18.50 \pm 0.23) - \frac{34320 \pm 530}{T} - 2 \log_{10} T \quad (1)$$

gives a linear plot of $\log_{10} P_{mm}$ vs reciprocal temperature for the temperature range 1977° to 2140°C. The accelerated grain growth reported to occur in the range 2000° to 2050°C suggests a net effect of the high vapor pressure existing in BeO prior to the transition to the cubic high-temperature form. Fragmentation of the large grains into a number of smaller regions with approximately the same orientation upon transformation (9,12) further suggests a change in vapor pressure at the transformation point. Vapor pressure

data (11) for slightly below and slightly above the transformation point (9.20×10^{-4} mm Hg at 2039°C and 1.67×10^{-3} mm Hg at 2081°C respectively, in vacuum) do not indicate a change in vapor pressure as a result of the phase change at 2050°C ; however the method of measuring the vapor pressure data may have been insensitive to discrimination of such change.

The vapor pressure data of Ref. 11 agrees well with that expected if it is assumed that vaporization proceeds by decomposition of BeO to the elements. Since this data did not identify the species present in the vapor nor discuss the chemical role of the tungsten effusion cell, the results are indeterminate. Later, work (13) on the vaporization of BeO and its reaction with tungsten in the temperature range 1900° to 2400°K showed the composition of the vapor mass, determined spectrometrically. It was shown that the vapor consisted predominantly of Be and O atoms and $(\text{BeO})_3$ and $(\text{BeO})_4$ molecules and smaller amounts of other molecules, O_2 , BeO, $(\text{BeO})_2$, $(\text{BeO})_5$, $(\text{BeO})_6$, WO_2 , WO_3 , and $\text{WO}_x(\text{BeO})_y$, where $x = 1, 2$ and $y = 1, 2, 3$. The dissociation energy of the BeO molecule was given as 4.6 ± 0.1 ev. The boiling point of BeO was roughly estimated to be $3850^\circ \pm 200^\circ\text{C}$, at which temperature the vapor was reported to consist mostly of $(\text{BeO})_4$ and smaller amounts of $(\text{BeO})_3$ and $(\text{BeO})_5$. The dissociation energy of BeO was given as 106 ± 3 kcal/mole. The great abundance of polymeric molecules in the vapor of BeO in contrast to the simplicity of the vapor of the other alkaline earth oxides is probably due to the ability of beryllium to form complex ions by virtue of its covalent tendency, as evidenced by complex ions formed in aqueous solutions.

The composition of the vapor above $\text{BeO}_{(s)}$ in a tungsten Knudsen cell at 2242°K reported in Ref. 13 is shown in Table 1. In the temperature range 2000° to 2400°K

Table 1
Composition of Vapor Above $\text{BeO}_{(s)}$ in a Tungsten
Knudsen Cell at 2242°K (Ref. 13)

| Molecule | Partial Pressure (atm) | Estimated Relative Ionization Cross Section* |
|-----------------------------|------------------------|--|
| Be | 5.0×10^{-7} | 1.0 |
| O | 5.0×10^{-7} | 0.2 |
| O_2 | 2.0×10^{-8} | 0.12 |
| BeO | 7.5×10^{-9} | 1.0 |
| $(\text{BeO})_2$ | 7.5×10^{-10} | 1.7 |
| $(\text{BeO})_3$ | 1.0×10^{-7} | 2.2 |
| $(\text{BeO})_4$ | 4.4×10^{-8} | 2.8 |
| $(\text{BeO})_5$ | 3.0×10^{-9} | 3.3 |
| WO_2 | 1.2×10^{-7} | 10.0 |
| WO_3 | 4.6×10^{-8} | 10.0 |
| $\text{WO}_2(\text{BeO})$ | 1.3×10^{-9} | 10.0 |
| $\text{WO}_3(\text{BeO})$ | 1.5×10^{-9} | 10.0 |
| $\text{WO}_2(\text{BeO})_2$ | 3.3×10^{-9} | 10.0 |
| $\text{WO}_2(\text{BeO})_2$ | 2.4×10^{-9} | 10.0 |
| $\text{WO}_2(\text{BeO})_3$ | 8.0×10^{-10} | 10.0 |
| $\text{WO}_3(\text{BeO})_3$ | 6.0×10^{-10} | 10.0 |
| $\text{WO}_2(\text{BeO})_4$ | 1.0×10^{-10} | 10.0 |
| Higher complexes | $< 10^{-10}$ | 10.0 |

*Ionization cross section is defined as $\sigma_{\text{O}}/\sigma_{\text{Be}}$.

the mass spectrum was reported (13) to contain a surprising complexity of species in the effusing vapor. In a current review (14) of the vapor pressure work on BeO, it was indicated that existing vapor pressure data on BeO is only in qualitative agreement, thus making the data approximate only.

The importance of an excited energy carrying state such as occurs in dissociated gas molecules or in chemical reaction and evaporation in producing an effect on the observed thermal conductivity cannot be overlooked.

The electrical resistivity of BeO (2.25 density) (15) measured in a nitrogen atmosphere is shown in Table 2. It will be noted that the resistivity decreases significantly from a value of 8×10^7 ohm-cm at 1000°C to a value of 1.6×10^3 ohm-cm at 2000°C .

Spectral emissivity ($\epsilon_{0.665}$) and total emissivity (ϵ_t) of BeO of density 2.778 g/cm^3 are shown in Table 3 (16).

Table 2
Resistivity of BeO (density 2.25) Sintered at 2100°C
Measured in Nitrogen Atmosphere (Ref. 15)

| Temperature ($^\circ\text{C}$) | Resistivity (ohm-cm) | Temperature ($^\circ\text{C}$) | Resistivity (ohm-cm) |
|-------------------------------------|-------------------------|-------------------------------------|-------------------------|
| 1000 | 8×10^7 | 1600 | 3.5×10^4 |
| 1100 | 1.6×10^7 | 1700 | 1.5×10^4 |
| 1200 | 4.0×10^6 | 1800 | 6.5×10^3 |
| 1300 | 8.0×10^5 | 1900 | 3.5×10^3 |
| 1400 | 2.5×10^5 | 2000 | 1.6×10^3 |
| 1500 | 8.0×10^4 | 2100 | 8.0×10^2 |

Table 3
Brightness Temperature T_B , Spectral
Emissivity ($\epsilon_{0.665}$), and Total Emissivity (ϵ_t) for
BeO (White-Air Fired) (Ref. 16)

| T ($^\circ\text{K}$) | $\epsilon_{0.665}^*$ | ϵ_t^* |
|------------------------|----------------------|----------------|
| 1104.6 | 0.212 | 0.336 |
| 1187.9 | 0.209 | 0.361 |
| 1271.0 | 0.210 | 0.392 |
| 1354.2 | 0.213 | 0.420 |
| 1437.1 | 0.217 | 0.439 |
| 1519.8 | 0.222 | 0.453 |
| 1602.4 | 0.228 | 0.463 |
| 1684.9 | 0.235 | 0.470 |
| 1767.2 | - | 0.474 |
| 1849.6 | - | 0.475 |
| 1890.7 | - | 0.475 |

*The values are estimated to be accurate to within 10% for spectral emissivity and to within 20% for total emissivity.

REVIEW OF EXISTING HYPOTHESES FOR HIGH-TEMPERATURE EXCITATION PROCESSES

The problem of anomalous increase in the observed thermal conductivity of single-phase BeO warrants a review of the existing knowledge on the subject of total heat transport in dielectric materials. Considerable disagreement exists in the literature regarding which of the various excitation mechanisms that have been proposed really account for an increase in thermal conductivity observed in both ceramics and semiconductors at high temperatures. Since this increase is probably not attributable to phonon transport, which follows a $1/T$ relationship, attempts have been made to account for it in the case of semiconductors on the basis of ambipolar transport of gap energy by electron-hole pairs (17,18), internal radiation (19), and various other excitation mechanisms (20). Similar attempts have been made to account for the existence of an anomalous rise in high-temperature thermal conductivity of several single-phase ceramics by radiative transport (2,21-24). In an attempt to rationalize the anomalous behavior of thermal conductivity in ceramics, the observed conductivity was also proposed (25) as some linear combination of phonon and electronic components, a radiative heat transfer component, and components resulting from transport of thermal energy by electron-hole pairs, excitons, and dissociated gas molecules operating simultaneously or individually to contribute to the total heat flow. Thus, four separate processes of thermal energy transfer have been proposed as contributing in some degree to total heat transfer, which include heat conduction by thermoelastic lattice vibrations, conduction by free electrons moving in the solid, conduction by excited atoms, and energy transfer by the passage of electromagnetic radiation. The total heat conduction in solid materials at high temperatures may therefore depend upon the sum of the contributions from any of these four modes of energy transfer. Conductivity due to thermoelastic lattice vibrations (phonon conduction) and conductivity due to electron energy transfer (electron conduction) are generally considered as being basic thermal conduction processes. Conduction by excited atoms (exciton conduction) and electromagnetic radiation (photon or radiation conduction), may be considered to be complimentary energy transfer processes. Total thermal conductivity in any solid may then be summarized by

$$k_{\text{total}} = k_{\text{ph}} + k_{\text{el}} + k_{\text{ex}} + k_{\text{r}}$$

where k_{ph} is thermal conductivity increment due to phonon transport, k_{el} is thermal conductivity increment due to electron transport, k_{ex} is thermal conductivity increment due to exciton transport, and k_{r} is thermal conductivity increment due to photon transport.

Phonon Conduction Parameter

Since thermal conductivity in dielectric materials is a structure sensitive property, single-phase, as well as polyphase polycrystalline aggregates are subject to various sources of thermal resistance. These include inhomogeneities in composition, microstructure, small-scale imperfections, and impurities.

In dielectrics, heat is transferred by thermally induced lattice vibration. When a temperature gradient exists in a material, vibrational quanta of thermal energy (phonons) (26) are considered to flow along the thermal gradient. The thermal conductivity of the material is subject to the inelastic collisions and the scatter of the phonons or by the mean free path of the phonons from analogy with kinetic theory. The thermal conductivity under these conditions has been expressed (27) as

$$k = 1/3 c_v \ell v \quad (2)$$

where c_v is the volume specific heat, ℓ is the phonon mean free path, and v is the elastic wave or phonon velocity. If lattice vibrations were completely harmonic in a material,

they would offer no resistance to phonon flow and the phonon mean free path as well as the thermal conduction in such material would be infinite. Actually, a number of scattering mechanisms may be operative in a material which limit the phonon mean free path. The magnitude of the additive thermal resistance depends upon the concentration, distribution, and size of the sources of thermal resistance listed in Table 4.

Photon Conduction Parameter

Thermal energy transfer through solids by transmission or absorption and reradiation of electromagnetic energy is a concept analogous to the heat transfer between photons and molecules in a gas. In the case of solids, instead of molecules or phonons the waves are considered as photons (electromagnetic radiation). The transfer of radiant energy between surfaces separated by a nonabsorbing medium has been treated extensively (28) and is generally well known. Information is lacking, however, on the situation when the space between the surfaces contains an absorbing or radiating medium. Depending on the absorption characteristics of the interposing medium and its thickness, (a) radiation may be transmitted between the surfaces, (b) radiation may be reflected at the boundaries between the medium and its surfaces, (c) radiation may be absorbed by the medium from its surfaces and reradiated again, (d) radiation may be emitted, absorbed, and reradiated by the medium. The matter of internal radiation in solid materials has been considered for glasses, ceramic coatings, ceramic oxides, and fibrous insulation. In all cases, the resulting approach for determining the internal radiant energy transport has been essentially the same, differing only in the assumptions made in the deviations of mathematical expressions to describe the phenomenon.

The phenomenon of radiation transport through a medium is a function of the scattering, absorption, and emission properties of the medium. The scattering and absorption properties of a material are generally treated together in its transmissive characteristics, while the radiative emission of a material is a function of the absorption and the temperature. Attempts which have been reported (24,33) for estimating the order of magnitude of possible effects from radiant energy transmission are largely oversimplification of a very complex phenomenon.

In one case (24), radiant energy conduction was expressed as

$$k_r = \frac{16}{3} \sigma n^2 T^3 l_r \quad (3)$$

where σ is the Stefan-Boltzmann constant, n is the refractive index, and l_r is the photon mean free path. The mean free path is limited by absorption and scattering and is dependent upon temperature and wavelength. If the temperature dependence of the mean free path compared to T^3 is small, then the thermal conductivity due to radiation would follow a T^3 dependency. This effect was measured in single crystals (23) and reported to be the case. A plot of the deviation (34) $\ln(k_t - k_{ph})$ versus $\ln T$, where k_t was total conductivity and k_{ph} is conductivity following a $1/T$ relationship, revealed a relation of the order of T^{17} instead of T^3 . Thus, the simple equation (3) is unable to explain the deviation or the role of radiant energy transmission. In another case (33) it was assumed for the deviation that the material which radiates has an emissivity of 1.00. This corresponded to the physical picture of a distribution of distinct radiating volume elements immersed in a transparent scattering medium. The optical density of the emitting elements was measured by an absorption constant. The actual situation was far more complex. The geometrical configuration to which the solution (33) applied was that of a semi-infinite slab bounded by two parallel planes perpendicular to the direction of heat flow. Wall effects were neglected in the solution and the equations referred to the interior of the material. Conductivity due to radiation transport for these assumptions was given as

$$k_r = \frac{8\sigma T_0^3}{\alpha + 2s} \quad (4)$$

Table 4
Sources of Resistance to Phonon Conductivity (Ref. 24)

| Source | Temp. Range | Temp. Dependence of Resistance | Remarks |
|---|---|--|--|
| Phonon-phonon interaction (Umklapp processes) | Very low temp. $T \ll \theta$ Below Debye temp. $T < \theta$ Above Debye temp. $T > \theta$ | T^{-3} $e^{-\theta/T}$ T' | |
| Boundaries (external) | Very low temp. $T \ll \theta$ | T^{-3} | |
| Boundaries (grain) | Very low temp. $T \ll \theta$ Above Debye temp. $T > \theta$ | T^{-3} No effect | Greatest effect for material with long mean free path. |
| Impurities | Very low temp. $T \ll \theta$ High temperature | T^{-1} Independent of T | Depends upon concentration and size, greater effect in lattice with long mean free path. |
| Porosity | Low temp. $T < \theta$ High temperature | Continuous pores Discontinuous pores T^3 | Proportional to conductivity of gas phase. Proportional to volume fraction of solid phase. Proportional to pore size, volume fraction, and emissivity. |

where σ is the Stefan-Boltzmann constant, α is the absorption coefficient (cm^{-1}), s is the scattering coefficient (cm^{-1}), k_r is thermal conductivity due to radiation transport, and T_0 is a reference temperature close to the temperatures actually occurring in the material where radiation transport takes place. The results obtainable from the above were only rough approximations according to the conclusions given.

Based on the above equation, however, Fig. 2 shows the ratio of heat transfer by radiation ($\text{cal}/\text{cm}^2\text{-sec}$) to the heat transfer by all other conduction processes ($\text{cal}/\text{cm}^2\text{-sec}$) plotted as a function of temperature for hypothetical material with thermal conductivity equal to the high-temperature conductivity of BeO. Thus, this plot gives an idea of the ratio of heat transfer by radiation to the heat transfer by all other conduction processes. The values of q_{rad}/q_k for temperatures above 2000°K indicate that radiation transport may be important to the overall conductivity of BeO at high temperatures, especially if q_k for the material is relatively small. At temperatures greater than 4000°K the heat transport by means of radiation transport could be the dominant process for energy dissipation.

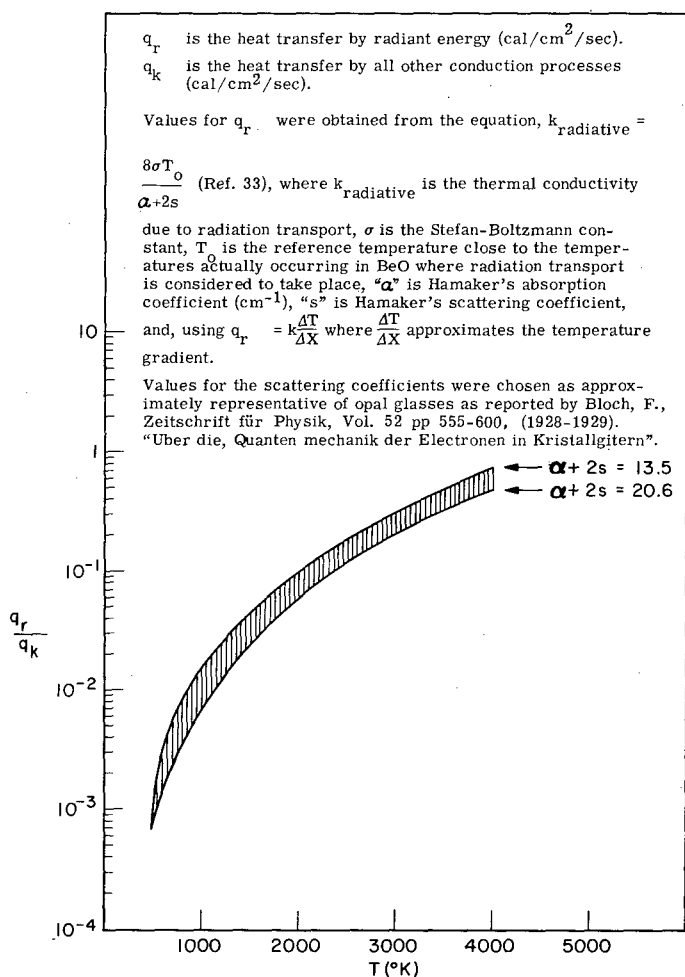


Fig. 2 - q_r/q_k vs temperature for thermal conductivity of BeO

Another treatment of the radiation conduction phenomenon in the interior of an infinite medium was reported in Ref. 35. The equations were deduced from the condition for radial energy flow through a large spherical surface (the interior of the Earth). By ignoring terms of the order of the inverse square of the spherical radius, the radiation conductivity deduced from this work should be applicable to the interior of an infinite slab bounded by parallel planes perpendicular to the direction of energy transport, ignoring boundary effects. The suggested approximate expression for radiative conductivity was given in Ref. 35 as

$$k_r = \frac{16n^2\sigma T^3}{3\epsilon} \quad (5)$$

where n is the average refractive index of the material over the wavelength regions of importance to the transfer process, σ is the Stefan-Boltzmann constant, T is the absolute temperature, and ϵ is the "opacity," an average value for the wavelength regions of importance to the transfer process and assumed to be temperature dependent. "Opacity" of the medium at wavelength λ and temperature T is defined as $\epsilon = \alpha + s$, where α is the absorption coefficient of the medium with no scattering centers and s is the scattering coefficient measured in a nonabsorbing medium containing scattering centers. For a typical inorganic crystal with $n = 1.7$, $\epsilon_0 = 5 \text{ cm}^{-1}$, $E = 3 \text{ eV}$, and $s_0 = 10 \text{ ohm}^{-1}\text{-cm}^{-1}$ a value is given in Ref. 35 for k_r equal to $0.048 \text{ cal/cm-sec-}^\circ\text{K}$ at 2500°K .

Exciton Conduction Parameter

The concept of thermal energy conduction by excitons (excitation energy) has been proposed in the field of heat transfer in order to explain the anomalous increase in conductivity of some dielectrics (24,36) and semiconductors (17,20,37) at extremely high temperatures. Excitons have been described as bound electron-hole pairs which are capable of diffusion throughout the material. Their energy states are intermediate between those of the valence band and the conduction continuum. It is believed that when a dielectric or semiconductor receives sufficient localized thermal energy, the electrons in the valence band can be excited to a higher energy level. If this energy is not quite high enough to place the electron in the conduction continuum, a tightly bound electron-hole pair is formed which is capable of transmitting its excitation to the valence electrons of neighboring atoms.

In Ref. 36 the excitation energy (exciton) contribution to thermal conductivity was given as

$$k_{ex} = \left(\frac{16\pi}{3}\right) \left(\frac{\sigma^3 T^2}{h^3}\right) M\ell \left[\left(\frac{\Delta E}{\sigma T} + 2\right)^2 + 2 \right] e^{-\Delta E/\sigma T} \quad (6)$$

where k_{ex} is conductivity due to exciton transport ($\text{cal/cm-sec-}^\circ\text{K}$), ΔE is the excitation energy for excitons (cal), σ is the Stefan-Boltzmann constant, M is the mass of the exciton in grams (often assumed to be equal to twice the mass of the electron), h is Planck's constant, T is temperature under consideration ($^\circ\text{K}$), and ℓ is mean free path of the exciton (cm).

Computations of k_{ex} are dependent upon knowledge of M , ℓ and ΔE , which must be obtained from experiment. Estimates of ΔE and ℓ were obtained (36) from thermal conductivity values of Al_2O_3 , BeO , and MgO , which are shown in Table 5. The values for ΔE and ℓ were obtained from high-temperature thermal conductivity data. The difference of the measured values for Al_2O_3 , MgO , and BeO from the sum of a $1/T$ temperature dependent phonon conductivity and a radiation conductivity calculated by Eq. (6) for k_r was attributed to exciton conductivity.

According to comments of Ref. 34, the probability of exciton conductivity due to electrons is at least four orders too small to account for the deviation or increased conductivity. Reference 34 concluded that none of the information reviewed (23,24,36) offered a satisfactory explanation of the deviation due to either exciton or radiation conduction.

Table 5
Values for Excitation Energy ΔE and the Mean Free Path l for Exciton Heat Conduction (Ref. 36)

| Oxide | ΔE (cal) | l |
|--------------------------------|------------------|-------|
| Al ₂ O ₃ | 1.42 | 560 Å |
| MgO | 1.35 | 840 Å |
| BeO | 0.43 | 27 Å |

Effects of Vaporization or Sublimation

At high temperatures, reactions involving vaporization, sublimation, and dissociation of vapor evolved from a solid add to the complexity of total heat transfer analysis. A large amount of energy is absorbed in the vaporization and dissociation processes, and temperature cannot be considered to be the driving force since a great deal of energy is chemically stored in the particles during the dissociation process. In general, metal oxides are formed exothermically and they tend to dissociate with increase in temperature. In the case of BeO, this compound exists as a solid over a considerable temperature range, and the vapor pressure of the BeO molecule is relatively low even at 2000°C. The heats of vaporization and of dissociation have been reported as 165 kcal and 106 kcal respectively (13). Since the evaporation and dissociation processes absorb energy, and if more atoms leave a heated surface than return to it as in a vacuum environment, the average energy of the molecules remaining in the solid will be lowered (i.e., the temperature will be lower). Upon recombination of the dissociated atoms on a surface considerable liberation of heat results in the form of a radiant energy. Whether the excitation processes due to vaporization, dissociation, ionization, and recombination make any significant contribution to the transfer of radiant energy through BeO is a difficult question.

EXPERIMENTAL

Approach

In designing the apparatus for exploring the radiant energy transmission through BeO, the major factor that governed the configuration of the apparatus was the need to reduce to a minimum the complicating variables inherent in the heat transfer problem. It was considered desirable to eliminate convection heat transfer and to drastically reduce conduction heat transfer in the sample material while leaving radiant energy transfer as the dominant process.

Other considerations entering into the choice of method included the desirability of restricting the sample volume to the smallest amount possible in view of the high temperature range desired and the need to maintain a high-vacuum environment, and the need to include adequate safety precautions to prevent any incidents involving toxic BeO. A high-vacuum environment not only eliminated the problem of convection heat transfer in the sample volume, but also provided the necessary protection to all the metallic components within the hot zone against oxidation and early failure from this cause.

In choosing a granular form of sample material, it was believed that the amount of heat transfer by conduction in this form of material could be drastically reduced to only that of point contact between grains, leaving radiation heat transfer as the dominant process. This viewpoint was partially based on the known fact that the effective thermal conductivity of a finely divided ceramic material compared to that of a solid of the same material is ordinarily several orders of magnitude lower than that of the solid.

It was decided that the basic form of apparatus consistent with the above requirements should consist of a ceramic container with a centrally located heater running lengthwise in it. This container would hold the sample material, while the heater would provide a source of radiant energy that would flow out radially from the center with isotherms of cylindrical shape. To prevent contact between the central heater and the granular sample material, a protection tube was necessary. Since this tube would necessarily have to be composed of BeO and because of its particular location, it was considered desirable to include it as a solid sample material and to observe its radiant energy transmission behavior together with that of the granular sample material.

The sample material must be heated to various temperatures to observe whether any significant changes occur in its radiant energy transmission characteristics. The most appropriate way of heating the sample material to a uniform temperature would be to use a resistance heater wound on the outside of the crucible with separate heaters included at top and bottom to offset end losses.

With a metallic resistor for the central heater and by measuring both the potential drop across a known gauge length and the total current, the effective thermal flux developed by the heater across its gauge length can be obtained.

By surrounding the heated parts of the system with suitable radiation shields and enclosing the entire assembly in a water cooled jacket on all sides, a cold wall furnace results. By mounting this assembly on a base plate and passing all the electrical, instrumentation, and water connections through vacuum sealed feed-throughs, a self-contained unit results which can be inserted into and attached to a vacuum bell jar or can be detached from it without disturbing any portion of the vacuum system.

An ideal temperature sensing system that would be desirable for this investigation was nonexistent. Such a system would have had to be capable of operating in a vacuum at very high temperatures and would have had to not only be sensitive to radiant energy but register quickly the changes in temperature caused by radiant energy heat transfer. The lack of such a system necessitated reliance upon thermocouple systems, which are rather insensitive in their response to radiant energy though rugged and quite reliable.

Description of Apparatus

The arrangement of the basic parts of the cold-wall high-temperature furnace apparatus is shown schematically in Fig. 3 (see facing page). In the figure the numbers identify the components as follows: (1) BeO crucible wound on the outside with 60-mil-diameter wire; (2) BeO cylinder; (3) central heater - 80-mil tungsten rod; (4) top heater - 60-mil tungsten wire - BeO ceramic; (5) bottom heater - 60-mil tungsten wire - BeO ceramic; (6) BeO protection tube; (7) potential drop leads - 3-mil tantalum wire; (8) four BeO support rods of 1/16 inch diameter spaced 90° apart; (9) BeO protection tube; (10) tungsten/iridium thermocouple - tantalum sheathed BeO thermocouple tube; (11) tungsten/iridium thermocouple; (12) tungsten/iridium thermocouple; (13) three radiation shields, each of 5-mil-thick tantalum; (14) four radiation shields, each of 5-mil-thick molybdenum, with 60-mil tungsten wire spacers; (15) nine radiation shields, each of 5-mil-thick molybdenum, with 60-mil tungsten wire spacers; (16) nine radiation shields, each of 5-mil-thick molybdenum, with 60-mil tungsten wire spacers; (17) double-walled water-cooled copper furnace jacket; (18) double-walled water-cooled bottom plate; (19) double-walled water-cooled top plate; (20) copper water-cooled top electrode assembly; (21) copper water-cooled bottom electrode assembly; (22) copper water-cooled power lead; (23) copper water-cooled power lead; (24) copper water-cooled power lead; (25) copper water-cooled power lead.

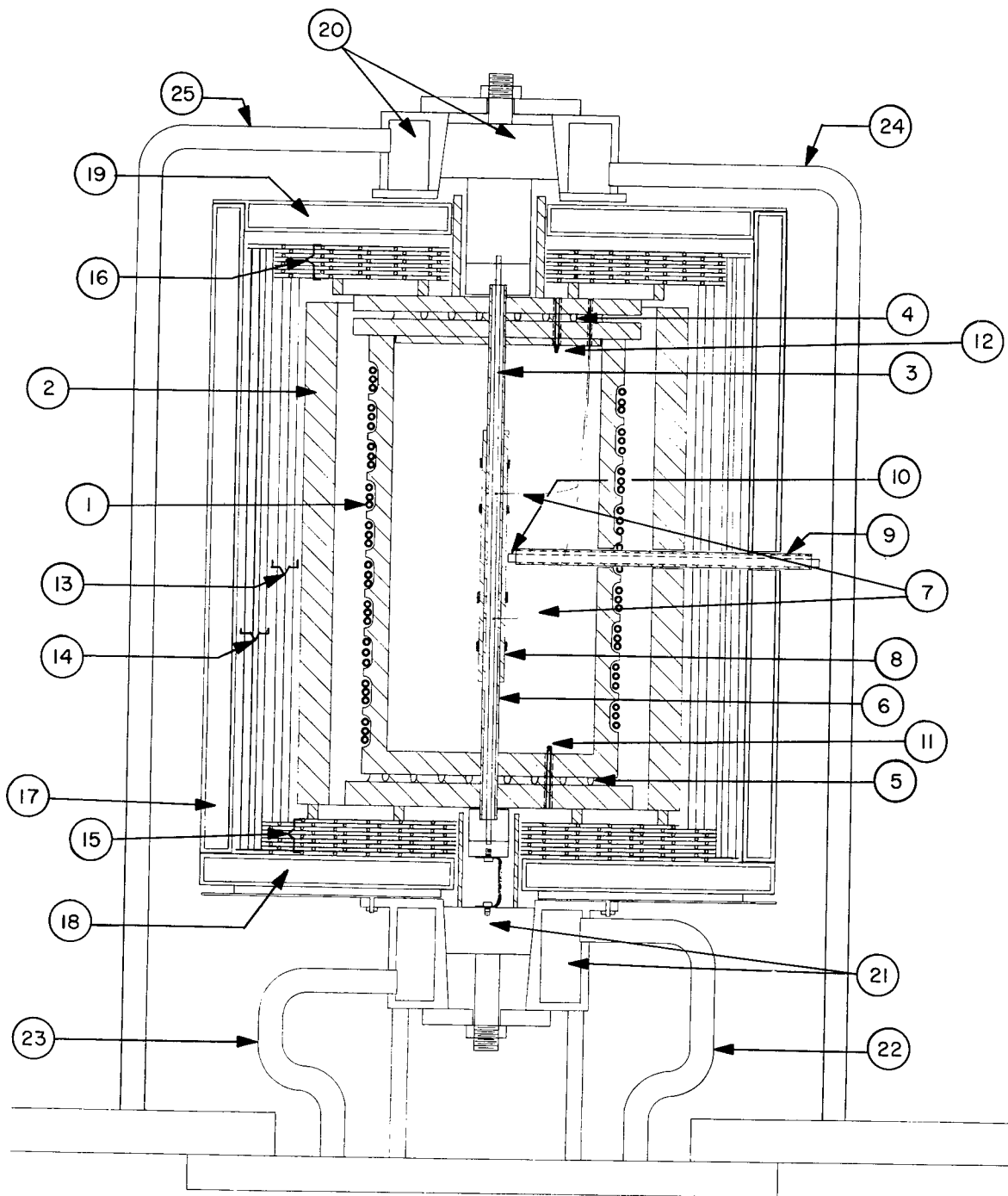


Fig. 3 - Schematic of the high-temperature vacuum furnace for the study of radiant energy transmission in BeO. The numbered components are described in the text on the preceding page (Page 12).

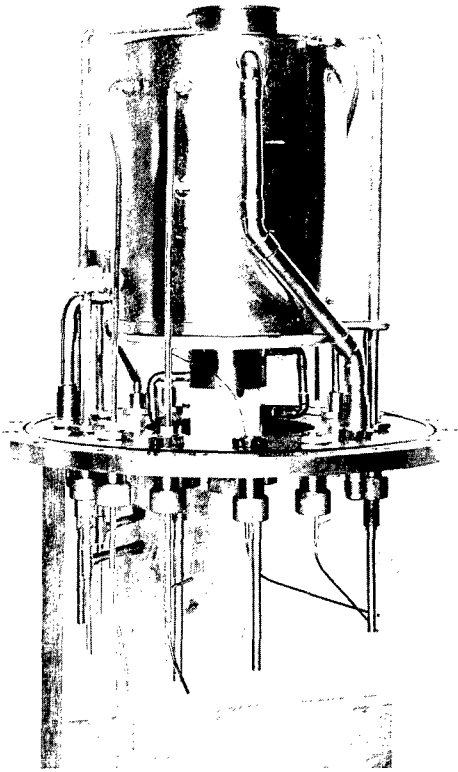


Fig. 4 - Cold-wall furnace assembly mounted on a vacuum bell-jar base plate

The complete furnace assembly mounted on a vacuum bell-jar base plate is shown in Fig. 4.

It is well to mention at the outset that all of the refractory ceramic components used in the furnace hot zone were composed of high-purity, high-fired BeO. This included the crucible for containing the granular sample material, top and bottom crucible heater plates, top heater cover, bottom support wafers, the protection tube for the central heater, thin support rods, electrical insulators for power leads and for thermocouples, various spacers, and small tubing. This was considered essential in order to avoid the inherent difficulties that usually occur when dissimilar refractory ceramic materials are in contact with each other at high temperatures. High-purity lamp-grade tungsten wire was used in all of the heater applications. Tungsten-iridium thermocouples were used for monitoring temperatures at all points in the hot zone.

The BeO crucible for containing the granular sample BeO material measured 4 inches o.d. by 3-1/4 inches i.d. by 6-5/8 inches high. A nine-turn spiral groove measuring 1/2 inch wide by 1/8 inch deep with 1/8-inch-thick walls was ground into the outside wall and this was wound with a three-strand, 60-mil tungsten wire heater. Three 1/4-inch-diameter holes bored through the crucible walls at points 120° apart and 3-1/4 inches down from the top served as ports for specially constructed thermocouples used for monitoring temperature effects in the BeO sample material. A 5/16-inch hole bored through the bottom of the crucible served as a port for a protection tube and the central heater wire enclosed concentrically within it.

A heater plate was provided at both top and bottom of the crucible. The top heater was constructed with raised sections 1/8 inch high on both sides of the plate. The raised section on the bottom side fitted into the inside diameter of the crucible and kept the heater plate centered in place. The raised section on the top side was slotted with six

parallel slots 1/8 inch deep which accommodated a grid type tungsten wire heater as illustrated in Fig. 5. A 5/16-inch-diameter hole bored through the plate at its center served as a port for the top end of the protection tube through which the central heater wire was passed. The characteristics of the bottom heater plate were similar to the top plate except that the raised section was omitted on the bottom side of the plate. A 5/16-inch central hole served as a port for the protection tube and the central heater wire. Both plates had two small holes bored through them for accommodating monitoring thermocouples as illustrated to the left of the central hole in Fig. 5. The crucible was supported on the bottom heater plate, which in turn rested on 1/4-inch-high sections of BeO tubing having a 1-inch o.d. and 3/16-inch wall thickness placed on the top of the bottom radiation shield assembly. This shield assembly in turn rested on the bottom of the water-cooled furnace jacket.

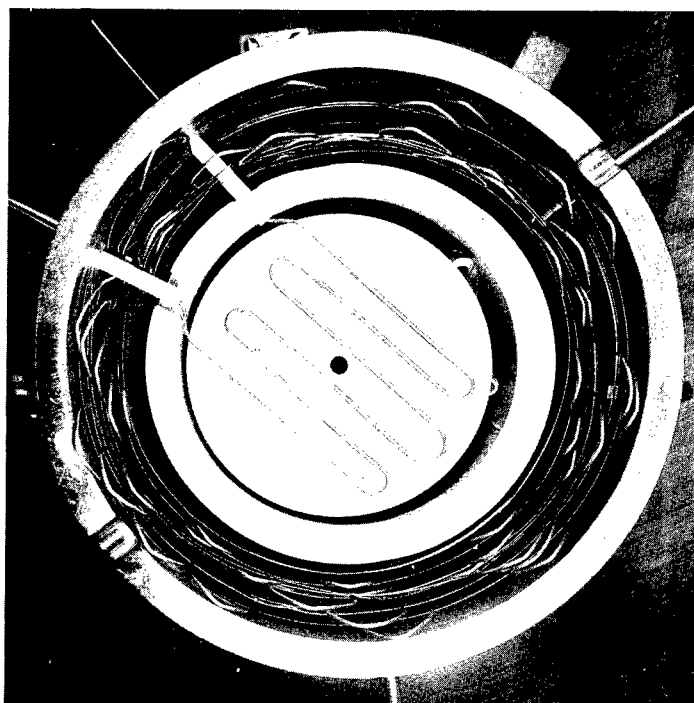


Fig. 5 - View of the top of the furnace showing the top heater and the side radiation shields

The radial source of radiant energy was from a central heater enclosed in a protection tube running lengthwise in the crucible as shown in Fig. 3. Since the central heater was only 8-1/2 inches long and the ends were connected to water cooled terminals, significant end losses were apparent. The effect of end losses is to decrease the voltage drop for the whole heater wire. As a result, the input of energy as well as the output of radiant energy over the heater length would be diminished and the power applied would not accurately reflect the radiant energy flux. The method used for eliminating or correcting for the end losses consisted of spot welding fine wire potential drop connections 2 inches apart in the center section of the heater wire. This section was considered to be far enough removed from the cooling terminals so that it could be considered uniform in temperature for high temperature ranges or very nearly so for lower temperatures.

The potential drop leads were initially planned to be of fine-wire tungsten so as to avoid thermoelectric effects, but the fragile nature of tungsten wire, particularly after it has been heated, proved this to be impractical. Fine-wire (3-mil) tantalum was substituted with reasonable success, and this combination was used up to the melting point of tantalum (2996°C). A slight error was introduced into the voltage drop readings by the use of tantalum with tungsten, since the couple between them develops nearly 23 millivolts at 2000°C; however, this was not considered serious under the experimental conditions. Calibration of the central heater wire versus temperature over a 2-inch gauge length is discussed in Appendix A.

The necessity of isolating the granular sample BeO material from contact with the central heater wire with a protection tube posed a problem with respect to the potential drop leads across the 2-inch gauge length. It was considered necessary to hold the inside diameter of the protection tube as close as practical to the outside diameter of the central heater wire. The protection tube size selected for this application measured 6.50 mm o.d. by 5.32 mm i.d. With an 80-mil-, or 2.03-mm-, diameter wire enclosed concentrically within the tube, there was left a space of only 1.64 mm or 65 mils between wire and tube. This space was not sufficient to fully enclose the central heater wire with potential drop leads attached. This problem was resolved by making up the protection tube in three sections, with the middle-section equal to the 2 inches gauge length. The ends of the middle-section were each notched to accommodate the fine wire. The protection tube was assembled around the heater wire by joining the three tube sections end to end and holding them in place by wiring 1/16-inch-diameter BeO rods, spaced 120° apart, across the joints, as shown in Fig. 3. The potential drop leads were then brought out of the hot zone through the top of the furnace.

Since metallic radiation shielding was used in the hot zone, it was necessary to insulate the crucible heater electrically. A BeO cylinder, 5-7/8 inches o.d. by 4-7/8 inches i.d. by 7-7/8 inches high, was centered around the crucible with BeO tubes as illustrated in Fig. 5. This arrangement also provided a means of supporting the thermocouples used to monitor temperatures within the crucible and assisted in outgassing and evacuation of the hot volume.

As shown in Figs. 3 and 5, metallic radiation shielding was used to thermally insulate the hot zone. The three shields nearest to the hot zone were of 5-mil polished tantalum sheet, while the four outer shields were of 5-mil polished molybdenum sheet. The individual turns were separated from each other by a wire grid made up from 60-mil tungsten wire. The top and bottom insulation consisted of an assembly of nine circular shields each of 5-mil polished tantalum sheet separated with tungsten wire grids. The top and bottom shield assemblies were kept separated from direct contact with the respective heater plates by means of short tubular BeO sections as shown.

The hot zone assembly was contained in a water-cooled furnace jacket made up in two parts from copper sheet. Double wall construction was used with suitable reinforcing between the walls to prevent not only buckling under vacuum but to also prevent any misalignment of the ports through which instrumentation passed. The reinforcing between the walls was arranged to also provide complete circulation of cooling water over all of the jacket surfaces. The main jacket consisted of cylindrical sides and a flat bottom; the sides were 8 inches i.d. by 1/2-inch wall by 10-3/8 inches overall height with a 5/8-inch-diameter water supply line and a 3/4-inch discharge line connected to it. The top jacket was constructed with a 3/16-inch lip so as to rest on the top of the main jacket with the water cooled section extending downward within the inside diameter of the main jacket. This cover measured 8-3/8 inches in diameter overall, with the cooling section measuring 8 inches in diameter by 1/2 inch thick. A 1-1/2-inch-diameter hole in the center served

as a port for the top electrode of the central heater. Cooling water connections were 3/8 inch for both supply and discharge. All water connections to the furnace jacket were hard-soldered, and lines were passed through vacuum seals in the base plate. By this arrangement there were no demountable water connections within the vacuum environment. Although the jacket assembly completely insulated the hot zone, there were sufficient openings to successfully outgas the assembly and to maintain a high vacuum of 1×10^{-6} torr under the highest operating temperatures reached.

The furnace assembly was mainly supported on the 18-inch-diameter stainless steel vacuum bell-jar base plate by the water lines passing through vacuum sealed feedthroughs. However, to permit vertical alignment of the assembly, the top of the bottom copper electrode was used as a fixed support for it. This electrode was kept in alignment with the base plate by the tubular section of alumina having parallel ends as shown in Fig. 4.

The central heater of 80-mil-diameter tungsten wire was kept positioned concentrically within the protection tube by the arrangement shown in Fig. 3. The wire was clamped rigidly to the top water-cooled copper electrode assembly by means of a split clamp, which was bored to retain the protection tube concentric with the wire. The bottom connection was made by clamping the wire to a split tantalum cylindrical block riding inside a tubular BeO guide. The tantalum block was connected electrically to the bottom water-cooled copper electrode with flexible copper braid. The tubular guide was kept in position by the hole in the bottom of the furnace jacket. By this arrangement the central heater was free to expand with temperature and could be kept concentric with the protection tube.

Temperatures at the bottom and top of the hot zone within the crucible were monitored by bare bead thermocouples, while specially constructed thermocouples were used to measure temperatures within the central planar zone of interest. These thermocouples were located on the same plane but spaced 120° apart with their junctions placed at different radial distances. One junction was located 3/32 inch from the protection tube, while the second junction was located 3/4 inch from it and the third junction 1-1/2 inches from it at the inner wall of the crucible. The arrangement of these thermocouples is illustrated in Fig. 6. The construction of the special thermocouples together with the calibration of the tungsten-iridium thermocouples used is discussed in Appendix B.

The arrangement as shown in Fig. 4 permitted the assembly of all sample material and components together with all connections for power, instrumentation, and water lines into a complete unit mounted on a base plate. This unit was then inserted into a stainless steel bell jar 14 inches in diameter by 24 inches in overall height and bolted to it. As a safety precaution tension on the bolts was maintained by spring pressure and the arrangement was so designed as to permit immediate relief of pressure should a water failure occur in the furnace assembly while at temperature.

The configuration of the bell jar and the layout of the vacuum system is illustrated in Fig. 7. The bell jar was equipped with a sight port for visual inspection of the interior while in operation, a 6-inch dial vacuum gauge for indicating quickly any significant vacuum pressure change, and a small 1/4-inch, bellows sealed, vacuum valve for breaking the vacuum with argon when necessary. A quick opening and closing, straight-through vacuum valve operated by a solenoid connected to a thermocouple gauge control provided for automatic isolation of the vacuum system in the event of a vacuum failure in the bell jar. The large chamber connected to the 6-inch-diameter vacuum line was a combination liquid nitrogen and dry ice-organic liquid cold trap which was used not as a cold trap but to make use of an existing component for making necessary vacuum connections in the system. Below this cold trap, there was another 6-inch-diameter straight-through vacuum throttle valve manually operated. Below this valve a 6-inch-diameter refrigerated optical baffle



Fig. 6 - View of the top of the furnace showing the arrangement of the crucible, thermal detectors on planar cross section, BeO sample tube in the center, BeO sleeve, side shields, and water-cooled furnace jacket

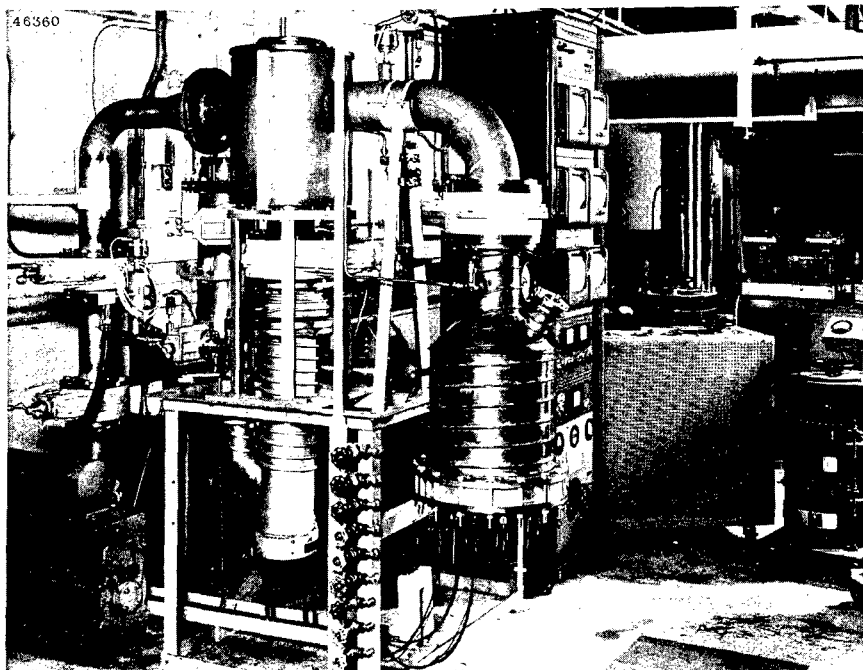


Fig. 7 - Arrangement of the vacuum bell jar containing the cold-wall furnace assembly and of the vacuum pumping system and instrumentation

was located directly over the opening to the 6-inch-diameter three-stage fractionating oil diffusion pump. To the left of the large cold trap a 4-inch-diameter line passed through two manually operated vacuum valves into a two-stage oil-sealed rotary mechanical pump with a pumping speed of 25 liters per second. A 2-inch-diameter holding pump line was also installed in the vacuum system to permit maintaining the diffusion pump in operation when the vacuum in the bell jar had to be broken for minor repairs to the furnace assembly. The 2-inch-diameter roughing line with its vacuum valve is visible in Fig. 7 leading from the exhaust port of the diffusion pump to the 4-inch-diameter line. The holding pump and the line leading to it are not visible, although the vacuum valve isolating the holding pump from the system is visible on the left bottom side of the large cold trap.

Vacuum pressures were measured with three different gauge systems: a thermocouple system interlocked with the vacuum valve above the bell jar, a cold cathode discharge gauge for following reduction of pressure below the limit of the thermocouple gauge during outgassing or roughing down operations, and a hot-wire ionization gauge for measuring stable pressure conditions during the experimental work with radiant energy.

Water temperature was monitored in all discharge lines leading from the furnace during its operation.

Separate power supplies together with controls were provided for each heater. The power applied to the central heater was measured with an accurate ammeter connected to an accurate current transformer. The voltage drop across the gauge length was measured by a vacuum tube voltmeter, accurate to the second decimal place. Temperatures and temperature responses to radiant energy were measured with precision potentiometers and an oscilloscope.

The granular fused BeO sample material was 8 to 10 mesh with a bulk density of 2.88 g/cm³ or about 96% of theoretical. The purity was about 99.5%, spectrographic analysis of which was as follows: aluminum, 0.15-0.25%; boron, 0.00007%; calcium, 0.15-0.25%; chromium, 0.001-0.002%; copper, 0.001-0.002%; iron, 0.10-0.20%; lead, 0.0003%; magnesium, 0.01-0.03%; manganese, 0.006-0.008%; nickel, 0.0005%; silicon, 0.10-0.20%; tin, 0.0002%; sodium, 0.003%; lithium, 0.0003%; silver, 0.00003%; carbon, trace; cadmium and zinc, not detected.

Petrographic examination of massive fused BeO, similar to the granular fused material, showed the presence of a high content of what appeared to be dark crystalline clear grains characteristic of transparent material in which incident visible light is internally scattered and absorbed within it. The lack of reflected light caused the grains to appear dark and indicated transparency. The massive fused material was observed to also contain gross gas porosity, which may have accounted for the somewhat low density. Individual grains, however, appeared to be quite dense and free from porosity. The characteristics of the porosity appeared to suggest that this was caused by the rejection of dissolved gases during solidification of the BeO from the molten state.

The tubular sample BeO material used as a protection tube for the central heater was white in color and its density was 2.8 g/cm³. Purity was 99.9% BeO with other elements in trace quantities only. The relatively low density, 93% of theoretical, is probably due to porosity. The tubing was formed by extrusion followed by sintering and high firing to 1900°C. Illumination of the tubing with a strong light beam showed it to be translucent, as illustrated in Fig. 8.

Experimental Procedure

The first step in the experimental work was to condition the components in the hot zone by outgassing all of the ceramic and metallic materials under vacuum. After ascertaining that the system was leaktight, it was roughed down to approximately 0.1 micron

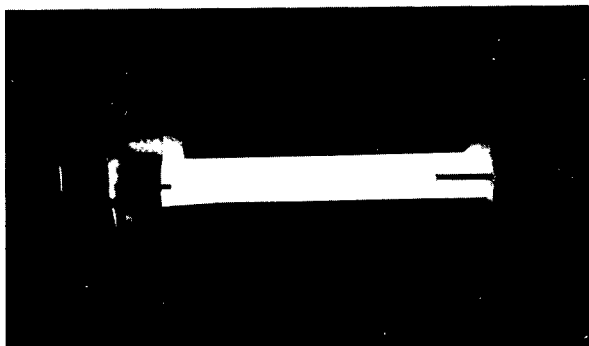


Fig. 8 - Translucency of the protection tube

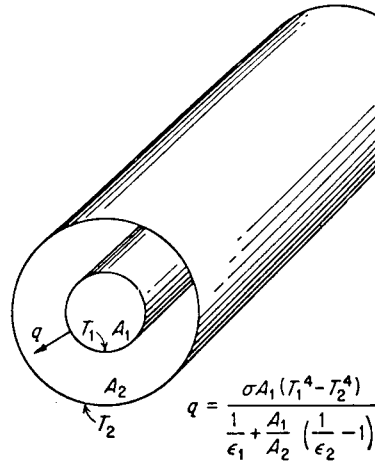
with the two-stage mechanical vacuum pump. At this point the diffusion pump was opened to the system and pumping continued until a stable pressure of 5×10^{-6} torr was obtained. The crucible heater was then activated to about 110°C to expel any moisture contained as absorbed water vapor in any of the materials. During this cycle no cooling water was circulated in the internal parts of the system. The pressure rise was kept below 0.01 micron during the initial outgassing. When the vacuum pressure reached a stable 5×10^{-6} torr, the temperature of the heater was increased in stages as fast as the pressure conditions due to outgassing would permit. Cooling water was applied to copper electrodes and the water-cooled furnace jacket. As temperature increased in the furnace system, the vacuum pressure was not permitted to exceed 5×10^{-5} torr. As outgassing diminished and the vacuum pressure entered the 10^{-6} -torr range, the heaters at the top and bottom were activated to assist in the final outgassing operation. Generally, the system was cleaned up of gas after the hot zone reached 1000°C and the vacuum pressure went into the 10^{-7} -torr range. This process generally took about two weeks of continuous pumping and heating to satisfactorily condition the system.

The procedure for studying the radiant energy transmission through BeO consisted of heating the entire crucible assembly to a given uniform temperature and then applying a pulse of a known amount of radiant energy from the central heater to the sample material for a given length of time.

The amount of radiant energy supplied by the central heater source was based on the temperature gradient between the maximum temperature attained by the heater and the ambient furnace temperature. The rate of total thermal radiation output was taken as the wattage input to the gauge section assuming that the gauge section was uniform in temperature.

Under the experimental conditions prevailing the radiant energy emitted from the central heater was first intercepted by the protection tube, which in turn became a radiant energy source when its temperature increased. With the central heater completely surrounded by a BeO protection tube it was necessary to determine the energy exchange between the heater and the tube when these were at different temperatures. Since the central heater wire and the BeO tube were not blackbodies, their surfaces would reflect thermal radiation to some extent and the amount of thermal radiant energy exchanged would be affected by the shape conditions existing between the two. Inasmuch as the experimental condition involved two concentric cylinders as illustrated in Fig. 9, the radiation angle factor (the fraction of the central heater's radiant energy intercepted by the protection tube) was equal to unity, since the inner body saw only the outer and nothing else and was therefore, exposed to all of the thermal radiation emitted by the central heater. Thus, the net radiant energy interchange between the two bodies, one of which was hotter than

Fig. 9 - Radiation exchange between two cylindrical surfaces



the other, was deduced from an energy balance where $q_{net} = q_{hotter} - q_{colder}$ and

$$q_{total} = \frac{A_1 \sigma (T_1^4 - T_2^4)}{\frac{1}{\epsilon_1} + \frac{A_1}{A_2} \left(\frac{1}{\epsilon_2} - 1 \right)} \tag{7}$$

where

- q = net radiant energy interchange (watts)
- A_1 = area of the hotter body (cm^2)
- A_2 = area of the colder body (cm^2)
- σ = Stefan-Boltzmann constant (5.6697×10^{-12} watt/sec- $^\circ K^4$)
- T_1 = absolute temperature of the hotter body ($^\circ K$)
- T_2 = absolute temperature of the colder body ($^\circ K$)
- ϵ_1 = emissivity of the hotter body
- ϵ_2 = emissivity of the colder body.

The above expression takes into consideration the radiation shape factor and the reflection factor. Hence, the net interchange between the central heater and the protection tube was not equivalent to the wattage input to the heater but smaller, and this fact had to be taken into consideration in the experimental work. The effect of the applied radiant energy flux upon the sample materials was monitored by thermocouple detectors at three points, 120° apart, across a planar cross section inside the crucible. The center-detector thermocouple located adjacent to the protection tube registered the temperature effect that the radiant energy pulse made on the BeO protection tube while the thermocouples embedded in the granular BeO mass, one halfway between tube and crucible wall (middle detector) and the other at the inside edge of the crucible wall (outer detector), registered the effect of the radiant energy emitted from the tube on the granular sample mass. The output of these thermocouples was followed with precision potentiometers, and photographs

were taken of the traces formed on the cathode-ray tube of the oscilloscope. No attempt was made to determine the amount of thermal radiation emitted from the protection tube to the granular BeO mass during a specific heat pulse, since one of the major unknown factors was the radiation transmissivity of the tube. When radiant energy impinges on a gray body, it may follow three alternate paths. Some of the energy may be absorbed, some may be reflected back from it, and some may be transmitted through the body as illustrated in Fig. 10. Thus, the absorptivity α , reflectivity ρ , and transmissivity τ com-

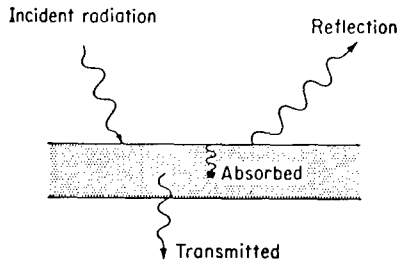


Fig. 10 - Alternatives for radiation impinging on a body

pletely specify the alternatives for the impinging energy and the sum of these factors $\alpha + \rho + \tau$ must equal unity. In the case of a transparent body considerable radiant energy may be transmitted through it without any appreciable increase in its ambient temperature. A translucent material may increase in temperature as radiant energy impinges upon it but it may also transmit some of this energy. With an opaque body transmissivity falls to zero and the impinging radiant energy will be subject to absorption and reflection only.

The rate of temperature rise of the central heater from ambient to maximum temperature as governed by power conditions of each heat pulse was obtained by dividing the I^2R loss by the specific heat of tungsten at maximum temperature. By comparing the rate of temperature rise in the central heater with the tem-

perature rise in the monitoring thermocouples outside of the protection tube the radiant energy exchange process was studied.

RESULTS AND DISCUSSION

A summary of experimental data is given in Table 6. Five series of experiments were conducted under various conditions of furnace temperature, central heater temperature and duration of individual heat pulses. The experimental data is arranged according to each series of experiments as indicated by column 1. Column 2 indicates the number of trials under a given set of trial conditions, while column 3 indicates the duration of each heat pulse applied to each trial. Columns 4, 5, and 6 indicate the amount of power applied across the gauge section of the central heater per heat pulse. Column 7 indicates the amount of power that would be required to heat the central heater to ambient temperature, while column 8 represents the net power radiated by the tungsten heater gauge length in excess of that required at the ambient temperature of the furnace. Column 9 indicates the net radiant energy intensity of tungsten, while column 10 indicates the maximum temperature reached by the gauge section of the central heater during each heat pulse and column 11 indicates the calculated time in seconds that it took the tungsten heater temperature to rise from the baseline ambient temperature prevailing in the furnace system at the beginning of each trial; the temperature variation between successive trials is noted by a plus and minus amount. Column 13 indicates the temperature differential between the maximum temperature reached by the central heater and the starting ambient temperature. Columns 14 through 22 indicate the data taken with three potentiometers (center, middle, and outer detectors) in monitoring the temperature effects across the furnace planar cross section as a result of the application of individual heat pulses. These data include the observed temperature rise, the response time representing the first indication of a change in emf, and the time to reach a peak in the temperature rise observed. Columns 23 through 30 indicate the data taken with an oscilloscope for thermocouples located at only the center and middle points of the planar cross section of the furnace system. These data are discussed in more detail in the text that follows.

The monitoring of the emf output of the thermocouple detectors with potentiometers in the series 1 trials was found to be somewhat inadequate because of sluggish response of the instruments to the emf developed by the thermocouples and the timing technique employed. The timing technique was to start a stop watch at the beginning of a heat pulse and stop it when the first indication of emf change was noted on the potentiometer. The first 27 trials were conducted at time intervals of 15 seconds per pulse, but this time interval tended to unbalance the ambient temperature level of the furnace system to an extent that it was considered desirable to reduce the duration of the heat pulse to 10 seconds. This interval was used in succeeding series, except for several pulses at 300 seconds duration to study the longer duration effect on the temperature rise characteristics of a heat pulse. The 10-second heat pulse was considered to be adequate, considering that thermal radiation as a type of electromagnetic radiation is propagated at the speed of light, 3×10^{10} cm/sec. Thus, it was assumed that if BeO developed transparency to thermal radiation at some elevated temperature, the temperature effects could probably be detected at the monitors within the 10-second duration without significantly disturbing the ambient temperature equilibrium.

In series 1 trials, a small temperature rise from 2° to 4°C was observed at the center detector in the ambient temperature range 1042° to 1240°C and a central heater temperature range 1227° to 1523°C . When the ambient temperature was increased to 1434°C and the central heater to 1803°C , the temperature rise observed was 11°C . With only a small additional increase in ambient temperature to 1446°C and a central heater temperature of 1999°C , a temperature rise of 22°C was noted. In this series of trials the time required for the central heater to reach maximum temperature above ambient was less than 1 second for temperature differences of from 78° to 369°C , while for a temperature difference of 553°C , listed in item 7 of Table 6, slightly more than 1 second was required to reach maximum temperature. The response time to first indication of an emf change due to the heat pulse varied from 2 to about 2.6 seconds in the ambient temperature range 1042° to 1240°C , while the time required to reach peak temperature rise exceeded both the 15-second and 10-second heat pulse lengths.

If the radiation intensity of BeO at ambient temperature is compared with that of tungsten at its maximum pulse temperature, it will be noted from Fig. 11 (the values of which are listed in Table C1 of Appendix C) and Table 7 (series 1), that for items 1, 2, and 3, BeO was radiating more energy than the tungsten even though the BeO was at a lower temperature. In the case of items 4 and 5 the radiation intensity of tungsten was slightly greater than that of BeO. The temperature effect of these trials upon the center detector was so slight that it was considered to be negligible. Items 6 and 7 (series 1), showed a temperature rise of 11° and 22.0°C respectively, with the tungsten having radiation intensities of 6.5 and 21 watts/cm² greater than those of the BeO. The temperature effect noted in these trials was considered to be due to the BeO tube absorbing the radiant energy incident upon it, converting this energy to heat, and reradiating it from its outer surface to the center detector. The heating process involved a time lag in response to the incident radiant energy and a heating time to peak temperature beyond the duration of the heat pulse. If the temperature effect at the center detector had been significantly influenced by radiant energy transmission through the BeO tube surrounding the center heater, a more prompt temperature response would have occurred, and the temperature would not have continued to rise beyond the end of the heat pulse. The BeO tube material, therefore, appeared to be opaque at temperatures up to about 1450°C .

In an attempt to obtain an improved rate of response to changes in the emf output of the detectors an oscilloscope was used to monitor the temperature changes in the series 2, 3, and 4 trials. Although the sensitivity of this instrument provided a fast response to changes in emf, considerable difficulty was experienced with it due to spurious interference believed to be of electromagnetic character and coming from radiation experiments being conducted within this laboratory at the same time. Attempts to shield or filter out this interference were not entirely satisfactory. This situation limited the amount of usable data and necessitated continued reliance upon the less sensitive potentiometric instruments.

Table 6
Summary of Experimental Data

| Item No. | 1 | 2 | 3 | 4 | 5 | 6 | 7 | 8 | 9 | 10 | 11 | 12 | 13 |
|----------|------------|---------------|------------------|------------------------|---------------------------------------|---------------------|---------------------------------|--|---|-----------------------|--------------------------|---------------------|--------------------------------------|
| | Series No. | No. of Trials | Pulse Time (sec) | Input to Source (amps) | Potential Drop, Gauge Section (volts) | Total Input (watts) | Power at Baseline Temp. (watts) | Energy Radiated, Gauge Section (net watts) | Radiant Energy Intensity (watts/cm ²) | Peak Pulse Temp. (°C) | Time to Peak Temp. (sec) | Baseline Temp. (°C) | Peak Temp. Minus Baseline Temp. (°C) |
| 1 | 1 | 13 | 15 | 57.97 | 0.371 | 21.51 | 8.96 | 12.55 | 3.87 | 1227 | 0.029 | 1042±1 | 185 |
| 2 | | 14 | 15 | 58.10 | 0.405 | 23.53 | 16.32 | 7.21 | 2.22 | 1285 | 0.005 | 1197±10 | 88 |
| 3 | | 1 | 10 | 70.8 | 0.530 | 37.52 | 16.76 | 20.76 | 6.40 | 1403 | 0.043 | 1205 | 198 |
| 4 | | 4 | 10 | 77.1 | 0.605 | 46.65 | 16.99 | 29.66 | 9.15 | 1487 | 0.121 | 1209±3 | 278 |
| 5 | | 11 | 10 | 76.8 | 0.636 | 48.84 | 18.94 | 29.90 | 9.22 | 1523 | 0.131 | 1240±3 | 283 |
| 6 | | 5 | 10 | 94.2 | 0.968 | 91.19 | 35.17 | 56.02 | 17.27 | 1803 | 0.333 | 1434±6 | 369 |
| 7 | | 5 | 10 | 120.5 | 1.210 | 145.81 | 36.58 | 109.23 | 33.68 | 1999 | 1.15 | 1446±5 | 553 |
| 8 | 2 | 4 | 10 | 142.5 | 1.66 | 236.55 | 11.38 | 225.17 | 69.43 | 2271 | 9.70 | 1102±10 | 1169 |
| 9 | | 2 | 10 | 140.0 | 1.736 | 243.04 | 39.52 | 203.52 | 62.76 | 2313 | 4.20 | 1471±2 | 842 |
| 10 | | 7 | 10 | 140.8 | 1.758 | 247.53 | 40.82 | 206.71 | 63.74 | 2327 | 4.26 | 1482±15 | 845 |
| 11 | | 4 | 10 | 142.0 | 1.79 | 254.18 | 42.70 | 211.48 | 65.21 | 2343 | 4.29 | 1498±4 | 845 |
| 12 | | 2 | 10 | 142.0 | 1.845 | 261.20 | 82.86 | 218.34 | 67.33 | 2361 | 1.67 | 1757±4 | 604 |
| 13 | 3 | 1 | 10 | 142.0 | 1.69 | 239.98 | 43.41 | 196.57 | 60.61 | 2289 | 3.43 | 1504 | 785 |
| 14 | | 2 | 10 | 140.0 | 1.705 | 238.70 | 43.52 | 195.18 | 60.19 | 2295 | 3.50 | 1505±1 | 790 |
| 15 | | 6 | 10 | 140.0 | 1.775 | 248.50 | 77.52 | 170.98 | 52.72 | 2335 | 1.68 | 1730±12 | 605 |
| 16 | | 1 | 10 | 140.0 | 1.85 | 259.00 | 115.80 | 143.20 | 44.16 | 2363 | 0.75 | 1907 | 456 |
| 17 | | 5 | 10 | 162.0 | 2.11 | 341.82 | 119.62 | 222.20 | 68.52 | 2471 | 1.32 | 1923 | 548 |
| 18 | | 2 | 10 | 188.0 | 2.64 | 496.32 | 150.78 | 345.54 | 106.55 | 2711 | 2.56 | 2033±5 | 678 |
| 19 | 4 | 1 | 10 | 120.0 | 1.31 | 157.20 | 42.23 | 114.97 | 35.45 | 2067 | 1.32 | 1494 | 573 |
| 20 | | 3 | 10 | 116.0 | 1.19 | 138.04 | 40.82 | 97.22 | 29.98 | 1979 | 0.84 | 1482±3 | 497 |
| 21 | | 1 | 300 | 114.6 | 1.17 | 134.08 | 40.23 | 93.85 | 28.94 | 1967 | 0.80 | 1482 | 485 |
| 22 | | 1 | 300 | 114.0 | 1.15 | 134.21 | 40.82 | 93.39 | 28.80 | 1959 | 0.74 | 1482 | 477 |
| 23 | | 1 | 300 | 113.4 | 1.15 | 130.41 | 40.82 | 89.59 | 27.63 | 1951 | 0.70 | 1477 | 474 |
| 24 | | 2 | 10 | 135.0 | 1.63 | 220.05 | 43.05 | 177.00 | 54.58 | 2231 | 2.74 | 1501±5 | 730 |
| 25 | | 2 | 10 | 132.0 | 1.57 | 207.24 | 62.86 | 144.38 | 44.52 | 2201 | 1.16 | 1661±4 | 540 |
| 26 | | 3 | 10 | 129.0 | 1.52 | 196.08 | 84.24 | 111.84 | 34.49 | 2171 | 0.51 | 1764±7 | 407 |
| 27 | | 1 | 10 | 132.0 | 1.57 | 207.24 | 84.64 | 144.38 | 44.52 | 2201 | 0.62 | 1766 | 435 |
| 28 | | 1 | 300 | 123.0 | 1.38 | 169.74 | 82.66 | 87.08 | 26.85 | 2101 | 0.31 | 1756 | 345 |
| 29 | | 5 | 4 | 10 | 132.0 | 1.57 | 207.24 | 98.85 | 108.39 | 33.42 | 2201 | 0.32 | 1836 |
| 30 | 2 | | 10 | 131.0 | 1.55 | 203.05 | 134.84 | 68.21 | 21.03 | 2191 | 0.19 | 1984±1 | 207 |
| 31 | 2 | | 10 | 139.5 | 1.72 | 239.94 | 134.84 | 105.10 | 32.41 | 2279 | 0.21 | 1984±1 | 295 |
| 32 | 2 | | 10 | 141.0 | 1.75 | 246.75 | 134.34 | 112.41 | 34.66 | 2295 | 0.25 | 1982±1 | 313 |

(Table continues)

Table 6 (cont'd)
Summary of Experimental Data

| Item No. | Potentiometric Data | | | | | | | | | Oscilloscope Data | | | | | | | |
|----------|---------------------|---------------------|-----------------|-----------------|---------------------|-----------------|-----------------|---------------------|-----------------|--|-----------------|---------------------|-----------------|---------------------|-----------------|---------------------|-----------------|
| | 14 | 15 | 16 | 17 | 18 | 19 | 20 | 21 | 22 | 23 | 24 | 25 | 26 | 27 | 28 | 29 | 30 |
| | Center Detector | | | Middle Detector | | | Outer Detector | | | Center Detector | | | | Middle Detector | | | |
| | Temp. Rise (°C) | Response Time (sec) | Peak Time (sec) | Temp. Rise (°C) | Response Time (sec) | Peak Time (sec) | Temp. Rise (°C) | Response Time (sec) | Peak Time (sec) | Trace No. | Temp. Rise (°C) | Response Time (sec) | Peak Time (sec) | Trace No. | Temp. Rise (°C) | Response Time (sec) | Peak Time (sec) |
| 1 | 2 | 2.57 | 16.23 | - | - | - | No Change | - | - | This series monitored with potentiometers only | | | | | | | |
| 2 | 3 | 2.00 | 17.59 | 1 | - | 17 | - | - | | | | | | | | | |
| 3 | 4 | 2.26 | 13.25 | - | - | - | - | - | | | | | | | | | |
| 4 | 4 | 2.20 | 10.46 | 1 | - | 21 | - | - | | | | | | | | | |
| 5 | 4 | 2.11 | 12.96 | 1 | - | - | - | - | | | | | | | | | |
| 6 | 11 | 1.69 | 12.00 | 1 | - | - | - | - | | | | | | | | | |
| 7 | 22 | 1.40 | - | 1 | 2.8 | - | - | - | | | | | | | | | |
| 8 | 40 | - | - | 5 | - | - | No Change | - | - | 2-CP1B-2 | 40 | - | - | - | - | - | |
| 9 | 23 | - | - | 4 | - | - | - | - | - | 2-CP2B-6 | 23 | - | - | 2MP2A-5 | 8 | - | - |
| 10 | 27 | - | - | 5 | - | - | - | - | - | 2-CP2C-7,2-CP21-13 | 31 | - | - | 2MP2,D,E,F,G,H-8-12 | 8 | - | - |
| 11 | 33 | - | - | 7 | - | - | - | - | - | 2-CP2J-14,2-CP2K-15 | 33 | - | - | 2MP2H-10 | 4 | 1 | 6 |
| 12 | - | - | - | 7 | - | - | - | - | - | 2-CP3B-19 | - | - | - | 2MP3A-18 | - | - | - |
| 13 | 19 | - | 11.5 | 3 | - | 13 | - | - | - | - | - | - | - | 3-MP1A-1 | - | - | - |
| 14 | 18 | - | 12.0 | 3 | - | 13 | - | - | - | - | - | - | - | 3-MP1B-2,3-MP1C-3 | - | - | - |
| 15 | 29 | ≈ 2 | 12.0 | 3 | - | 8 | - | - | - | - | - | - | - | 3-MP1C-9 | 4 | 0.5 | 8.5 |
| 16 | 18 | - | 13.2 | 1 | - | - | - | - | - | - | - | - | - | 3-MP2A-11 | 8 | 1 | 9 |
| 17 | 22 | ≈ 1 | 14.7 | 8 | 2 | 7 | 5 | ≈ 1.8 | 5 | - | - | - | - | 3-MP2D-14 | 8 | 1 | 8 |
| 18 | 43 | ≈ 1 | - | - | - | - | 15 | - | - | - | - | - | - | - | - | - | - |
| 19 | 33 | - | 10.2 | - | - | - | - | - | - | - | - | - | - | - | - | - | - |
| 20 | 43 | 0.6 | 11.0 | 3 | - | >10 | - | - | - | 4-CP1B-2,4-CP1D-12 | 42 | 1.5 | 8.5 | 4-MP1B-2,4-MP1B-3 | 4,4 | 5,3 | 18,7 |
| 21 | 285 | - | 300.0 | 43 | 92.8 | - | - | - | - | 4-CP1EL-15 | 83,108 | 6 | 36,90 | 4-MP1EL-15 | 8,5,16 | 66 | 51,150,75 |
| 22 | 286 | - | 300.0 | 36 | 76.4 | 339 | - | - | - | - | - | - | - | - | - | - | - |
| 23 | 286 | - | 300.0 | 38 | 79.2 | 474 | - | - | - | 4-CP1ELRR-27 | 42,84 | 3 | 6,51,75 | 4-MP1ELRR-27 | 4,17,8 | 66 | 69,150,150 |
| 24 | 21 | - | 9.75 | 3 | 11.0 | - | - | - | - | - | - | - | - | - | - | - | - |
| 25 | 19 | - | 11.8 | 2 | 10.0 | - | - | - | - | - | - | - | - | MP1A,MP1B,MP1C | 2,4,3 | 5,5,3 | 10,15,13 |
| 26 | 21 | 3.65 | 22.4 | - | - | - | - | - | - | - | - | - | - | - | - | - | - |
| 27 | 23 | 3.77 | 24.65 | - | - | - | - | - | - | - | - | - | - | - | - | - | - |
| 28 | 341 | <1 | 314.0 | 77 | 46.2 | 431 | 47 | 71 | 508 | - | - | - | - | - | - | - | - |
| 29 | 29 | <1 | 20.3 | 3 | 45.0 | 121 | - | - | - | This series monitored with potentiometers only | | | | | | | |
| 30 | 23 | ≈ 1 | - | 3 | 11.2 | - | - | - | - | | | | | | | | |
| 31 | 27 | 1 | 21.0 | 3 | 12.2 | 108 | - | - | - | | | | | | | | |
| 32 | 26 | 1.2 | 21.0 | 5 | 13.0 | 107 | - | - | - | | | | | | | | |

NAVAL RESEARCH LABORATORY

UNCLASSIFIED

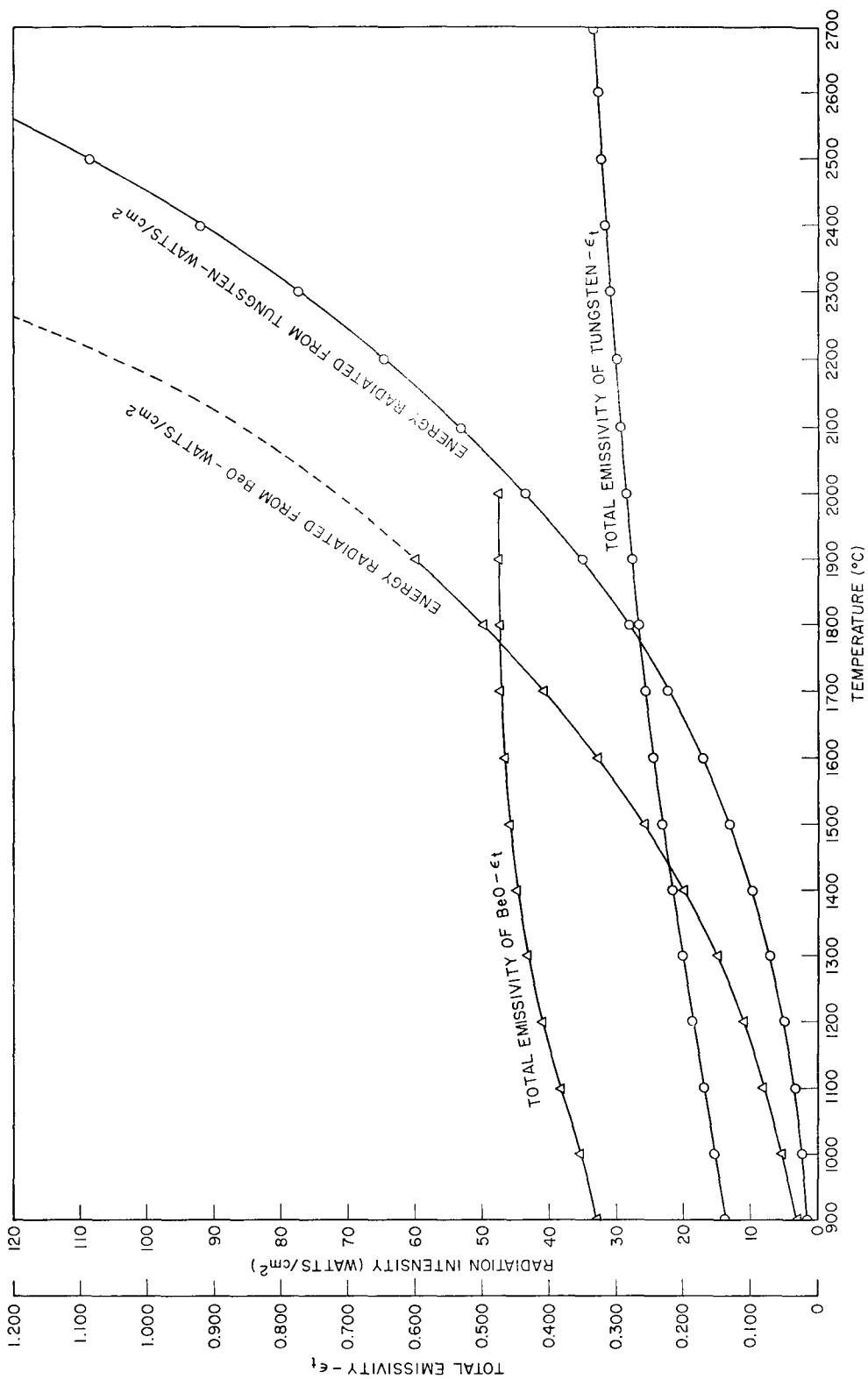


Fig. 11 - Total emissivity and radiation intensity of tungsten and BeO as a function of temperature

Table 7
Radiation Intensity of Tungsten and BeO

| Item No. | Series No. | Baseline Temp. (°C) | Max. Heater Temp. (°C) | Radiation Intensity (RI) (watts/cm ²) | | |
|----------|------------|---------------------|------------------------|---|-------|-------|
| | | | | W | BeO | ΔRI |
| 1 | 1 | 1042 | - | 2.7 | 6.5 | - |
| | | - | 1227 | 5.7 | - | -0.8 |
| | | 1197 | - | 5.0 | 11.0 | - |
| | | - | 1285 | 6.75 | - | -3.25 |
| | | 1205 | - | 5.2 | 11.3 | - |
| | | - | 1403 | 10.1 | - | -1.2 |
| | | 1209 | - | 5.3 | 11.5 | - |
| 2 | 2 | - | 1487 | 12.7 | - | +1.2 |
| | | 1240 | - | 5.8 | 12.5 | - |
| | | - | 1523 | 14.0 | - | +1.5 |
| | | 1434 | - | 11.0 | 22.0 | - |
| | | - | 1803 | 28.5 | - | +6.5 |
| | | 1446 | - | 11.2 | 22.5 | - |
| | | - | 1999 | 43.5 | - | +21.0 |
| 3 | 3 | 1102 | - | 3.5 | 8.2 | - |
| | | - | 2271 | 73.7 | - | +65.5 |
| | | 1471 | - | 12.0 | 24.0 | - |
| | | - | 2313 | 79.0 | - | +55.0 |
| | | 1482 | - | 12.5 | 24.7 | - |
| | | - | 2327 | 81.0 | - | +56.3 |
| | | 1498 | - | 13.1 | 25.9 | - |
| 4 | 4 | - | 2343 | 83.0 | - | +57.1 |
| | | 1757 | - | 25.5 | 45.7 | - |
| | | - | 2361 | 86.1 | - | +40.4 |
| | | 1504 | - | 13.5 | 26.2 | - |
| | | - | 2289 | 75.8 | - | +49.6 |
| | | 1505 | - | 13.5 | 26.2 | - |
| | | - | 2295 | 76.5 | - | +50.3 |
| 5 | 5 | 1730 | - | 26.5 | 43.2 | - |
| | | - | 2335 | 82.0 | - | +36.8 |
| | | 1907 | - | 35.7 | 60.5* | - |
| | | - | 2363 | 86.2 | - | +15.7 |
| | | 1923 | - | 37.1 | 62.2* | - |
| | | - | 2471 | 103.0 | - | +40.8 |
| | | 2033 | - | 46.5 | 75.6 | - |
| 6 | 6 | - | 2711 | 150.0 | - | +74.4 |
| | | - | - | - | - | - |

* Estimated

Table continues

Table 7 (cont'd)
Radiation Intensity of Tungsten and BeO

| Item No. | Series No. | Baseline Temp. (°C) | Max. Heater Temp. (°C) | Radiation Intensity (RI) (watts/cm ²) | | |
|----------|------------|---------------------|------------------------|---|-------|-------|
| | | | | W | BeO | ΔRI |
| 19 | 4 | 1494 | - | 13.0 | 25.5 | - |
| | | - | 2067 | 49.7 | - | +24.2 |
| 20 | | 1482 | - | 12.5 | 24.7 | - |
| | | - | 1979 | 42.0 | - | +17.3 |
| 21 | | 1477 | - | 12.3 | 24.5 | - |
| | | - | 1967 | 40.7 | - | +16.2 |
| 22 | | 1482 | - | 12.5 | 24.7 | - |
| | | - | 1959 | 40.1 | - | +15.4 |
| 23 | | 1482 | - | 12.5 | 24.7 | - |
| | | - | 1951 | 39.3 | - | +14.6 |
| 24 | | 1501 | - | 13.2 | 26.0 | - |
| | | - | 2231 | 68.0 | - | +42.0 |
| 25 | | 1661 | - | 20.2 | 37.5 | - |
| | | - | 2201 | 64.5 | - | +27.0 |
| 26 | | 1764 | - | 26.0 | 46.5 | - |
| | | - | 2171 | 61.0 | - | +15.5 |
| 27 | | 1766 | - | 26.0 | 46.5 | - |
| | | - | 2201 | 64.5 | - | +18.0 |
| 28 | 1756 | - | 25.5 | 45.5 | - | |
| | - | 2101 | 53.1 | - | +7.6 | |
| 29 | 5 | 1836 | - | 30.5 | 53.2 | - |
| | | - | 2201 | 64.5 | - | +11.3 |
| 30 | | 1984 | - | 42.2 | 69.5 | - |
| | | - | 2191 | 63.2 | - | -6.3 |
| 31 | | 1984 | - | 42.2 | 69.5 | - |
| | | - | 2279 | 74.5 | - | +5.0 |
| 32 | | 1982 | - | 42.0 | 69.0 | - |
| | | - | 2295 | 76.5 | - | +7.5 |
| 33 | | 1913 | - | 36.5 | 61.3 | - |
| | - | 2327 | 81.0 | - | +19.7 | |

The series 2 trials were conducted with tungsten central heater radiation intensities well above those of BeO at ambient temperature. The radiation intensity differences between the tungsten at maximum temperature and the BeO ambient temperature ranged from about 40 to 65.5 watts/cm² as shown in the tabulation for series 2 trials in Table 7.

The temperature effects noted at the center detector for trials listed under item 8, series 2 trials, Tables 6 and 7, are shown in Fig. 12. The grid pattern of this figure and

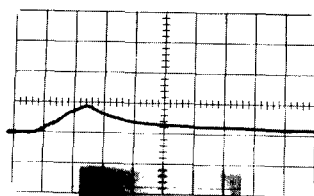


Fig. 12 - Temperature rise of 40°C at the center detector for item 8, series 2 trials (baseline temperature, 1102°C; heater maximum temperature, 2271°C; 10-second pulse)

similar figures to follow represented time on the horizontal axis and the emf output of the detector on the vertical axis. Each major division on the horizontal axis represented 5 seconds of elapsed time (unless otherwise stated) and each major division on the vertical axis represented 1 millivolt or 41.66°C .

As shown in Fig. 12, the temperature effect at the center detector was a 40°C rise within the 10-second heat pulse from an ambient temperature of 1102°C . The center heater reached a maximum temperature of 2271°C in 9.7 seconds, having a radiation intensity at peak temperature of 65.5 watts/cm^2 above that of BeO at ambient temperature. There appeared to be a delay of about 2 seconds before any change occurred in the emf baseline value. Once the temperature started to rise, the rate of rise appeared to be steady at about 4.5°C per second to peak with an abrupt change in emf at the end of the heating pulse. The temperature dropped from the peak of 40°C to about 8°C in about 18 seconds, after which the temperature tapered off very gradually indicating a slight rise in the ambient furnace temperature.

The response of the center detector was rather slow considering the magnitude of the radiation intensity incident upon the BeO tube material. The tungsten center heater increased from an ambient temperature of 1102°C to a peak temperature of 2271°C , a differential of 1169°C , in 9.7 seconds for a rate of about 120°C per second. The nature of the heating curve of Fig. 12 and the abrupt discontinuity at the end of the heating cycle, however, indicated a possibility that BeO had transmitted certain wavelengths of thermal radiation at the low temperature of 1100°C .

Raising the ambient temperature to 1498°C and using a central heater temperature of 2343°C for a difference in temperature of 845°C produced the temperature effect at the center detector as shown in Figs. 13 and 14. The temperature rise obtained was 33°C with about a 1-second delay before any change occurred in the emf from the baseline. The rate of rise was linear at about 4.2°C per second. The same abrupt change in emf occurred at the end of the heating cycle in this set of trials as was observed in those represented by Fig. 12. Although ambient and center heater temperatures had been increased by about 400° and 72°C respectively, there was no comparable increase in temperature effect. In fact, the temperature rise obtained was smaller by about 7°C . Assuming that BeO possessed a capability of transmitting some radiant energy in the ambient temperature range of these trials, it did not exhibit any increase in tendency to transmit a greater amount of radiant energy at 1500°C than it did at 1100°C . Considering the amount of radiation intensity to produce a 40°C rise as 0.61 watt/cm^2 - $^{\circ}\text{C}$ compared to 0.58 watt/cm^2 - $^{\circ}\text{C}$ for a 33°C rise, it appeared as if the amount of radiation intensity was a greater factor in producing a temperature effect than the factor of ambient temperature.

Fig. 13 - Temperature rise of 33°C at the center detector for item 11 (baseline temperature, 1498°C ; heater maximum temperature, 2343°C ; 10-second pulse)

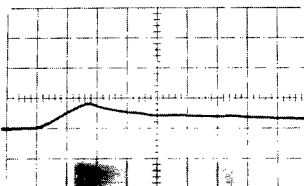
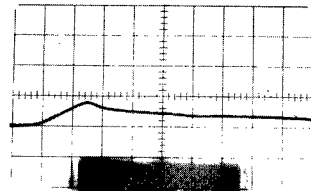


Fig. 14 - Another trace showing a temperature rise of 33°C for the conditions as given in Fig. 13

The temperature effect obtained at the middle detector in series 2 trials was from 4° to 7°C. The change in emf was so gradual and so slight that it was not possible to determine the response time nor the time to reach peak temperature from photographs of the oscilloscope traces. A typical trace is shown in Fig. 15 in which the change in emf from baseline appears to be about 4°C. The temperature effect at the middle detector was complicated by a tendency of the ambient temperature to rise slightly with the application of a heat pulse. The high radiation intensities developed by the central heater over the short intervals of time were sufficient to unbalance the ambient temperature equilibrium within the granular BeO mass, making it frequently necessary to allow the temperature of the furnace system to stabilize before proceeding with additional trials.

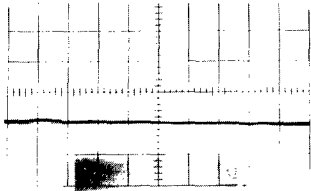


Fig. 15 - Temperature rise of 4°C at the middle detector for item 11 (baseline temperature, 1498°C; heater maximum temperature, 2343°C; 10-second pulse) .

There was no measurable temperature effect observed at the outer detector during series 2 trials.

The temperature effects represented by Figs. 12, 13, and 14 appear to be related in some degree to the radiant energy emitted from the primary source. Whether a portion of the total radiant energy incident upon the BeO passed through it without interacting with it or whether the temperature effect was caused by radiant energy being emitted only by the BeO as its temperature increased poses a question.

The character of the temperature effect was similar in all three figures, even though there were differences in the ambient and central heater temperature conditions. The rather prompt temperature response of the center detector and the abrupt change in emf at the end of a heating pulse indicated that a part of the temperature effect could have been caused by direct transmission of radiant energy through the BeO tube. It is necessary to take into account, however, that as the temperature of the BeO increased, the amount of radiant energy emitted by it also increased. Therefore, the temperature effect observed at the center detector could be considered as partly due to transmitted radiant energy through the BeO and partly due to radiant energy emitted by the BeO. The abrupt change in emf at the end of the heating pulse, however, could be interpreted as being caused solely by the abrupt cessation of radiant energy transmission from the central heater at power cutoff. Since the heat capacity of tungsten is considerably lower than that of BeO, the temperature of the tungsten would be expected to drop rapidly after power cutoff with a sharp reduction in radiant energy emission from it. The relatively high heat capacity of BeO (>0.5 cal/g) at high temperatures would tend to limit the rate of temperature rise from a high-intensity radiant energy pulse and also limit the rate of temperature drop during cooling. This would tend to indicate that the temperature effects observed at the center detector could not be attributed entirely to the absorption of the incident radiation by the tube and subsequent reradiation of the absorbed energy to the center detector.

In series 3 trials the ambient temperature ranged from about 1500° to 2033°C, while the central heater temperature ranged from about 2290° to 2711°C. At an ambient temperature of about 1505°C and a central heater maximum temperature of 2290°C there was a net radiation intensity of about 50 watts/cm². The temperature effect produced at the center detector was a rise of 19°C in 10 seconds. With an ambient temperature of 1730°C and a center heater maximum temperature of 2335°C there was a net radiation intensity of 36.8 watts/cm². The temperature effect in this case was a rise of 29°C in 10 seconds. When the ambient temperature was increased to 1907°C and the center heater maximum temperature to 2363°C, the net radiant energy intensity reduced to about 15.7 watts/cm². The temperature effect was a rise of only 18°C. With the ambient temperature at 1923°C and the center heater maximum temperature at 2471°C, the net radiation intensity was 40.8 watts/cm²,

which produced a temperature effect of 22°C . Finally with the ambient temperature at 2033°C and the center heater maximum temperature at 2711°C , the net radiation intensity was 74.4 watts/cm^2 , which produced a temperature rise of 43°C at the center detector.

The temperature effects, obtained at an ambient temperature of about 1500°C and at temperatures above this, were somewhat lower in series 3 trials than those obtained in series 2 trials for similar ambient temperature conditions. Even at the highest ambient temperature of 2033°C and the high net thermal radiant energy intensity of 74.4 watts/cm^2 delivered from the tungsten source at 2711°C , the temperature effect observed at both the center detector and the middle detector was lower than that expected from the trend exhibited in the series 2 trials. One contributing factor which probably caused the amounts of radiant energy transferred in the sample BeO materials to be lower was the coating of sample materials with metallic films. Some evaporation of tungsten occurred from the central heater with the tungsten vapor being deposited onto the inner surface of the sample BeO tube. This film altered somewhat the radiant energy receptive characteristics of the BeO. From the vapor pressure data shown in Fig. C1 of Appendix C, it is obvious that at the temperatures employed in the experimental work, some evaporation occurred from all of the elements contained in the hot zone of the apparatus. Since the tungsten of the central heater was heated to high temperatures and the BeO tube surrounding the heater and the granular BeO outside the tube were generally at somewhat lower temperatures the evaporated tungsten condensed upon the cooler inner surface of the sample BeO tube. This condensed tungsten, though relatively thin, was probably sufficiently thick to alter the radiant energy transfer properties of the BeO tube. In the case of the granular BeO material, the individual grains became coated with thin metallic films, particularly in the vicinity of the tantalum-sheathed thermal detectors. The presence of metallic coatings on the sample materials obviously interfered with the radiant energy transfer into the BeO, since metals are considered opaque to thermal radiation. The thickness of these coatings was apparently great enough to reduce the degree of the temperature effect.

The temperature effects at the middle detector are illustrated by Figs. 16 and 17, in which temperature peaks were reached in 8 and 7 seconds respectively. The rather prompt response of the middle detector indicated the possible transmission of a small amount of radiant energy. The emf reversal at power cutoff was somewhat obscured by the slight increase in ambient temperature conditions as indicated by the gradual temperature gradient from pulse peak to the initial ambient temperature.

Fig. 16 - Temperature rise of 3°C at the middle detector for item 15 (baseline temperature, 1730°C ; maximum heater temperature, 2335°C ; 10-second pulse)

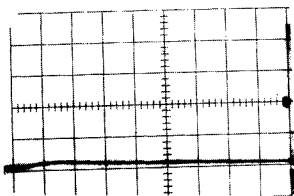
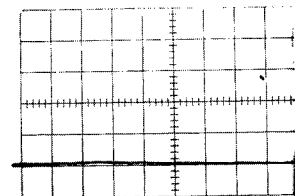


Fig. 17 - Temperature rise of 8°C at the middle detector for item 17 (baseline temperature, 1923°C ; maximum heater temperature, 2471°C ; 10-second pulse)

The operation of the apparatus for prolonged periods at high temperatures in vacuum resulted in deterioration of the metallic components in the hot zone of the furnace system.

In view of the test results of series 3 trials being lower than expected, it was necessary to completely overhaul the hot zone section of the apparatus and to replace all of the essential components.

Series 4 trials, therefore, were started with uncontaminated BeO sample materials and new metallic components. The first four trials were conducted at an ambient temperature of about 1490°C, and 10-second pulse maximum temperatures of about 2020°C, and a net radiant energy intensity of about 20.7 watts/cm². Under these conditions a temperature effect of a 40°C rise was observed at the center detector and a 3°C rise at the middle detector. Typical results obtained at the center detector are shown in Fig. 18 and a repeat in Fig. 19 made under the same conditions. A relatively prompt response occurred to the radiant energy from the central heater. There was a delay of about 1 second before any change occurred in the baseline emf, about another second to reach a relatively uniform rate of emf increase, and 8 seconds to reach peak emf. As was seen in Figs. 12, 13, and 14 of series 2 trials a sharp change in emf was again observed in these trials at power cutoff. The characteristics of the curves of Figs. 18 and 19 and those of Figs. 12, 13, and 14 suggest that a certain amount of the incident radiant energy was rapidly transferred from the BeO to the center detector either by direct transmission or by simultaneous emission and absorption as will be discussed. The circumstances, however, would appear to favor the latter mode of radiant energy transfer.

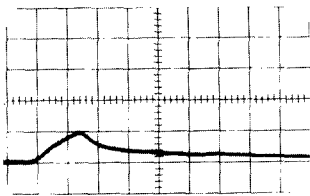
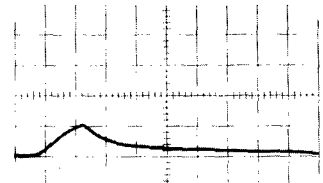


Fig. 18 - Temperature rise of 40°C at the center detector for item 20 (baseline temperature, 1482°C; maximum heater temperature, 1979°C; 10-second pulse)

Fig. 19 - Temperature rise of 42°C for the same conditions as in Fig. 18



The temperature effects at the middle detector for the same pulse conditions as prevailed for Figs. 18 and 19 were not as clearly discernible. The emf responses obtained are shown in Figs. 20, 21, and 22. In Fig. 20, an emf increase was obtained corresponding to a 3°C rise; however, neither the point of initial emf change nor the change at power cutoff was apparent. The emf values in Figs. 21 and 22 indicated virtually no change with respect to the baseline value; thus, there was no measurable temperature effect in the granular BeO from the tungsten source of radiant energy or from the radiant energy radiated by the BeO tube as a result of its 40°C rise.

In an attempt to clarify some of the questions concerning the radiant energy transfer process in BeO, three successive trials were made, each of 300 seconds duration. The purpose of extending the pulse time was to determine the effects of radiant energy intensity on BeO as it heated over a greater period of time. The temperature conditions for the first three trials were as follows: the ambient temperature range was 1477° to 1482°C; the center heater maximum temperature range was 1951° to 1967°C; the net amount of

Fig. 20 - Temperature rise of 3°C at the middle detector for item 20 (baseline temperature, 1482°C; maximum heater temperature, 1979°C; 10-second pulse)

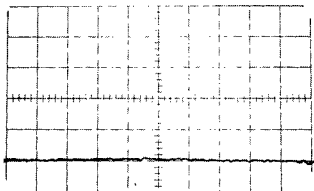
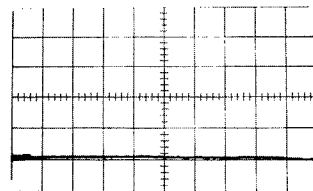


Fig. 21 - Temperature rise of 3°C at the middle detector for the same conditions as in Fig. 20

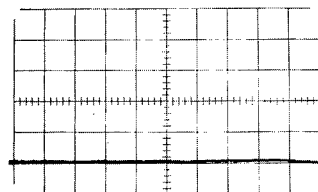
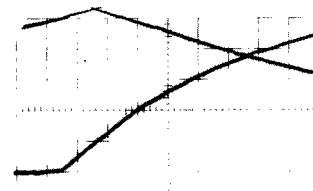


Fig. 22 - Temperature rise of 3°C at the middle detector for the same conditions as in Fig. 20

radiant energy intensity ranged from 14.6 to 16.2 watts/cm². The net result of these trials was an emf rise equivalent to 286°C in 300 seconds at the center detector and an average rise of 39°C at the middle detector in times exceeding the 300-second pulse duration.

The temperature effect obtained at the center detector for an ambient temperature of 1477°C and a center heater temperature of 1967°C for a net radiant energy intensity of 16.2 watts/cm² is shown in Fig. 23. In this figure and succeeding figures pertaining to the trials of 300 seconds duration each major division on the horizontal axis of the grid pattern represented 15 seconds of elapsed time. The value of each major division on the vertical axis remained the same as in previous figures at 41.66°C. The lower curve of Fig. 23 pertained to the first 135 seconds of the total pulse time of 300 seconds. The upper curve on the left was a continuation of the lower curve and the upper curve on the right was a cooling curve after peak. The upper curve was an attempt to obtain a complete record of the temperature effect on a single photographic record.

Fig. 23 - Temperature rise of 286°C at the center detector for item 21 (baseline temperature, 1477°C; maximum heater temperature, 1967°C; 300-second pulse)



Considering the lower curve only, a delay of about 9 seconds from zero time occurred before any significant change in emf was evident from the baseline value. The emf change was practically linear for the next 36 seconds, corresponding to a rise in temperature of about 83°C or about 2.3°C per second. The emf change over the next 90 seconds of the

figure corresponded to an additional rise in temperature of about 100°C or about 1.1°C per second. The rate of emf change for the remaining 165 seconds of temperature rise (not shown) of the trial diminished gradually corresponding to an additional rise of 103°C or about 0.63°C per second. The average temperature rise over the elapsed time of 300 seconds was at the rate of about 0.95°C per second.

Considering the temperature conditions of this trial, the central heater reached a maximum temperature of 1967°C from an ambient temperature of 1477°C in 0.8 second. The rate of temperature rise at the source of radiant energy for the 490°C difference between ambient and maximum was 612.5°C per second. The radiant energy intensity over the 490°C rise increased from the ambient intensity of about 12.5 watts/cm² to about 40.7 watts/cm² maximum intensity for a net increase of 28.2 watts/cm². Due to the effects of reflection and shape factors, the amount of radiation intensity involved in the net radiant energy interchange between the tungsten source and the BeO tube was calculated to be 16.2 watts/cm² instead of 28.2 watts/cm², as was shown by Fig. 9 and in accordance with Eq. (7).

Considering next the temperature effect of the above radiant energy intensity on the BeO tube, a longer delay occurred in the initial response to the heat pulse than was observed in the 10-second-pulse trials. No explanation can be made of this unless the timing of the start of the heating cycle was in error. Since the tungsten source reached maximum temperature in less than 1 second, it was expected that the response should have been more prompt than that shown in Fig. 23. The linear rate of the initial emf rise, corresponding to a temperature rise of 83°C at the center detector from an ambient of 1477°C indicated that the energy radiated from the BeO tube also increased linearly with its increase in temperature. According to Fig. 11, at the ambient temperature of 1477°C BeO radiated energy at the rate of 24.5 watts/cm² and at 1560°C radiated 30 watts/cm², a difference of 5.5 watts/cm², for the 83°C temperature interval observed at the center detector. For the next 100°C rise from 1560°C to 1660°C the energy radiated increased 7.5 watts/cm² to 37.5 watts/cm². For the next 103°C from 1660°C to 1763°C , the peak temperature reached at the center detector, the energy radiated from the BeO tube increased 8.7 watts/cm² to 46.2 watts/cm². In contrast the radiant energy output of the tungsten source was about 12.3 watts/cm² at the ambient temperature of 1477°C and 40.7 watts/cm² at its maximum temperature of 1967°C for a net output increase of 28.4 watts/cm² for the 490°C temperature difference.

In reviewing the results shown in Fig. 23, some aspects of the temperature effect as represented by the changes in emf with time indicated a predominantly absorption and reradiation process with very little radiant energy throughput. The radiant energy emitted by the tungsten source was probably partly reflected, partly scattered, and the rest absorbed in the BeO with simultaneous emission of a part of the absorbed energy. The radiant energy interchange apparently proceeded at a uniform rate of increase for the first 36 seconds after the emf started to rise. During this interval, in which the center detector showed a temperature rise of 83°C , the difference in amount of radiant energy radiated by the tungsten at 1967°C and the BeO at 1560°C was 10.7 watts/cm². During the next interval of 90 seconds the difference in energy radiated by the tungsten at 1967°C and the BeO at 1660°C was 3.2 watts/cm². Since the temperature of the central heater source was constant, the gradual decrease in the rate of emf increase over this interval was probably due to the decrease in the rate of heat transfer to the BeO tube as the BeO tube increased in temperature. Finally, for the remaining 165-second interval (not shown) the difference in energy radiated by the tungsten and the BeO at the terminal temperature of 1763°C representing the 286°C rise over a 300-second interval was 5.5 watts/cm² in favor of the BeO. From this it would appear that the BeO radiated more energy than it received in the latter stage of the 300-second trial. This anomaly may be due to an increase in the temperature of the tungsten source as the BeO tube temperature increased. At the BeO terminal temperature of 1763°C , it radiated about 46.2 watts/cm²,

while the tungsten would have to be at 2030°C to radiate an equal amount. Since the emf was observed to be still rising at the end of the 300-second period, it could be assumed that the temperature of the tungsten source had increased to some value above 2030°C . If, however, the temperature of the tungsten did not increase as was assumed, then the temperature effect observed in the latter stages of the emf rise would have been caused by direct transmission of radiant energy through the BeO onto the center detector. In such an event, the terminal temperature of the BeO would not have reached 1763°C but remained at about 1650°C , with the radiant energy passing through the BeO without further raising its temperature. This latter circumstance seems improbable, since absorption of radiant energy in BeO increases with temperature in all of the shorter wavelengths and intensities shift toward these wavelengths.

The temperature effect observed at the middle detector for the 300-second trials is illustrated by Fig. 24. The three curves indicate the emf change with time, starting with the bottom curve from left to right and proceeding to the middle and to the top curve in the same sequence. The peak emf indicated by the top curve was reached in about 474 seconds and corresponded to a temperature rise of 33°C . Separate potentiometric measurement indicated, however, that the peak temperature was 38°C . The bottom curve showed no emf change from baseline value for about 79 seconds, after which it increased to a value corresponding to about 4°C over the next 56 seconds. The middle curve covered a time span of 150 seconds and indicated an emf increase which corresponded to about an 18°C rise, while the top curve covered a time span of about 140 seconds and indicated an emf increase to peak corresponding to about a 10°C rise. There was no indication from the data obtained at the middle detector that the temperature effect obtained was related to any direct transmission of radiant energy through the granular BeO. The gradual temperature rise after the long delay from the start of the radiant energy pulse and the long time interval from the end of the 300-second pulse to reach peak temperature indicated that the hot granular BeO was being heated very slowly by the radiant energy emitted from the BeO tube, and because of the scattering of this radiant energy and because of the high heat capacity of BeO the temperature of the granular BeO did not increase significantly. Therefore, the amount of radiant energy that was emitted by the granular BeO as a result of this very small temperature rise produced only a very minor temperature effect at the middle detector.

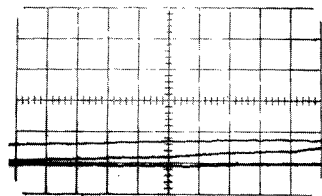


Fig. 24 - Temperature rise of 33°C at the middle detector for item 21 (baseline temperature, 1477°C ; maximum heater temperature, 1967°C ; 300-second pulse). The three curve segments go from left to right in sequence.

The temperature effect at the center detector for a 300-second trial under higher ambient and maximum heater conditions is shown in Fig. 25. The ambient temperature was 1756°C , and the maximum heater temperature was 2101°C . The total emf change corresponded to a temperature rise of 341°C in a time interval of 314 seconds. Referring to Fig. 25, the bottom curve shows the emf change during the first 132 seconds of the pulse. The two other curves intended as a continuation of the bottom curve could not be completely recorded on the same photograph. The curve descending from left to right is a portion of the emf decay from the peak.

Considering the case of the lower curve only, the total emf change in the first 132 seconds corresponded to a 179°C rise for an average rise of about 1.36°C per second.

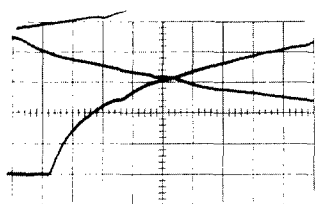


Fig. 25 - Temperature rise of 341°C at the center detector for item 28 (baseline temperature, 1756°C ; maximum heater temperature, 2101°C ; 300-second pulse)

This was distributed as follows: for the first 7.5-second interval the emf change corresponded to a 42°C rise for a rate of 5.0°C per second, for the next 13.5-second interval the emf change started to slow down and corresponded to an additional 42°C rise for a rate of about 3.1°C per second, for the next interval of 36 seconds the emf change corresponded to an additional 42°C rise for a rate of 1.17°C per second, for the next interval of 52.5 seconds the emf change was an additional 42°C for a rate of 0.8°C per second, and the remaining 22.5-second interval corresponded to an additional 13.5°C rise for a rate of about 0.60°C per second.

The steeper initial emf surge seen in Fig. 25 as compared to that in Fig. 23, appeared to be associated with the possibility that at the higher baseline temperature considerably more of the incident radiant energy was transferred in the BeO for a brief period by simultaneous emission and absorption in depth without an accompanying temperature change. As the BeO interacted with and absorbed radiant energy, its temperature increased. The thermal resistivity of BeO, however, acted to reduce the rate of temperature rise and thus limited the radiant energy intensity emitted by the BeO. From the shape of the temperature-time curves of both Figs. 23 and 25, it appeared as if both followed an exponential type relation after the initial surge.

The temperature effect observed at the middle detector for this trial is shown by the three emf-vs-time curves of Fig. 26. The total temperature rise observed was 75°C in an elapsed time of 431 seconds to peak. There appeared to be a delay of about 85 seconds from zero time before any evidence of a change in emf occurred. In the remaining interval of 50 seconds on the bottom curve the emf increase corresponded to about 8°C . The emf change shown on the middle curve was practically linear and corresponded to an additional temperature rise of about 42°C over an interval of 150 seconds for a rate of temperature rise of about 0.28°C per second. On the top curve the emf change followed the same rate as the middle curve for about 45 seconds, corresponding to an additional rise of about 17°C , after which the rate of emf change to peak corresponded to a temperature rise of about 10°C in 75 seconds. The very gradual increase in temperature effect observed at the middle detector after a prolonged delay did not indicate any evidence that this effect was due to the transmission of radiant energy through the granular BeO. The time interval from the end of the 300-second pulse to peak emf was 131 seconds. If the temperature effect had been due to either direct transmission or radiant energy through the hot granular BeO or due to the simultaneous emission and absorption of radiant energy in depth, a more prompt response should have resulted. In this case, scattering of the radiant energy by the individual grains of BeO was undoubtedly more pronounced than would have occurred had this been a continuous solid. In addition, the factors of reflection and refraction at the surfaces of individual grains likewise had some limiting effects on the transfer of the radiant energy to the middle detector. Due to the slow response and the rather small increase in temperature observed in this trial, it was decided that heating of the BeO progressed between individual grains primarily by the absorption and reradiation of radiant energy, while some conduction occurred between grains at contact points. The evidence did not indicate any significant simultaneous emission and absorption in depth or direct transmission of radiant energy through the hot granular material. If there was any radiant transmission by either of these processes, the effects were obscured. Considering the high radiant energy radiating capability of BeO,

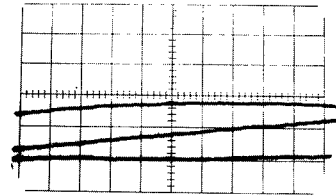


Fig. 26 - Temperature rise of 75°C at the middle detector for item 28 (baseline temperature, 1756°C ; maximum heater temperature, 2101°C ; 300-second pulse)

it should be pointed out that each grain becomes a significant radiator when the temperature of the material is raised, which makes it difficult to discriminate how the radiant energy is transferred.

The temperature effect observed at the outer detector for this trial corresponded to a rise of 47°C above the initial ambient temperature of 1756°C . The time interval to the first indication of an emf change was about 71 seconds, while it required 508 seconds to reach a peak emf corresponding to the 47°C rise. The effect was so gradual that it was decided that this phase of the trial was due partially to the gradual heating of the grains by progressive absorption of radiant energy and the transfer of energy by reradiation to adjacent grains and by conduction at contact points. The proximity of the outer detector to the outer furnace heater was also a factor in the temperature rise observed. A slight rise in the temperature of the granular mass had an effect on the temperature stability of the heated enclosure. Thus, a small part of the total temperature rise of 47°C was probably due to disturbing the temperature equilibrium of the furnace system. Considering the fact that the radiant energy at the center detector corresponded to a maximum net intensity of 28 watts/cm^2 , a net intensity at the middle detector of 5 watts/cm^2 , and a net intensity at the outer detector of about 3 watts/cm^2 , all based on the emittance of tungsten, it is readily seen that granular BeO even though it is translucent in character attenuated roughly about 90% of the incident radiant energy traversing the 3.81-cm (1.5-in.) planar cross section of the granular BeO mass at the center of the gauge section.

The remaining trials in series 4 were conducted at ambient temperatures of 1501° , 1661° , 1764° , and 1766°C and maximum heater temperatures of 2231° , 2201° , 2171° , and 2201°C respectively. The resulting temperature effects observed at the center detector corresponded to temperature rises of 21° , 19° , 21° , and 23°C in time intervals to peak of about 10, 12, 22, and 25 seconds respectively. At an ambient temperature of 1501°C and heater temperature of 2231°C the net radiant energy intensity difference between BeO at ambient temperature and the tungsten heater at maximum temperature was 42 watts/cm^2 ; at an ambient temperature of 1661°C and a maximum heater temperature of 2201°C the net difference was 27.0 watts/cm^2 ; at an ambient temperature of 1764°C and a maximum heater temperature of 2171°C the net difference was 14.5 watts/cm^2 ; at an ambient temperature of 1766°C and a maximum heater temperature of 2201°C the net difference was 18 watts/cm^2 . There appeared to be no significant temperature effects produced at the center detector by increasing the ambient temperature from about 1500°C to about 1765°C nor from variations in the net radiant energy intensities incident on the BeO.

The temperature effects at the middle detector for the above temperature conditions were very minor, corresponding to about a 3°C rise.

The above results observed at the center detector and at the middle detector indicated that evaporation from the tungsten and from the tantalum sheathed thermocouple detectors onto the sample BeO materials had probably affected the surface characteristic of the sample materials to some extent, thereby changing the radiant energy transfer conditions. As a result the temperature effects observed are considered to be lower than would be expected if the surfaces of the sample materials had remained free of metallic films.

The experimental data shown in Figs. 12, 13, 14, 19, 23, and 25 were analyzed by considering the transfer of thermal energy from the tungsten source into the BeO from an exponential temperature-time relation standpoint. Since the BeO tube was relatively thin, the thermal resistance of the material was considered to be small and the rate of heat transfer was considered to be governed almost wholly by the surface thermal resistance. This situation would not prevail, however, in the case of thick sections, since the rate of heat transfer would be governed almost entirely by the thermal resistance of BeO. Surface thermal conductivity was considered as the unit rate of radiant energy transfer to or from a surface and denoted by k' . Correspondingly, $1/k'$ denoted surface thermal resistivity. Thermal conductivity (k) was considered as the quantity of thermal energy which passed through a unit area of unit thickness having unit difference of temperature between opposing faces. Thermal resistivity was considered to be the reciprocal of thermal conductivity and denoted by $1/k$. Thus, in the case of thick sections the rate of heat transfer through BeO under given temperature conditions would be governed by both factors of k and k' .

The temperature-vs-time aspect of the experimental data was considered to be complex, since this relation involved many variables and unknown quantities. Thus, only approximate solutions would be obtained by calculations.

The general character of the temperature-vs-time relation is illustrated in Fig. 27 by the ideal case of heating a solid by radiant energy transfer to the surfaces of the solid from a source at constant temperature. If the temperature rise is constant, the temperature-time relation would be that indicated by the line AC of Fig. 27. However, as the temperature of the source of radiant energy is constant, the rate of heat transfer to the solid continually decreases as the temperature of the solid rises, and the temperature-time relation is that exhibited by the curve AE, which approaches asymptotically the temperature of the radiant energy source indicated by the horizontal line BD.

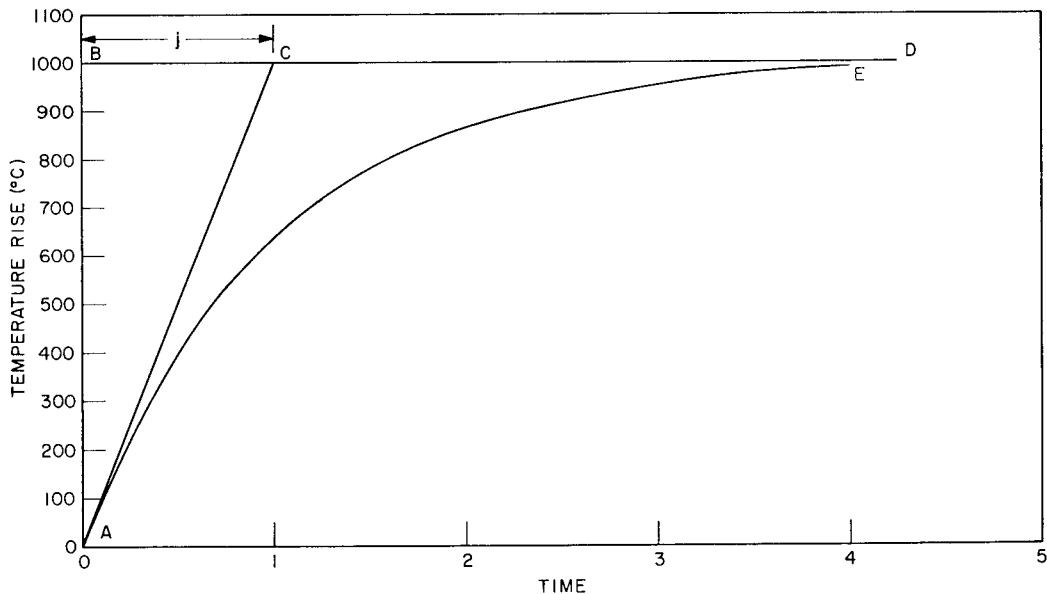


Fig. 27 - Radiant heating of a solid in the ideal case. Curve AE indicates the heating of the solid when the source is at the temperature indicated by BD. Line AC indicates the heating when the temperature rise is constant.

The exponential temperature-time relation may be expressed by the equation

$$\theta_t = \theta_m (1 - e^{-t/j}) \quad (8)$$

where θ_t is the temperature rise corresponding to time t , θ_m is the maximum temperature rise, e is the base of natural logarithms (2.718), and j is the time constant for the given conditions.

The value of the time constant j for each set of conditions is given by the intercept of AC on BD as may be seen in Fig. 27. Equation (8) can be written

$$\theta_t / \theta_m = 1 - e^{-t/j} \quad (9)$$

That is, at any time t after the beginning of the heating period the temperature rise of the solid is a fraction of the maximum temperature rise, this fraction being the value $(1 - e^{-t/j})$. The curve of Fig. 28 shows values of the exponent t/j for corresponding values of fractions of the maximum temperature change. For example, if $t = 0.70j$, or $t/j = 0.70$, the temperature rise is one half of the maximum rise, while for $t = j$, $\theta_t = 0.63\theta_m$. Thus, at the end of a time period equal to four times the time constant j , the temperature rise would be 98% of its maximum value.

The initial rate of temperature rise is given by the slope of the tangent AC, Fig. 27. The slope of the heating curve AE at any given time is the measure of the rate of temperature rise at that time. The initial temperature of the solid minus the constant applied temperature is the maximum temperature rise. Hence, if the initial rate of temperature rise, that is, the slope of the line AC in a given case is observed, the value of the time constant j can be obtained, and the time required for heating the solid to any particular temperature below the constant temperature of the source of radiant energy can be calculated by Eq. (8).

Since the temperature of the mass of a solid is raised by the absorption of thermal energy in the solid and by its distribution within the volume, the rate of the penetration depends on thermal conductivity of the substance and on its specific heat and density, the product of the specific heat and density being the heat storage capacity per unit volume of the substance.

Thermal diffusivity, defined as the ratio of its thermal conductivity to its thermal energy storage capacity per unit volume may be expressed by the equation

$$h^2 = k/\rho c_p \quad (10)$$

where h^2 is the thermal diffusivity, k is the thermal conductivity, ρ is the density, and c_p is the specific heat. All other conditions being the same, the rate of temperature rise of two materials will be the faster for the material having the higher thermal diffusivity.

Thermal diffusivity of a substance varies with temperature. This variation is due mainly to variations in thermal conductivity and specific heat with temperature. The distinction between thin and thick solids relates primarily to the influence of thermal diffusivity on the rates of heating. In the case of a thin solid, the influence of thermal diffusivity on the rate of temperature change of the solid is probably negligible. Thus, for a thin solid exposed to a given temperature, higher than that of the solid, the rate of temperature change in the solid is determined practically wholly by its surface thermal conductivity. With a thick solid, the rate of temperature change at any point within the solid during its exposure to thermal energy is governed by both its surface thermal conductivity and its thermal diffusivity. The use of thin and thick in this sense, of course,

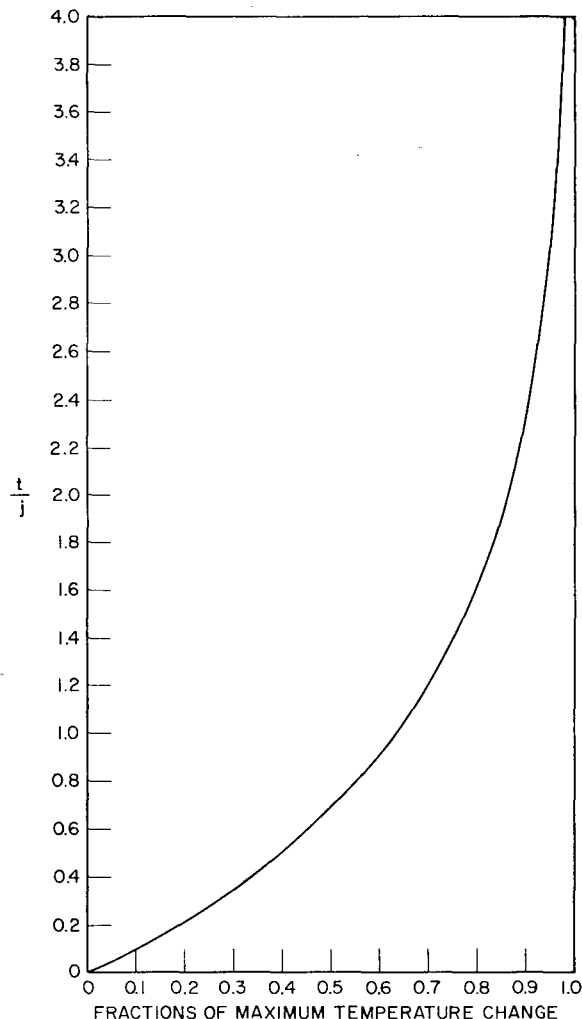


Fig. 28 - Values of the exponent t/j in Eq. (9)

must be related to the nature of the solid material, since under certain conditions a path of heat transfer that would apply to one kind of thin solid may also apply to a thick solid of another kind.

Considering the temperature effect observed in Fig. 12, in which the baseline temperature was 1102°C and the maximum source temperature was 2271°C , the initial rate of emf change corresponded to a temperature rise of 4.5°C per second. Using this initial rate, a temperature-vs-time heating curve, shown in Fig. 29, was constructed from values calculated according to Eq. (8). (The calculated values used in plotting Figs. 29 through 33 are listed in Table C2 of Appendix C.) The time interval j was found to be 263 seconds, which represented the time required for the temperature to rise 1169°C based on the initial rate of heating being maintained constant. Since the source temperature was constant and the rate of heat transfer to the BeO tube continually decreased as its temperature rose, curve AE represented the actual temperature-vs-time relation. The time to reach 98% of the maximum source temperature was calculated to be about 1050 seconds for the experimental conditions.

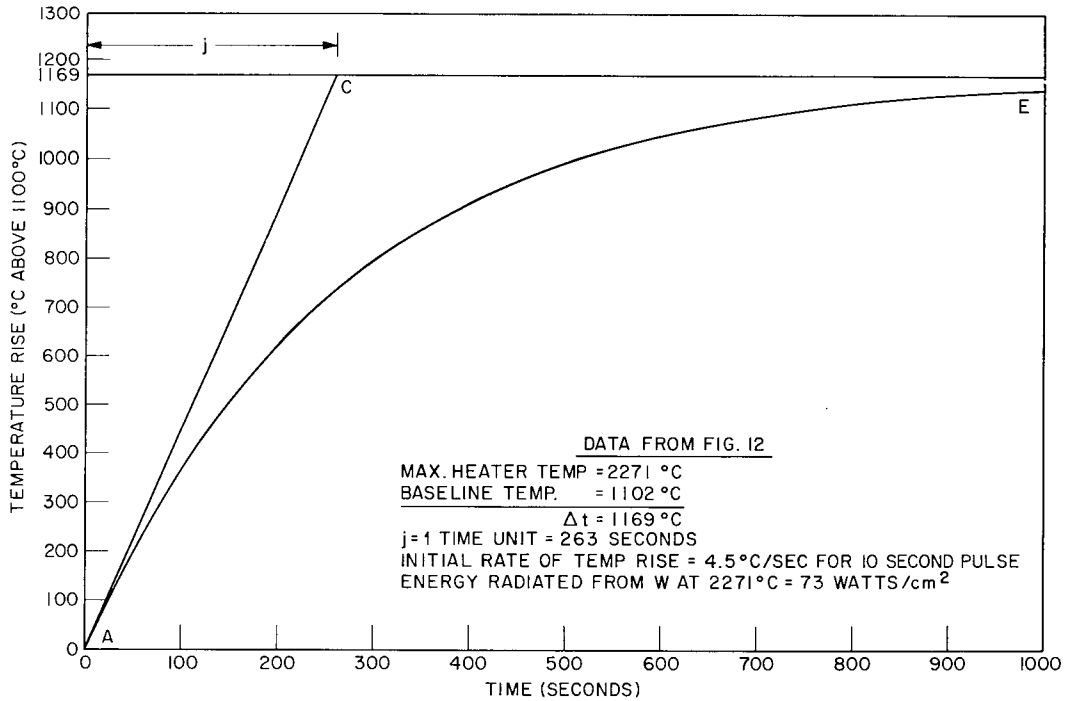


Fig. 29 - Temperature-vs-time curve for the trial of Fig. 12

The temperature effect shown in Figs. 13 and 14 occurred under higher temperature conditions, with the baseline temperature at 1498°C and the source temperature at 2343°C. The initial rate of temperature rise in this case was 4.23°C per second. The temperature-vs-time heating curve is shown in Fig. 30 for the experimental temperature conditions in this case. The time interval j was found to be 200 seconds, the time required for the temperature to rise 845°C based on maintaining the initial rate of temperature rise.

For the temperature effect observed in Figs. 18 and 19, the experimental temperature conditions consisted of a baseline temperature of 1482°C and a maximum source temperature of 1979°C. Since the sample materials were fresh in this case, they were considered to be free from evaporated metallic films. The initial rate of temperature rise was 6°C per second, from which the temperature time curve shown in Fig. 31 was constructed. The time interval j was found to be 82 seconds for the temperature to rise 497°C.

The experimental temperature conditions for the 300-second-pulse trial represented by Fig. 23 consisted of a baseline temperature of 1477°C and a maximum source temperature of 1967°C. The initial rate of temperature rise was 2.8°C per second from which the temperature-vs-time curve shown in Fig. 32 was obtained. The time interval j was found to be 175 seconds for the temperature rise of 490°C based on the initial rate being maintained.

Referring to Fig. 23, a temperature rise of 184°C was observed to occur in the first 128 seconds of the 300-second pulse, while a maximum of 286°C was observed in 300 seconds. According to Fig. 32, the temperature should have risen about 250°C in 128 seconds and should have reached 400°C or about 81% of the maximum temperature rise of 490°C in 300 seconds, if at any time after the beginning of the heating period the temperature rise was a fraction of the maximum temperature rise according to the fraction

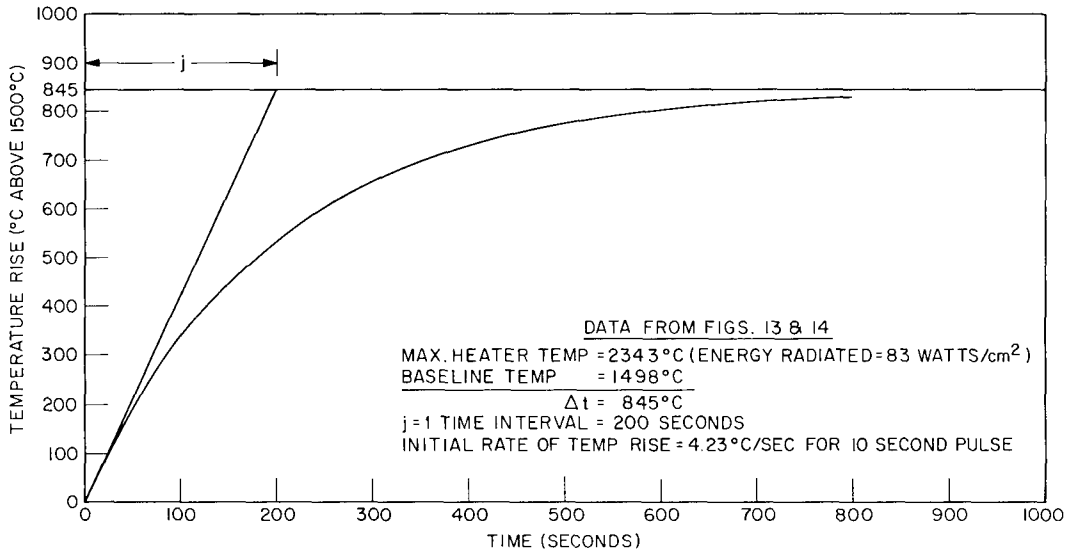


Fig. 30 - Temperature-vs-time curve for the trials of Figs. 13 and 14

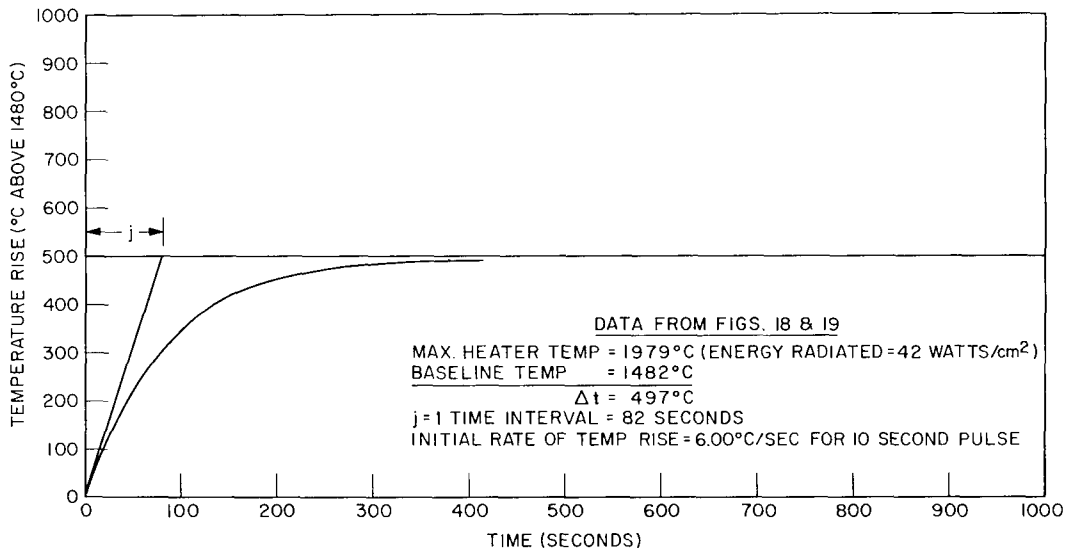


Fig. 31 - Temperature-vs-time curve for the trials of Figs. 18 and 19

$(1 - e^{-t/j})$. It is obvious from curve (b) in Fig. 32 that the temperature effect at the center detector did not follow very closely the calculated temperature-vs-time relation of curve (a). It was considered probable that the temperature rise of the BeO tube may have followed this type of relation and the discrepancy between the values for the temperature rise observed at the center detector and the calculated values could be attributed partly to the inadequate response of the center thermocouple detector to radiant energy. On the other hand, there was another possibility, however, that the temperature of the BeO did not rise as rapidly as was indicated in Fig. 32.

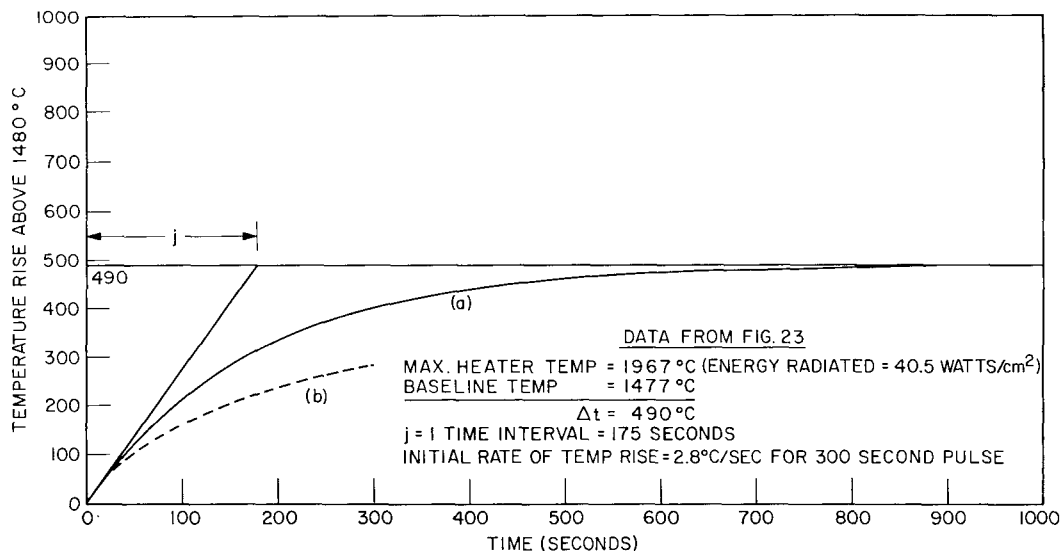


Fig. 32 - Temperature-vs-time curve for the trial of Fig. 23. Curve (a) is the calculated curve, while curve (b) is the observed measurement at the center detector.

The experimental temperature conditions for the 300-second trial represented by Fig. 25 consisted of a baseline temperature of 1756°C and a maximum source temperature of 2101°C. The initial rate of emf rise corresponded to a temperature rise of 5.0°C per second, and the time interval j based on this rate was found to be 70 seconds. The calculated temperature-vs-time curve is shown in Fig. 33. Referring to Fig. 25, an emf rise corresponding to 180°C occurred in the first 132 seconds of the 300-second pulse, while the maximum temperature rise of 341°C occurred in 314 seconds. In this case the actual temperatures observed at the center detector (curve (b) of Fig. 33) did not follow the exponential trend of values for curve (a). Since the maximum temperature of 341°C reached by the center detector was nearly that of the source at the end of the trial, it was suspected that the conditions involving the center detector had changed. It was found upon subsequent examination of the BeO tube that cracks had developed in it and that the center detector had probably received radiant energy directly from the tungsten source. In the first 132-second part of this trial, however, the BeO tube was considered to be crack-free. The initial surge of emf rise appeared to be about the same for BeO at 1756°C as it was for BeO at 1482°C (Fig. 31). This appeared to show that the higher initial BeO temperature did not produce any increased effects from exposure to radiant energy.

Comparing Figs. 29 and 30, it will be noted that the initial rates of temperature rise were quite similar although the baseline temperatures were 400°C apart. On the basis of a 300-second interval, however, the temperature-time curve of Fig. 29 indicates a temperature rise of about 800°C whereas the curve of Fig. 30 indicates a rise of only 650°C. Considering the baseline temperatures were 1102°C for Fig. 29 and 1498°C for Fig. 30 with net radiant energy intensities of about 70 watts/cm² in each case, the seemingly faster heating in the case of Fig. 29 may possibly be related to the thermal resistivity of BeO, which would range between 16.6 sec-°C-cm/cal for 1102°C and 28.6 sec-°C-cm/cal for 1900°C in covering the 800°C rise. In the case of Fig. 30, the initial thermal resistivity would be higher due to the higher baseline temperature of 1498°C, the value being about 24 sec-°C-cm/cal. This would tend to reduce the initial heating rate, as apparently occurred. It has been reported (34) that the thermal resistivity of BeO reaches a maximum at about 1825°C with a significant decline in thermal resistivity at higher temperatures. Accordingly, the heating rate would be expected to decline up to the temperature of maximum resistivity and then increase again as the thermal resistivity decreased.

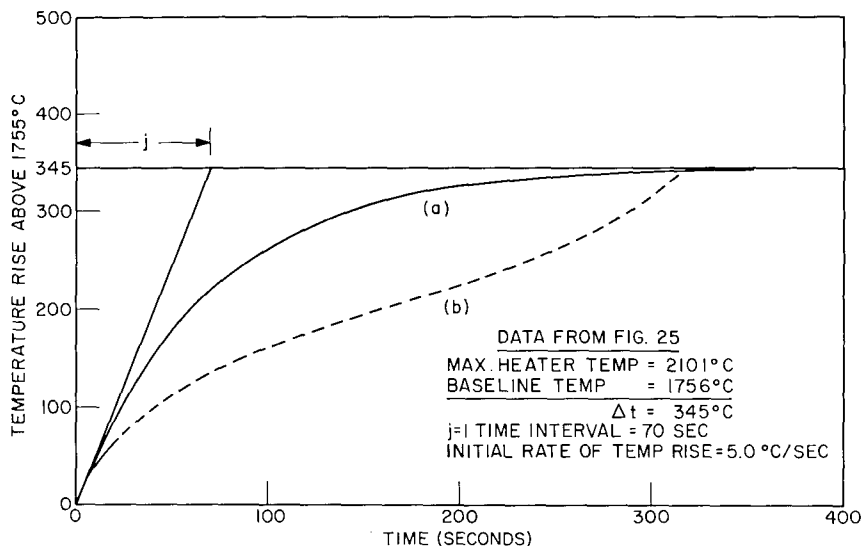


Fig. 33 - Temperature-vs-time curve for the trial of Fig. 25

Comparing the heating rates of Figs. 31 and 32, it will be noted that the baseline temperatures as well as the net radiant energy intensities from the tungsten source were very similar, yet the initial heating rate varied from 6°C per second for Fig. 31 to 2.8°C per second for Fig. 32. Since the experimental temperature and radiant energy conditions were nearly alike in both cases, the thermal resistivity of the BeO should have been practically the same in each case and the initial rate of heating should not have varied significantly. The initial rate of emf rise seen in Figs. 18 and 19 was interpreted as a surge of radiant energy that was momentarily transferred to the center detector from the BeO. It was assumed that radiant energy from the tungsten source was rapidly transferred in the hot BeO for a few seconds without it interacting with the radiant energy surge. As soon as the BeO interacted with the incident radiant energy, its temperature began to rise, which in turn increased its thermal resistivity, which tended to limit the rate of temperature rise and the subsequent emission of radiant energy from the BeO. This sequence appeared to be evident in the first 132 seconds of Fig. 25. Thus, with the exception of the brief initial surge of radiant energy throughput in the hot BeO, the thermal behavior involving the transfer of radiant energy appeared to be very similar to that of an opaque refractory material.

The balance of the series 4 10-second trials in which the experimental temperature conditions were varied from about 1500° to 1765°C showed an increase in time to reach a peak emf. From Table 6 it will be noted that from a baseline temperature of 1500°C the peak of temperature rise was reached in 9.8 seconds, while from a baseline of 1661°C the peak was reached in 11.8 seconds and from a baseline of 1765°C the peak was reached in about 23 seconds. This seemed to indicate that thermal resistivity had exerted an influence in limiting the temperature rise in the BeO and its subsequent emittance of radiant energy.

Attempts were made in series 5 trials to obtain the effects of incident radiant energy on BeO at baseline temperatures from 1836°C to about 1985°C . At these higher temperatures difficulties developed with the use of oscilloscopes for monitoring the emf rise, and potentiometers had to be used. At a baseline temperature of 1836°C and a maximum source temperature of 2200°C the emf rise corresponded to a peak of 29°C , which was reached in 20 seconds from a 10-second pulse. The net difference of radiant energy

between the intensity of BeO at baseline and that of the tungsten source was about 11.5 watts/cm². At a baseline temperature of 1985°C and maximum source temperature of 2190°C the emf rise corresponded to 23°C. The radiant energy intensities of BeO and the tungsten source were about equal in this case. At a baseline of 1985°C and a maximum source temperature of 2280°C, the emf rise corresponded to 27°C with a net difference between intensities of 5 watts/cm². At a baseline of about 1980°C and a maximum source temperature of 2295°C the emf rise corresponded to 26°C with a net difference in intensities of 7.5 watts/cm². The time to reach peak emf in each case was about 20 seconds for a 10-second pulse. The small emf and sluggish effects produced at the center detector at high baseline temperatures indicated that the transfer of radiant energy into the BeO from the source was poor.

The temperature effects observed at the middle detector in series 5 trials corresponded to very minor temperature rises above baseline. In the first three 10-second trials the emf rise corresponded to 3°C in each case, while a 5°C rise was observed in the fourth trial. The time to reach peak emf was unrealistically long being in excess of 100 seconds in each case.

The net results of the series 5 trials indicated that hot BeO at temperatures approaching 2000°C did not exhibit any expansion of a possible diathermic tendency it may have possessed at lower temperatures. In fact, there seemed to be a trend toward complete opaqueness as the material was heated toward higher temperatures. This trend seemed to be verified in Fig. 34, in which the absorption of radiation energy is seen to increase at all wavelengths with increasing temperature.

Generally, nonconductors are opaque; they absorb the major part of impinging radiant energy and radiate comparatively much heat. White oxides are generally considered to have a low emissivity in the long-wavelength, visible, and near infrared regions. The emissivity increases with wavelength for wavelengths above about 5 μ. They are nearly black at 10 μ and at high temperatures, indicating high absorptivity of radiant energy. The spectral emissivity of BeO having a grain size of 0.5 μ was shown in Fig. 34 for temperatures 1500°, 1700°, and 2000°K. The distribution shows that BeO is a poor emitter in the visible range of wavelengths and that all the higher values of emissive power fall into the infrared region of the spectrum. As temperature increases, the emissive power increases for all wavelengths. From this BeO would be expected to absorb radiant energy more strongly the higher the temperature and thus become more black. This effect was apparent in Fig. 11, where the energy radiated was seen to increase with increase in temperature.

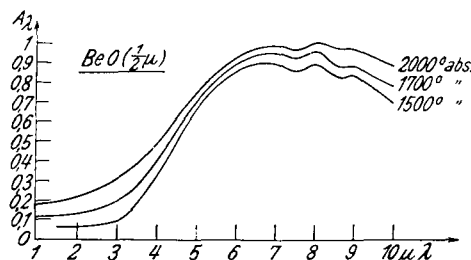


Fig. 34 - Spectral emissivity of BeO vs wavelength (from Ref. 38)

Considering the radiant energy radiated by a body at various temperatures it will be seen from Fig. 35 that the maximum energy radiated increases as temperature increases and that the wavelength at which the maximum energy is radiated becomes shorter. The intensity of radiant energy W_{λ_m} measured in watts/cm² emitted at the wavelength of peak radiation " λ_m " measured in microns increases approximately as the fifth power of the absolute temperature of the blackbody as given by

$$W_{\lambda_m} = 1.3T^5 \times 10^{-15}. \tag{11}$$

Doubling the absolute temperature of a blackbody source increases its peak radiation energy thirty-two fold.

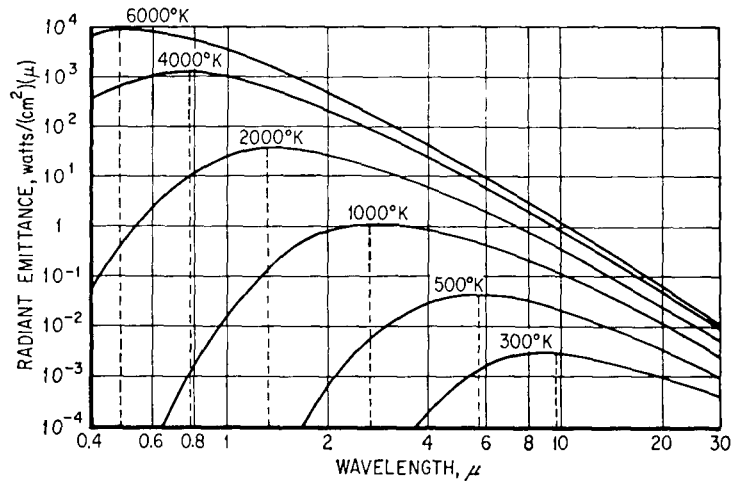


Fig. 35 - Blackbody radiant emittance vs wavelength (from Ref. 39)

The spectral-radiant emittance distribution curves for tungsten and for a blackbody at 2450°K (2177°C) are shown in Fig. 36. An ordinate is shown drawn through the two curves at a wavelength of 1.6 μ. The ratio of ordinate (or height) of the tungsten curve (a) to that of the blackbody curve (b) at 1.6 μ gives the spectral emittance of the tungsten at 2450°K (2177°C) and 1.6 μ. Thus, at this temperature, the radiant energy peak is at about 1.2 μ. At a temperature of about 2280°C the radiant energy peak is at about 1.14 μ, and at this temperature about 61% of the radiant energy radiates from tungsten between wavelengths of 0.7 μ and 2 μ, in which about 13% radiates between 0.7 μ and 1 μ and 48% between 1 μ and 2 μ. At a temperature of about 2500°C the radiation peak shifts to about 0.95 μ, with about 64% of the energy radiated between wavelengths 0.7 μ and 2 μ, of which 17% is radiated between 0.7 μ and 1 μ and 47% between 1 μ and 2 μ.

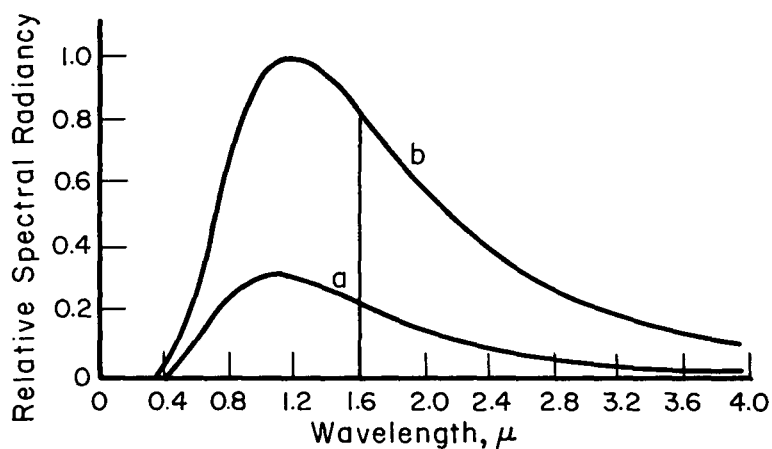


Fig. 36 - Spectral radiancy distribution curves for (a) tungsten and (b) a blackbody at 2450°K (2177°C) (from Ref. 40)

At high temperatures a material may be opaque to certain wavelengths of radiant energy and transparent to others or it may become more or less transparent to a varying range of wavelengths of radiant energy as the temperature is changed. Theoretically, no specimen of a material is completely opaque except at infinite thickness, yet it may be considered to be opaque at some thickness which produces no observable difference in opacity between that thickness and an infinite thickness.

For a material of infinite thickness, all radiant energy incident upon it is either reflected or absorbed. The thickness which can be considered as infinite depends, for practical purposes, on the absorption coefficient as given by $X_{\infty} \approx 3.5/\alpha$ where X_{∞} is the infinite thickness and α is the absorption coefficient.

The absorption coefficient depends strongly on the wavelength of incident radiation. In the case of glasses, it varies from about 0.1 cm^{-1} for wavelengths below about 2.5μ to about 10 cm^{-1} for wavelengths above 2.5μ (41). A 0.3-cm thickness is effectively infinite (opaque) at room temperature, where most of the radiant energy is at long wavelengths, but at elevated temperatures a 35-cm thickness is necessary as an infinite thickness. Translucent oxides have an absorption coefficient of from 10 to 30 per cm in the visible range of wavelengths, so that sample thicknesses of 0.1 to 0.3 cm are effectively infinite or opaque.

Besides emittance (ϵ), and absorbance (a), a translucent material has reflectance (ρ) and transmittance (τ). At any wavelength, $\epsilon + \rho + \tau = 1$. A thick section has a lower τ than a thin section. If τ decreases, then emittance or reflectance must increase. Because reflectance is primarily a surface phenomenon and remains sensibly constant, a thick section of translucent material will have a higher emittance. For example, glass has a high transmittance in the visible range of wavelengths and low emittance, while at wavelengths of 5μ to 7μ transmittance is low but emittance is high.

Considering the spectral emittance of BeO when heated to high temperatures as was shown in Fig. 34, it will be noted that the maximum emittance occurs in the wavelength range 7μ to 8μ , whereas it is at a minimum in the wavelength range below about 2μ . As shown in Fig. 34, the increase in emittance with temperature in the short wavelength region is more pronounced than the emittance at the longer wavelengths. From this it follows that absorbance of radiant energy also increases in the short wavelength region in order to provide greater emittance at these wavelengths. As a result of the greater emittance, it would be expected that translucent BeO would exhibit no increase in transmittance but rather a decrease. Assuming that the curves of Figs. 12, 13, and 14 resulted from the transmittance of radiant energy through the BeO tube, their similarity indicated that there was no increase in transmittance when the ambient temperature was increased from 1102° to 1498°C . In fact, the temperature effect at 1498°C was about 7°C lower than that observed at 1102°C . This trend would indicate that transmittance of radiant energy decreased as the temperature of the BeO was increased.

From the limited optical property data available on BeO, polycrystalline translucent material has been reported (10,42) to be relatively opaque below a wavelength of 30μ , while some transmission was observed above this wavelength, reaching a saturation value for transmission in the wavelength region from 90μ to 120μ . Maximum reflectance was reported to occur between wavelengths of 9μ and 13μ . Absorbance data versus wavelength indicated absorption peaks at 4.9μ and 6.4μ with greater absorption observed in the region from 4μ to 4.6μ than in the 6.4μ region. Although these data pertained to the problem of infrared transmission in BeO, the results nevertheless were informative.

The behavior of translucent BeO towards pulses of radiant energy in the series 2 trials appeared to be largely characteristic of an opaque material with perhaps a very

minor indication of diathermancy (the property of affording free passage to radiant energy). It is desirable to discuss this aspect in a nonmathematical manner in order to elucidate the underlying physical phenomena.

In the more familiar problems involving radiant energy transfer, opaque solids interact with radiant energy only at their surfaces, and conduction is the only mechanism by which heat is redistributed throughout the interior of a material. Perfectly diathermic solids do not interact with radiant energy at all; however, they may be practically opaque to certain wavelengths of radiant energy. In contrast with diathermic materials, diathermanous materials absorb radiation not just at their surfaces but in depth, resulting in internal radiative effects which may also participate in the heat distribution throughout the interior of the material. The emission and absorption of radiant energy are thus bulk, rather than surface, phenomena. The interaction of the simultaneous emission and absorption of radiant energy throughout the volume leads to a dependence of the emittance of diathermanous solids on their thicknesses. This interaction also leads to a mechanism of radiative heat transfer in the interior of a diathermanous material entailing not the familiar transmission of radiation through it but involving internal radiant energy interchanges between adjacent layers.

A fundamental factor that cannot be overlooked in the process of emission and absorption in depth is the temperature of the material. If the temperature of the material is low in comparison with the temperature of the source of radiant energy, its own emittance will be negligible in comparison with the intensity of the radiant flux traversing it. If, however, the temperature of a diathermanous material is raised, either by deliberate heating or by absorption of radiant energy, the material itself becomes a significant radiator of radiant energy. The radiant energy radiated by it would be, in part, that which originated from the radiant energy source and, in part, the radiant energy originated in the material itself. This process, therefore, involves the interaction of simultaneous emission and absorption of radiant energy throughout the material.

Assuming that the radiant energy radiated from a source is in the form of diffuse radiation, the flux density will depend on the temperature and nature of the source. A fraction of this flux density will fall in the region of certain wavelengths to which a diathermanous solid may be opaque. As this diffuse radiant energy impinges on the diathermanous solid, a fraction will be reflected. Those components of the unreflected radiant energy to which the solid is opaque will be absorbed at the surface. The remainder of the incident radiant energy will be refracted into the solid and partly absorbed as it crosses the solid. Of the radiant energy that may reach the opposite surface of the solid, a part will re-emerge from it and a part will be internally reflected. More of the reflected part will be absorbed as it recrosses the solid, to be partly reflected once again at the first surface. These multiple reflections will continue, given enough time, until the radiant energy is completely attenuated by absorption and by losses across the surfaces of the solid. Thus, some of the radiant energy is delivered directly from the source to the interior of a diathermanous material and promptly redistributed. In contrast, an opaque material absorbs all the radiant energy that is not reflected at its surface, and the energy reaches the interior of the material only by the slower process of thermal conduction.

In the radiant energy interchange concept discussed above, some of the radiation from a source is absorbed at the surface, and some throughout the thickness of the material, while the radiant energy emitted by the solid originates partly from the surface and partly from the interior of the solid. The proportions emitted are governed by the properties and temperature of the diathermanous solid and not by those of the source.

Internal effects from radiant energy impinging on a diathermanous solid are of course confined to those wavelengths to which the material may exhibit some diathermancy. Spectral absorption coefficients are important factors for ascertaining the effect of temperature on the diathermancy of a material and the relation to the change in spectral

composition of blackbody radiation at various temperatures. For example, at room temperature 90% of the energy of blackbody radiation is contained in the range of long wavelengths; as temperature increases, the spectral distribution shifts toward shorter wavelengths, to which a material may be diathermanous. Thus, silicate glasses are virtually opaque to radiation of wavelengths longer than about 4.5μ , transmitting only about 10% of the radiation from a blackbody at room temperature. At 1000°C , the spectral distribution has shifted so much that the glasses are diathermanous to about 70% of the radiation from a blackbody. In the case of glasses, diathermancy is not a unique physical property; rather it is determined by the wavelength dependence of its absorption coefficients and the spectral composition of the radiation in question.

In the process of emission and absorption in depth, two different physical situations are possible. In the first, the diathermanous solid does not contain scattering centers within its volume. The radiant energy radiated is derived from the emission and absorption within the interior of the radiating solid and from the effects of multiple reflections from boundaries as the radiant energy attempts to escape from the radiator. In the second physical situation, the radiant energy traversing the solid is diverted and attenuated by scattering processes in addition to the processes of simultaneous emission and absorption from the various layers of the material. Radiant energy in this case is not only absorbed by the material of the layer, but it is also scattered by pores and grain boundaries in the layer. In addition, the surface and internal reflections of radiant energy contribute effects. These factors influence the character of the radiant energy emitted from a material so that it is almost perfectly diffuse, whereas the radiant energy impinging on the material surface is partly collimated by refraction as it enters the surface of the material.

Considering the behavior of hot translucent BeO to be opaque, the radiant energy incident upon the inner surface of the tube is partly reflected and partly absorbed at the surface. The absorbed energy reaches the interior only by the relatively slow process of thermal conduction. The energy radiated at the opposite surface would originate entirely at that surface.

On the other hand, if the impinging radiant energy is considered to be absorbed in depth the incident energy is delivered directly to the interior of the material and absorbed throughout its thickness with simultaneous emission and absorption throughout the volume of the material. This interaction involves not the transmission of radiant energy through the material but the internal interchange of radiant energy between adjacent layers, which results in heat distribution throughout its interior (43). Considering the high specific heat of BeO at high temperatures, which is calculated to be 0.577 cal/g at 2100°C from an equation reported in Ref. 44, a considerable amount of absorbed radiant energy is stored by virtue of its heat capacity. (Specific heat values for BeO are plotted in Fig. C2 of Appendix C.) Thus, an appreciable amount of radiant energy can be accommodated in the material as heat without causing a large increase in the temperature of the material. Not all of the internally emitted radiant energy radiates from the material, since some is absorbed on its path to the surface, some is internally reflected, and some as it reaches a surface is refracted across it. It is the entry of the refracted portion into the medium surrounding the radiator that is commonly known as radiant energy emission. Thus, the ability of the BeO to emit radiant energy is characterized by the rate at which the energy is emitted in all directions from a unit volume of the material at a given temperature.

The initial surge of emf change observed at the center detector appeared to be associated with the possibility of simultaneous emission and absorption in depth of the incident radiant energy intensity by the BeO without an accompanying change in temperature. As soon as the BeO interacted with incident radiant energy, the temperature of the BeO began to rise with an accompanying rise in specific heat, in emittance, and in thermal resistivity. The increase in emittance with temperature was undoubtedly accompanied by the absorption of increasing amounts of radiant energy, thereby, reducing the amount of radiant energy that could be transferred by simultaneous emission and absorption. This would

explain in some degree the rather prompt reduction in the rate of emf rise from the initial rate. In view of the radiating characteristics of BeO at elevated temperatures it was somewhat difficult to assign a number value that was possibly transferred in the BeO initially. If the emittance of tungsten is used for a rough estimate of this, then for a 42°C rise from a baseline temperature of 1756°C to 1800°C the amount of radiant energy transferred to the center detector initially was estimated to be roughly 0.08 watts per second or about 0.5 watt in 6 seconds, neglecting losses from the center detector by radiation and conduction. This amount of radiant energy was considered to be very small and indicated that no large throughput of radiant energy occurred in hot BeO.

SUMMARY

The radiant energy throughput in hot BeO was explored by five series of experiments in the temperature range from 1000° to 2000°C. Two types of BeO material were employed, a thin translucent BeO tube and a granular fused material.

In the temperature range from 1000° to 1250°C and a low intensity of incident radiant energy, a negligible temperature effect (<4°C) was observed at the center detector, while at the same time there were no detectable effects observed at the middle or outer detectors. The major portion of the radiant energy emitted by the tungsten source was absorbed on the inner surface of the BeO tube, converted to heat and then distributed throughout the material by the relatively slow process of conduction. Since the temperature effect observed at the center was produced entirely from radiant energy being emitted by the BeO tube, it is obvious from the small effects obtained that there was no transmission of radiant energy through the BeO and that the effects obtained were produced by reradiation from the BeO tube as a result of a small rise in its temperature.

When the temperature of the BeO was increased to about 1445°C, the incident intensity appeared to have some influence on the speed with which a temperature effect occurred at the center detector. As the incident intensity was increased the response time of the emf rise and the time to reach peak emf at the center detector were both somewhat lower. This indicated that the transfer of radiant energy in the BeO was somewhat sensitive to the intensity of incident radiant energy. The results of the series 1 experiments, however, did not appear to show that the BeO tube material was significantly transparent in the temperature range from 1000° to 1445°C. In this case the radiant energy transfer in hot BeO appeared to proceed by the process of absorption at the inner surface, conduction, and reradiation.

In the series 2 experiments, the BeO baseline temperature ranged from 1100° to 1760°C, while the net radiant energy intensities were maintained from about 63 to 70 watts/cm² above baseline values. The temperature effects observed at the center detector indicated the possibility that some radiant energy throughput had occurred briefly in the BeO at the start of each heating cycle. The prompt emf rise noted at the center detector at the start together with the relatively high initial rate of emf rise and the abrupt drop in emf at the end of the heating pulse was interpreted as indicating that some of the high intensity emitted by the tungsten source was transmitted either through the BeO or by a process involving simultaneous emission and absorption in depth. The results obtained, however, seemed to favor the latter process, since the rate of emf rise appeared to fall off appreciably as the BeO became hotter during a heating pulse.

The temperature effects obtained at the middle detector in the series 2 experiments were very minor, ranging from a rise of from 4° to 7°C. This indicated that the BeO tube emitted a very weak radiant energy intensity as a result of the heat pulse. Consequently, the temperature of the BeO tube must not have risen much above that indicated at the

center detector. The radiant energy transfer in the granular material was expected to be considerably less than that expected in a continuous solid, since extensive scattering of the radiant energy occurred. A slight indication of a prompt response to the incident radiation was noted in part of the trials and not in others, leaving the matter of radiant energy transmission in the granular material in doubt.

There were no detectable indications of any temperature effects at the outer detector.

In the series 3 experiments, the BeO baseline temperature varied from 1500° to 2035°C, while the incident source intensity varied from about 44 to 107 watts/cm² above the baseline value. The temperature effects obtained at the center detector were somewhat lower than those obtained in the series 2 experiments. The trend, observed in the series 1 and 2 experiments, for the temperature effect to increase with increase in baseline temperature and radiant energy intensity did not materialize in the series 3 experiments. Prolonged exposure of the metallic components to high temperatures in vacuum caused evaporation to occur. The presence of evaporated films on the inner surface of the BeO was believed to have produced changes in the emissivity of the surface which adversely affected its radiant energy transfer. This was particularly evident in the case where the BeO baseline temperature was at 2035°C and the incident radiant energy intensity was 107 watts/cm². This high baseline temperature and high intensity produced an emf rise corresponding to only 43°C.

The temperature effects observed at the middle detector were also lower than those observed in the series 2 experiments. This would follow from the weaker intensities emitted by the tube.

The temperature effects observed at the outer detector were mainly negligible and uncertain due to slight unbalancing of the temperature of the furnace wall heater.

In the series 4 experiments, the BeO materials and metallic components were replaced with fresh materials. The BeO baseline temperatures ranged from 1475° to 1770°C, while the radiant energy intensity ranged from 27 to 55 watts/cm². Experiments were conducted at pulse intervals of 10 seconds and 300 seconds. The temperature effects obtained at the center detector with the 300-second trials suggested that the BeO followed an exponential type of temperature-vs-time heating curve. This trend was examined by constructing temperature-vs-time curves based on the initial rate of emf rise. The results indicated that the rate of heating at the center detector appeared to show a trend similar to the exponential temperature-vs-time relation but there was a greater drop in temperature rise with time. The initial rate of emf rise indicated a brief surge of radiant energy throughout from the tungsten source to the center detector. This was interpreted to be due to radiant energy transfer in the BeO by simultaneous emission and absorption in depth without an accompanying temperature change occurring in the BeO. As soon as the BeO interacted with the incident radiant energy, its temperature began to rise, which further increased its thermal resistivity. The high heat capacity of hot BeO would tend to cause it to soak up considerable amounts of absorbed energy without any rapid increase in temperature. The interaction of the simultaneous emission and absorption was considered to involve a dependence of the emittance on the thickness. The interaction was also considered to involve a mechanism of radiant energy transfer in the interior of hot BeO involving not the transmission of radiant energy through it but by internal radiant energy interchanges between adjacent layers. This concept was supported by the fact that at the baseline temperature the emittance of BeO was considerably below the source intensity. Thus, the initial emf effects originated from the source as a result of simultaneous emission and absorption in depth. As heating of the BeO occurred, it radiated increased amounts of radiant energy which originated in the material itself. Thus, as the BeO became hotter, its own radiant energy emittance increased in intensity, thereby

reducing the overall net effectiveness of the incident intensity and obscuring the amount of radiant energy transferred by simultaneous emission and absorption. In view of this situation it was not possible to assign a realistic numerical value to the amount of radiant energy that was transferred by simultaneous emission and absorption. Since the total temperature effects obtained were quite small, the amount of thermal energy transferred by simultaneous emission and absorption was considered to be very small.

The temperature effects of the 300-second pulses observed at the middle detector involved lengthy time intervals for a first indication of an emf rise and for reaching a peak in emf rise. The emf rises corresponded to temperatures of 36° to 43°C. The sluggish response to radiant energy emitted by the BeO tube together with the low temperature-rises indicated that the interchange of radiant energy in the granular material was affected by scattering and proceeded by absorption of radiant energy at grain surfaces with subsequent re-emission to adjacent grains and reabsorption. This resulted in a slow increase in temperature and in emittance. The effects observed at the middle detector were interpreted as a good indication that hot BeO material did not develop any significant diathermic tendency but behaved essentially as an opaque refractory material.

The temperature effects observed at the outer detector were too small and too uncertain to warrant consideration from a radiant energy standpoint.

There appeared to be no significant increase in the temperature effects as a result of increasing the BeO baseline temperature to higher values. The series 5 experiments were conducted at baseline temperatures from 1836° to 1984°C and radiant energy intensities above baseline from 21 to 34.5 watts/cm². The temperature rise observed at the center detector ranged from 23° to 29°C. The time required for the first indication of emf rise varied from about 1.5 to 3 seconds, while the time to reach peak in emf rise was about 21 seconds. It is obvious from the results that there was no significant effect produced from the relatively high intensity incident upon BeO at temperatures approaching 2000°C. Considering the rapidity with which the tungsten source reached maximum temperature and the length of time required for the center detector to reach the peak in emf rise in 10 seconds, the radiant interchange was predominantly a process governed by absorption at the inner surface of the tube, distribution of heat by conduction, and reradiation at the outer surface. The intensity reradiated was obviously small; according to Fig. 11 an estimate of this value would be about 3 watts/cm² for the highest temperature reached.

CONCLUSIONS

Thin continuous BeO translucent material heated to temperatures from 1000° to 2000°C did not show any significant throughput of radiant energy upon exposure to pulses of high-intensity radiant energy. From 1000° to 1800°C there appeared to be an initial effect from the incident radiant energy intensity applied, depending to some degree on the intensity. This effect was interpreted as being due to the exposed surface of the BeO being raised to a high temperature so rapidly that little heat soaked into the thickness of the BeO and the temperature of the mass of the material did not immediately rise. It was postulated that during this short interval some interchange of incident radiant energy occurred by a process involving simultaneous emission and absorption of radiant energy in depth. As soon as the temperature of the BeO began to rise, however, this process of radiant energy interchange appeared to be superseded by the normal process of absorption of radiant energy at one surface, conversion of the absorbed energy into heat, and redistribution of the heat in the mass by conduction with an accompanying rise in temperature, resulting in the BeO becoming a radiator. Since the source of radiant energy was considered constant during a pulse, it was thought that the BeO followed an exponential temperature-vs-time relation based on the initial rate of temperature rise observed at the

center detector. The actual rate of temperature rise, however, deviated considerably from the calculated value, which indicated that as the temperature of the BeO increased, its thermal resistivity also increased, which apparently kept the temperature from increasing as rapidly as was anticipated. This resulted in a smaller amount of radiant energy being transferred to the center detector.

As the BeO temperatures were increased from 1800° to 2000°C, there were no significant increases in the effects observed. The initial rate of emf rise did not appear to differ from that of the emf peak. This was interpreted to mean that as BeO became hotter it radiated energy at such a rate that the effectiveness of the radiant energy emitted by the source was reduced. Thus, BeO at a temperature of 1985°C radiated at about the same rate as tungsten did at a temperature of about 2240°C. As was observed at lower BeO temperatures the somewhat low temperature effects obtained from radiant energy interchange in the hot BeO at high temperature was due to a somewhat low radiant energy intensity. From this it was concluded that the degree of radiant energy intensity influenced to some degree the radiant energy interchange in BeO; however the intensities employed in this exploratory work were found to be insufficient to produce any significant transmission of radiant energy in hot BeO up to 2000°C.

ACKNOWLEDGMENTS

The valuable assistance of the following personnel is acknowledged: Ronald W. Scott for his contribution in the construction and assembly of vital sheet metal parts of the apparatus and in the shaping of tungsten components, Keith Burnworth for his contribution in the assembly and operation of the vacuum system and for overall operation of the apparatus during the high temperature phases of work, Clarence R. Forsht and C. Nicholas Zillotti for their contributions to the electrical phases of the work, and Wilson Reaves for his contribution in the operation of oscilloscope instruments.

REFERENCES

1. Taylor, R.E., "A High Temperature Thermal Conductivity Apparatus," Atomics International, Canoga Park, California, Report ASD-TDR-62-348, Contract No. AF33(657)7136, Project No. 4776, Task No. 6, Apr. 1962
2. McQuarrie, M., "Thermal Conductivity: VII, Analysis of Variation of Conductivity with Temperature for Al_2O_3 , BeO and MgO," J. Am. Ceram. Soc. 37 (No. 2, Part II): 91-95 (Feb. 1, 1954)
3. Wyckoff, R.W.G., "Crystal Structures," Vol. I, Ch. III, text pp. 19-23, table p. 31, illustration p. 4, New York:Interscience, 1960
4. Hückel, W., "Structural Chemistry of Inorganic Compounds," p. 788, New York:Elsevier, 1951
5. Pauling, L., "The Nature of the Chemical Bond," p. 24, Cornell University Press, 1945
6. Baker, T.W., and Baldock, P.J., "A High Temperature Phase Transformation in Beryllia," Metallurgy Division, Atomic Energy Research Establishment, Harwell, Berkshire, Report AERE M-1017, Feb. 1962
7. Smith, D.K., Cline, C.F., and Frechette, V.D., "A High Temperature Crystallographic Phase Inversion in BeO," J. Nucl. Mater. 6(No. 3):265-270 (Aug. 1962)
8. Austerman, S.B., "High Temperature Phase Transformation in Beryllium Oxide - Thermal Arrest Measurements," Atomics International, Report NAA-SR-7654, Feb. 15, 1963
9. Austerman, S.B., "Decrepitation of Beryllium Oxide at High Temperatures," Atomics International Report NAA-SR-6428, Sept. 30, 1961
10. McClelland, J.D., Richardson, J.H., and Franklin, L.R., "Fabrication and Properties of Translucent Beryllium Oxide," Atomics International Report NAA-SR-6454, Contract: AT(11-1)-Gen. 8, Nov. 1961
11. Erway, N.D., and Seifert, R.L., "Vapor Pressure of Beryllium Oxide," J. Electrochem. Soc. 98(No. 3):83-88 (Mar. 1951)
12. Austerman, S.B., "Sub-Crystal Formation in BeO Crystals at High Temperature," J. Nucl. Mater. 6(No. 3):332-333 (1962)
13. Chupka, W.A., Berkowitz, J., and Giese, C.F., "Vaporization of Beryllium Oxide and its Reaction with Tungsten," J. Chem. Phys. 30(No. 3):827-834 (Mar. 1959)
14. Ackerman, R.J., and Thorn, R.J., "Vaporization of Oxides," ch. 2, pp. 46-48, in "Progress in Ceramic Science," vol. 1, J.E. Burke, editor, New York:Pergamon, 1961
15. Foëx, M., "Conductibilités électriques de la glucine et de la magnésie aux températures élevées" (Electrical Conductivity of BeO and MgO at High Temperatures), Comptes Rendus 214:665-666 (1942)

16. Seifert, R.L., "The Spectral Emissivity and Total Emissivity of Beryllium Oxide," *Phys. Rev.* 73(No. 10):1181-1187 (May 15, 1948)
17. Busch, G., and Schneider, M., "Heat Conduction in Semiconductors," *Physica* 20:1084-1086 (1954); Fröhlich, H., and Kittel, C., Remark on the paper by Prof. G. Busch, *Physica* 20:1086 (1954)
18. Price, P.J., "Ambipolar Thermodiffusion of Electrons and Holes in Semiconductors," *Philosophical Magazine* 46:1252-1260 (1955); "Electronic Thermal Conduction in Semiconductors," *Phys. Rev.* 95:596(A) (1954)
19. Devyatkova, E.D., Moizhes, B. Ya., and Smirnov, I.A., "Thermal Conductivity of Tellurium Containing Different Concentrations of Additional Elements in the Temperature Range 80-480°K," *Soviet Phys. - Solid State* 1:555-569 (1959)
20. Joffé, A.F., "Heat Transfer in Semiconductors," *Can. J. Phys.* 34:1342-1355 (Dec. 1956); "Properties of Various Semiconductors," *Phys. Chem. Solids* 8:6-14 (1959)
21. Kingery, W.D., and McQuarrie, M.C., "Thermal Conductivity: I, Concepts of Measurement and Factors Affecting Thermal Conductivity of Ceramic Materials," *J. Am. Ceram. Soc.*, Part II, 37(No. 2):67-72 (Feb. 1, 1954)
22. Kingery, W.D., "Thermal Conductivity: XII, Temperature Dependence of Conductivity for Single-Phase Ceramics," *J. Am. Ceram. Soc.* 38(No. 7):251-255 (July 1955)
23. Charvat, F.R., and Kingery, W.D., "Thermal Conductivity: XIII, Effect of Microstructure on Conductivity of Single-Phase Ceramics," *J. Am. Ceram. Soc.* 40(No. 9):306-315 (Sept. 1957)
24. Lee, D.W., and Kingery, W.D., "Radiation Energy Transfer and Thermal Conductivity of Ceramic Oxides," *J. Am. Ceram. Soc.* 43(No. 11):594-607 (Nov. 1960)
25. Whitmore, D.H., "Excitation Processes in Ceramics and Anomalous Increase in Thermal Conductivity at Elevated Temperatures," *J. Appl. Phys.* 31(No. 6):1109-1112 (June 1960)
26. Peierls, R., "Zur kinetischen Theorie der Wärmeleitung in Kristallen," *Ann. Physik* 3:1055-1101 (1929)
27. Debye, P., "Vorträge über die Kinetische Theorie der Materie und Elektrizität" (Papers on the Kinetic Theory of Matter and Electricity), *Göttinger Wolfskehlvorträge*, Leipzig and Berlin:Teubner, 1914
28. (a) Jakob, M., "Heat Transfer," vols. I and II, New York:John Wiley, 1949; (b) Chandrasekhar, S., "Radiative Transfer," New York:Dover, 1960; (c) Hottel, H.C., "Radiant Heat Transfer," ch. 3 in "Heat Transmission," 3rd edition, New York:McGraw-Hill, 1954; (d) Carslaw, H.S., and Jaeger, J.C., "Conduction of Heat in Solids," 2nd edition, London:Oxford University 1959
29. (a) Berman, R., "The Thermal Conductivity of Dielectric Solids at Low Temperatures," *Advan. Phys.* 2:103-140 (1953); (b) Klemens, P.G., "Thermal Conductivity and Lattice Vibrational Modes," *Solid State Phys.* 7:1-98 (1958)
30. Berman, R., Foster, E.L., and Rosenberg, H.M., "The Thermal Conductivity of Irradiated Dielectric Crystals at Low Temperatures," Report of the Conference on Defects in Crystalline Solids, Physical Society, London, 1955, pp. 321-327

31. Francl, J., and Kingery, W.D., "Thermal Conductivity: IX, Experimental Investigation of Effect of Porosity on Thermal Conductivity," J. Am. Ceram. Soc. 37:(No. 2, Part II): 99-107 (1954)
32. Vasilos, T., and Kingery, W.D., "Thermal Conductivity: XI, Conductivity of Some Refractory Carbides and Nitrides," J. Am. Ceram. Soc. 37(No. 9):409-414 (1954)
33. Hamaker, H.C., "Radiation and Heat Conduction in Light-Scattering Material": "I. Reflection and Transmission," Philips Res. Rep. 2:55-67 (1947); "II. General Equations Including Heat Conduction," Philips Res. Rep. 2:103-111 (1947); "III. Application of the Theory," Philips Res. Rep. 2:112-125 (1947); "IV. Various Extensions and a Generalized Theory," Philips Res. Rep. 2:420-425 (1947)
34. Taylor, R.E., "Thermal Conductivity and Expansion of Beryllia at High Temperatures," J. Am. Ceram. Soc. 45(No. 2):74-78 (Feb. 1962)
35. Clark, S.P., Jr., "Radiative Transfer in the Earth's Mantle," Trans. Am. Geophys. Union 38(No. 6):931-938 (1957)
36. Jamieson, J.C., and Lawson, A.W., "High-Temperature Heat Conductivity of Some Metal Oxides," J. Appl. Phys. 29(No. 9):1313-1314 (Sept. 1958)
37. Pikus, G.E., Zhur. Tekh. Fiz. 26:36 (1956)
38. Ritzow, G., "Die Temperaturstrahlung glühender Oxyde und Oxydgemische im ultraroten Spektralgebiet," Ann. Physik 19:785 (1934)
39. Hackforth, H.L., "Infrared Radiation," New York:McGraw-Hill, 1960
40. "Emissivity and Emittance," DMIC Memorandum 72, Battelle Memorial Institute, Columbus, Ohio, Nov. 10, 1960, p. 9
41. Kingery, W.D., "Property Measurements at High Temperatures," New York:Wiley, 93, 1959
42. Kendall, E.G., and McClelland, J.D., "Materials and Structures, Beryllium Containing Materials Program," Report TDR-930(2240-66) TR-1, Period July 1-December 31, 1961, Contract AF04(647)-930, Aerospace Corp., El Segundo, California
43. Gardon, R., "A Review of Radiant Heat Transfer in Glass," Symposium on Heat Transfer Phenomena in Glass, Philadelphia, April 24-28, 1960
44. Kandyba, V.V., Kantor, P.B., Krasovetsskaya, R.M., and Fomichev, E.N., Dokl. Akad. Nauk 131:566-567 (1960), Translation AEC-TR-4310, 1960

APPENDIX A

CALIBRATION OF GAUGE SECTION OF TUNGSTEN WIRE SOURCE

A single 80-mil-diameter tungsten wire was used as a source of radiant energy, mounted vertically between water-cooled terminals in a vacuum furnace. A gauge section of 2 inches length having 3-mil tantalum potential-drop leads spot welded to each end of the gauge section was calibrated in the temperature range from 847° to 2996°C, the melting point of tantalum. Brightness temperatures were determined by sighting on the center of the gauge section with an NBS-calibrated optical pyrometer. The current and the potential drop were recorded for each temperature. Brightness temperatures were corrected to true temperatures.

The calibration results are tabulated in Table A1 and plotted in Fig. A1. Also shown in Fig. A1 is an estimate of the cooling effects of the water-cooled leads on the tungsten wire. It was estimated that at wire temperatures above 1325°C the end effects of the water-cooled leads did not produce any temperature gradient in the gauge section.

Table A1
Compilation for Fig. A1

| Brightness Temp. (°C) | Corrected Temp. (°C) | Current (amps) | Pot. Drop (volts) | Vacuum Press. (torr) |
|-----------------------|----------------------|----------------|-------------------|----------------------|
| 847 | 892 | 38.4 | 0.172 | 8×10^{-7} |
| 980 | 1042 | 48.0 | 0.258 | 1×10^{-6} |
| 1081 | 1157 | 56.3 | 0.330 | 2×10^{-6} |
| 1170 | 1257 | 64.0 | 0.410 | 2.8×10^{-6} |
| 1249 | 1342 | 70.4 | 0.488 | 2×10^{-6} |
| 1338 | 1442 | 77.5 | 0.575 | 1.9×10^{-6} |
| 1418 | 1532 | 84.8 | 0.660 | 2.1×10^{-6} |
| 1550 | 1687 | 96.0 | 0.830 | 3.2×10^{-6} |
| 1642 | 1794 | 103.8 | 0.970 | 4.3×10^{-6} |
| 1730 | 1900 | 112.0 | 1.11 | 5.7×10^{-6} |
| 1849 | 2044 | 122.5 | 1.30 | 7.5×10^{-6} |
| 1940 | 2152 | 131.3 | 1.46 | 9.8×10^{-6} |
| 2006 | 2232 | 138.8 | 1.60 | 1×10^{-5} |
| 2088 | 2334 | 145.6 | 1.79 | 1.4×10^{-5} |
| 2139 | 2397 | 152.5 | 1.93 | 2×10^{-5} |
| 2208 | 2482 | 160.0 | 2.10 | 1.8×10^{-5} |
| 2289 | 2584 | 170.0 | 2.33 | 3.4×10^{-5} |
| 2390 | 2712 | 182.4 | 2.65 | 5.6×10^{-5} |
| 2453 | 2792 | 191.3 | 2.86 | 9×10^{-5} |
| 2520 | 2882 | 203.2 | 3.15 | 5.6×10^{-5} |
| 2565 | 2940 | 211.2 | 3.39 | 7×10^{-5} |
| 2602 | 2995 | 221.3 | 3.60 | 1×10^{-4} |

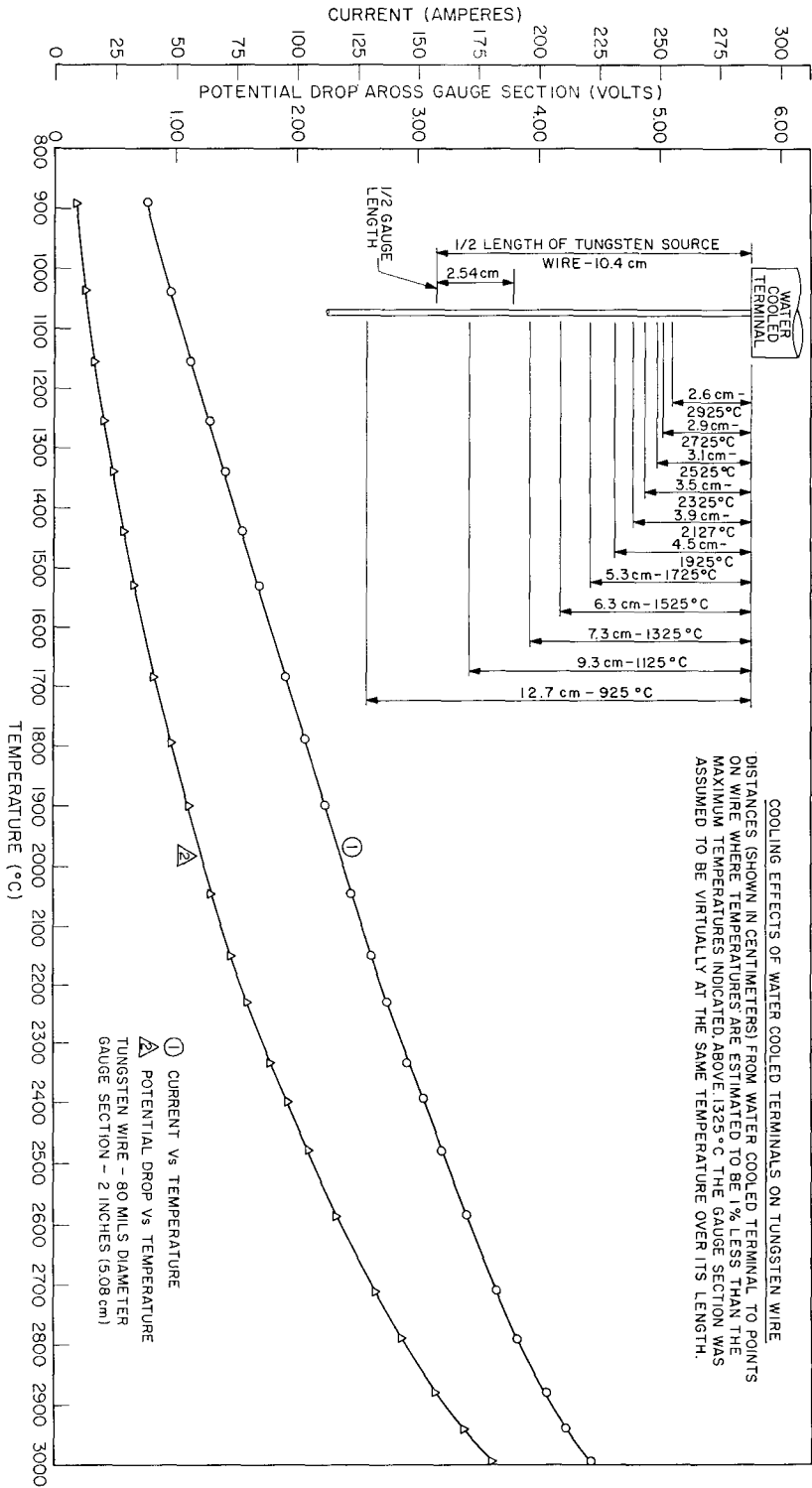


Fig. A1 - Calibration of tungsten radiant energy source

APPENDIX B

THERMOCOUPLE DETECTORS AND CALIBRATION DATA

THERMOCOUPLE DETECTORS

The principle of using a thermocouple as a detector of thermal radiation was based upon absorption of radiant energy and its conversion to heat. This heating produces secondary phenomena in the detector in the form of an electromotive force. Since the thermocouple type of detector depends upon the heating effect from radiant energy for its operation, it was assumed that it would respond to a given amount of radiant energy regardless of its wavelength.

Thermocouples do not require cooling, and their sensitivity is essentially constant over a broad spectral band of wavelengths comprising the thermal radiation region from about 0.1 to 100 μ . This range extends from the ultraviolet to the far infrared, as indicated in the electromagnetic spectrum depicted in Fig. B1.*

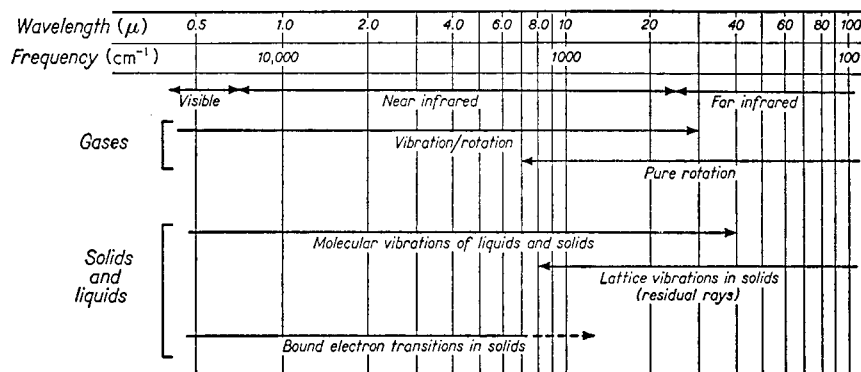


Fig. B1 - The infrared spectrum, and the origin of spectra

Since the output of thermocouples is produced by the heating effect of incident thermal radiation, they can be considered as power detectors whose output is proportional to the total energy of the absorbed radiant energy. As thermal radiant energy detectors, thermocouples are more sensitive to radiant energy below incandescence; however, this type of detector was considered to be the best choice to monitor the temperature effects under the experimental conditions employed.

In view of the high-temperature requirements of the experimental work, it was necessary to consider thermocouple materials which would provide the following characteristics: high emf, high melting point of all components, and chemical stability in vacuum and in contact with BeO insulating material. The thermocouple system selected for this

*G.K.T. Conn and D.G. Avery, "Infrared Methods," New York:Academic, 1960.

work was based on the tungsten/iridium combination constructed as shown in Fig. B2. The hot junction was welded to the 1/8-inch-diameter flat tip of the tantalum sheath as shown. The 24 gauge thermocouple elements were embedded in powdered BeO with the assembly contained in a tantalum sheath making a pressure tight closure. This type detector was used to monitor the temperature effects across the planar cross section of the sample BeO materials.

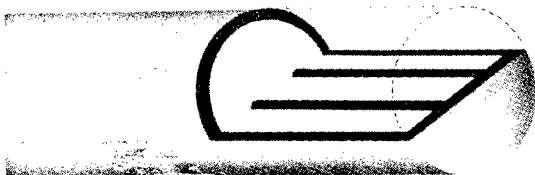


Fig. B2 - Cutaway sketch showing the hot junction tungsten/iridium thermocouple welded to the flat tip of the tantalum sheath making a pressure-tight closure

Conventional bare hot junction tungsten/iridium thermocouples, insulated with two-hole high-purity BeO thermocouple tubing were used to monitor the top and bottom heater temperatures of the hot zone.

CALIBRATION OF TUNGSTEN/IRIDIUM THERMOCOUPLES

The tungsten/iridium thermocouples were calibrated in vacuum using an NBS-calibrated Pt/Pt-13%Rh thermocouple as a reference from 1000° to about 1500°C. An NBS-calibrated optical pyrometer of the disappearing filament type was used above 1500°C.

The calibration was conducted in a vertical tube furnace equipped with a single-turn-sheet tantalum resistance element electrically heated. A tantalum block, suspended within the single-turn heater, was used as a common medium for comparing the emf developed by the W/Ir couple with that of the Pt/Pt-13%Rh couple at a given temperature. This block was also used in conjunction with the optical pyrometer to determine the temperature for a given emf developed by the W/Ir couple at the higher temperatures. The calibration data tabulated in Table B1 are shown plotted in Fig. B3. These data were in close agreement with published data on the W/Ir system.

Table B1
Compilation of Emf-vs-Temperature Data for a W/Ir Thermocouple

| Temp. (°C) | Emf (mv) |
|------------|----------|------------|----------|------------|----------|------------|----------|------------|----------|
| 1000 | 14.4 | 1200 | 19.2 | 1400 | 24.1 | 1600 | 29.0 | 1800 | 33.9 |
| 10 | 14.6 | 10 | 19.5 | 10 | 24.4 | 10 | 29.2 | 10 | 34.1 |
| 20 | 14.8 | 20 | 19.7 | 20 | 24.6 | 20 | 29.5 | 20 | 34.4 |
| 30 | 15.1 | 30 | 20.0 | 30 | 24.8 | 30 | 29.7 | 30 | 34.6 |
| 40 | 15.3 | 40 | 20.2 | 40 | 25.1 | 40 | 30.0 | 40 | 34.8 |
| 50 | 15.6 | 50 | 20.4 | 50 | 25.3 | 50 | 30.2 | 50 | 35.1 |
| 60 | 15.8 | 60 | 20.7 | 60 | 25.6 | 60 | 30.5 | 60 | 35.3 |
| 70 | 16.0 | 70 | 20.9 | 70 | 25.8 | 70 | 30.7 | 70 | 35.6 |
| 80 | 16.3 | 80 | 21.2 | 80 | 26.1 | 80 | 31.0 | 80 | 35.8 |
| 90 | 16.5 | 90 | 21.4 | 90 | 26.3 | 90 | 31.2 | 90 | 36.1 |
| 1100 | 16.8 | 1300 | 21.6 | 1500 | 26.6 | 1700 | 31.4 | 1900 | 36.3 |
| 10 | 17.0 | 10 | 21.9 | 10 | 26.8 | 10 | 31.7 | 10 | 36.6 |
| 20 | 17.3 | 20 | 22.2 | 20 | 27.0 | 20 | 31.9 | 20 | 36.8 |
| 30 | 17.5 | 30 | 22.4 | 30 | 27.3 | 30 | 32.2 | 30 | 37.0 |
| 40 | 17.8 | 40 | 22.7 | 40 | 27.5 | 40 | 32.4 | 40 | 37.3 |
| 50 | 18.0 | 50 | 22.9 | 50 | 27.8 | 50 | 32.7 | 50 | 37.5 |
| 60 | 18.2 | 60 | 23.2 | 60 | 28.0 | 60 | 32.9 | 60 | 37.8 |
| 70 | 18.5 | 70 | 23.4 | 70 | 28.3 | 70 | 33.1 | 70 | 38.0 |
| 80 | 18.8 | 80 | 23.6 | 80 | 28.5 | 80 | 33.4 | 80 | 38.2 |
| 90 | 19.0 | 90 | 23.9 | 90 | 28.8 | 90 | 33.6 | 90 | 38.5 |
| 1200 | 19.2 | 1400 | 24.1 | 1600 | 29.0 | 1800 | 33.9 | 2000 | 38.7 |

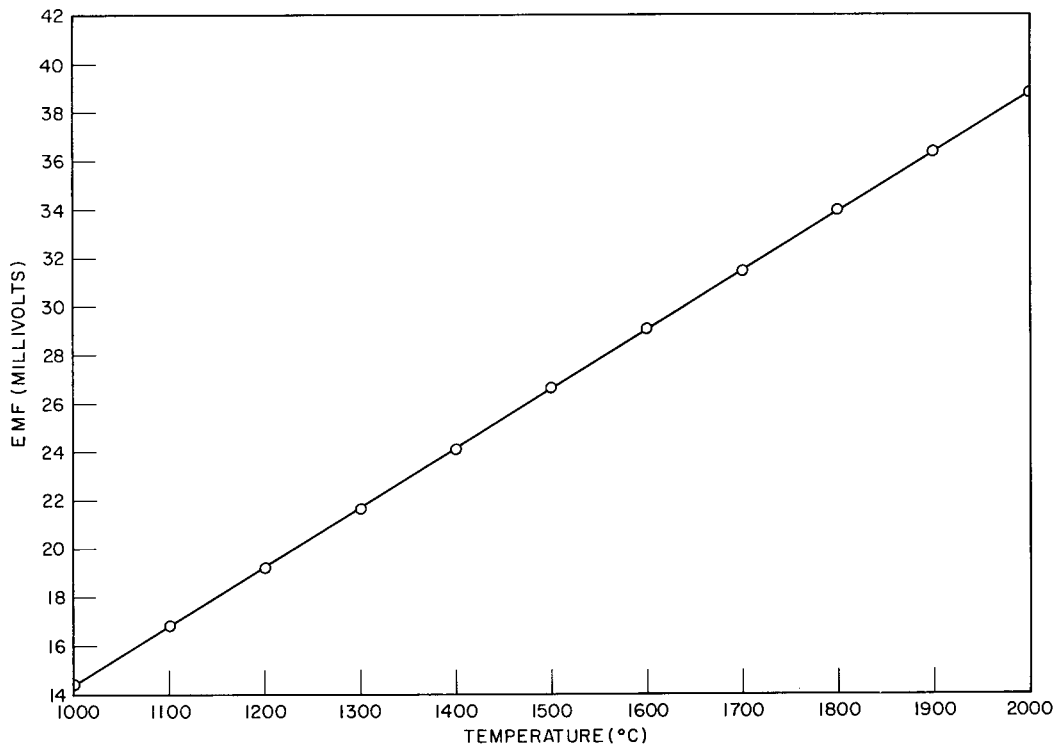


Fig. B3 - Calibration curve for W/Ir thermocouples

APPENDIX C

MISCELLANEOUS PROPERTIES

Table C1 is a compilation of the thermal properties involving total emissivity and energy radiated for BeO and tungsten in the temperature range 900° to 3000°C that were used in plotting Fig. 11.

Vapor pressure data for materials used in the high-temperature zones are compiled and plotted in Fig. C1. These materials included BeO, iridium, tantalum, and tungsten. The vapor pressures for BeO were calculated from the equation

$$\log_{10} p = 18.5 - \frac{34,230}{T} - 2 \log_{10} T$$

taken from Ref. 11. The vapor pressures for iridium, tantalum, and tungsten were taken from Table I of RCA Review 23:567-586 (Dec. 1962).

The values used in plotting Figs. 29 through 33 are compiled in Table C2. These values were calculated in accordance with Eq. (8), using initial rates of temperature rise determined from trials shown in the figures indicated at the bottom of Table C2.

Figure C2 is a plot of the specific heat of BeO, calculated from the equation

$$C_p = 9.471 + 2.090 \times 10^{-3} T \text{ cal/mole-}^\circ\text{K (1200}^\circ\text{-2820}^\circ\text{K melt point)}$$

as given by Ref. 44. The values plotted are tabulated in the figure.

Table C1
THERMAL PROPERTIES OF BeO AND TUNGSTEN
(FOR FIG. 11)

| Temp. (°C) | Total Emmissivity | | Energy Radiated (watts/cm ²) | |
|---------------|-------------------|-------|--|----------|
| | W | BeO | From W | From BeO |
| 900 | 0.139 | 0.330 | 1.524 | 3.16 |
| 1000 | 0.154 | 0.354 | 2.3337 | 5.34 |
| 1100 | 0.170 | 0.383 | 3.484 | 7.81 |
| 1200 | 0.187 | 0.412 | 5.08 | 11.11 |
| 1300 | 0.203 | 0.434 | 7.17 | 15.17 |
| 1400 | 0.218 | 0.449 | 9.83 | 20.07 |
| 1500 | 0.232 | 0.460 | 13.24 | 25.92 |
| 1600 | 0.245 | 0.468 | 17.38 | 32.81 |
| 1700 | 0.257 | 0.473 | 22.32 | 40.79 |
| 1800 | 0.267 | 0.474 | 28.17 | 49.87 |
| 1900 | 0.277 | 0.475 | 35.19 | 60.00 |
| 2000 | 0.286 | 0.475 | 43.55 | |
| 2100 | 0.294 | | 53.13 | |
| 2200 | 0.301 | | 64.41 | |
| 2300 | 0.309 | | 77.24 | |
| 2400 | 0.316 | | 92.04 | |
| 2500 | 0.322 | | 108.39 | |
| 2600 | 0.327 | | 126.92 | |
| 2700 | 0.333 | | 145.24 | |
| 2800 | 0.336 | | 171.13 | |
| 2900 | 0.340* | | 196.12 | |
| 3000 | 0.343* | | 224.17 | |

*Extrapolated Values

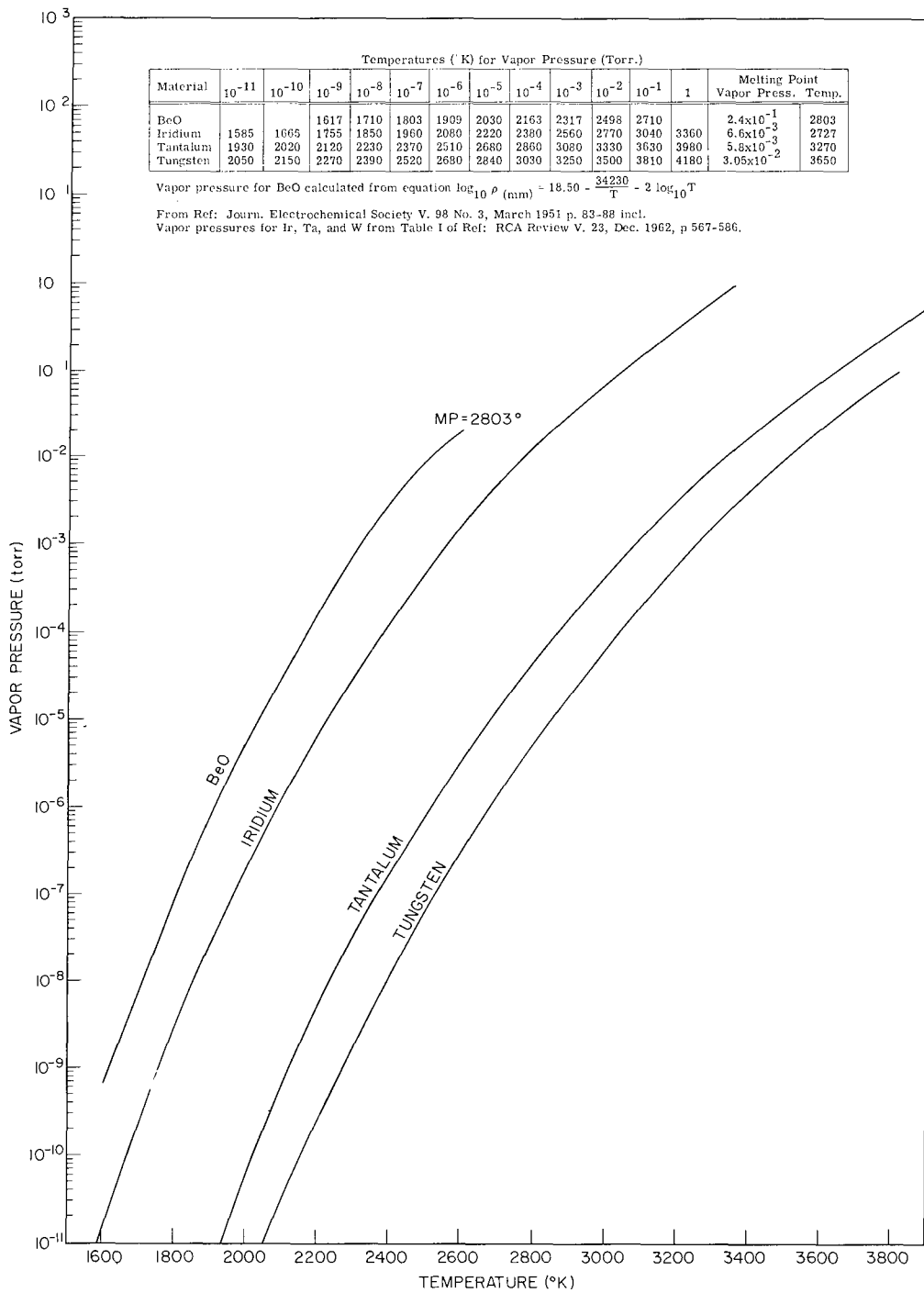


Fig. C1 - Vapor pressures of BeO, iridium, tantalum, and tungsten

Table C2
 COMPILATIONS FOR TEMPERATURE-VS-TIME CURVES

| t/j | Data for Fig. 29 | | Data for Fig. 30 | | Data for Fig. 31 | | Data for Fig. 32 | | Data for Fig. 33 | |
|-----|--|-----------------|--|-----------------|--|-----------------|--|-----------------|--|-----------------|
| | Time (sec) | Temp. Rise (°C) | Time (sec) | Temp. Rise (°C) | Time (sec) | Temp. Rise (°C) | Time (sec) | Temp. Rise (°C) | Time (sec) | Temp. Rise (°C) |
| 0.1 | 26.3 | 111 | 20.0 | 80 | 8.2 | 47 | 17.6 | 47 | 7 | 33 |
| 0.2 | 52.6 | 212 | 40.0 | 153 | 16.4 | 90 | 35.2 | 89 | 14 | 63 |
| 0.4 | 105.2 | 385 | 80.0 | 279 | 32.8 | 164 | 70.4 | 162 | 28 | 113 |
| 0.6 | 157.8 | 527 | 120.0 | 381 | 49.2 | 224 | 105.6 | 221 | 42 | 156 |
| 0.8 | 210.4 | 644 | 160.0 | 465 | 65.6 | 274 | 140.8 | 270 | 56 | 190 |
| 1.0 | 263.0 | 739 | 200.0 | 534 | 82.0 | 314 | 176.0 | 310 | 70 | 218 |
| 1.2 | 315.6 | 817 | 240.0 | 591 | 98.4 | 347 | 211.2 | 342 | 84 | 241 |
| 1.4 | 368.2 | 881 | 280.0 | 637 | 114.8 | 374 | 246.4 | 369 | 98 | 260 |
| 1.6 | 420.8 | 934 | 320.0 | 674 | 131.2 | 397 | 281.6 | 391 | 112 | 275 |
| 1.8 | 473.4 | 976 | 360.0 | 705 | 147.6 | 415 | 316.8 | 409 | 126 | 288 |
| 2.0 | 526.0 | 1011 | 400.0 | 731 | 164.0 | 430 | 352.0 | 424 | 140 | 298 |
| 2.2 | 578.6 | 1039 | 440.0 | 751 | 180.4 | 442 | 387.2 | 436 | 154 | 307 |
| 2.4 | 631.2 | 1063 | 480.0 | 768 | 196.8 | 452 | 422.4 | 446 | 168 | 314 |
| 2.6 | 683.8 | 1082 | 520.0 | 782 | 213.2 | 460 | 457.6 | 454 | 182 | 319 |
| 2.8 | 736.4 | 1098 | 560.0 | 794 | 229.6 | 467 | 492.8 | 460 | 196 | 324 |
| 3.0 | 789.0 | 1111 | 600.0 | 803 | 246.0 | 472 | 528.0 | 466 | 210 | 328 |
| 3.2 | 841.6 | 1121 | 640.0 | 811 | 262.4 | 477 | 563.2 | 470 | 224 | 331 |
| 3.4 | 894.2 | 1130 | 680.0 | 817 | 278.8 | 480 | 598.4 | 474 | 238 | 334 |
| 3.6 | 946.8 | 1137 | 720.0 | 822 | 295.2 | 483 | 633.6 | 477 | 252 | 336 |
| 3.8 | 999.4 | 1143 | 760.0 | 826 | 311.6 | 486 | 668.8 | 479 | 266 | 337 |
| 4.0 | 1052.0 | 1148 | 800.0 | 830 | 328.0 | 488 | 704.0 | 481 | 280 | 339 |
| 4.5 | 1183.5 | 1156 | 900.0 | 831 | 369.0 | 491 | 792.0 | 485 | 315 | 341 |
| 5.0 | 1315.0 | 1161 | 1000.0 | 836 | 410.0 | 494 | 880.0 | 487 | 350 | 343 |
| | j = 263 sec. Initial rate of temp. rise = 4.5°C/sec. (Trial of Fig. 12.) | | j = 200 sec. Initial rate of temp. rise = 4.23°C/sec. (Trial of Figs. 13 and 14.) | | j = 82 sec. Initial rate of temp. rise = 6°C/sec. (Trial of Figs. 18 and 19.) | | j = 176 sec. Initial rate of temp. rise = 2.8°C/sec. (Trial of Fig. 23.) | | j = 70 sec. Initial rate of temp. rise = 5.00°C/sec. (Trial of Fig. 25.) | |

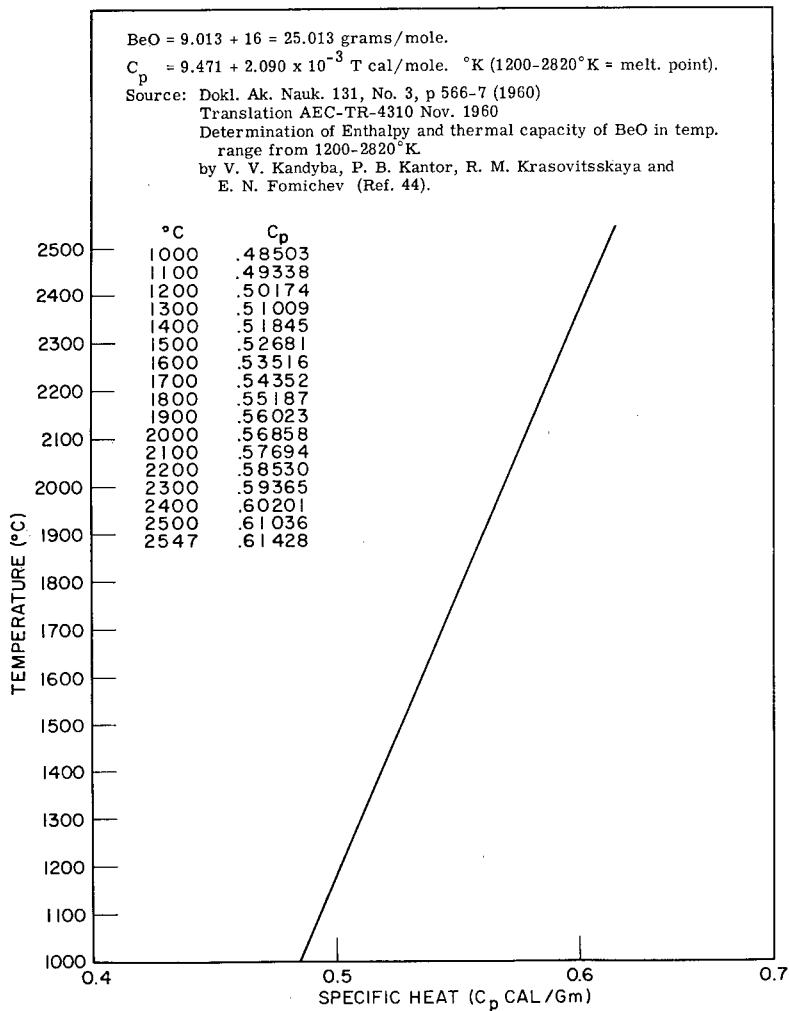


Fig. C2 - Specific heat of BeO

DOCUMENT CONTROL DATA - R&D

(Security classification of title, body of abstract and indexing annotation must be entered when the overall report is classified)

| | | | |
|---|--|---|--|
| 1. ORIGINATING ACTIVITY (Corporate author) U.S. Naval Research Laboratory Washington, D.C. 20390 | | 2 a. REPORT SECURITY CLASSIFICATION UNCLASSIFIED | |
| | | 2 b. GROUP | |
| 3. REPORT TITLE AN EXPLORATORY STUDY OF RADIANT ENERGY TRANSPORT IN BeO | | | |
| 4. DESCRIPTIVE NOTES (Type of report and inclusive dates) A final report on one phase of the problem. | | | |
| 5. AUTHOR(S) (Last name, first name, initial) Chapin, E.J., and Howe, D.G. | | | |
| 6. REPORT DATE March 22, 1965 | 7 a. TOTAL NO. OF PAGES 73 | 7 b. NO. OF REFS 44 | |
| 8 a. CONTRACT OR GRANT NO. NRL Problem M01-15 | 9 a. ORIGINATOR'S REPORT NUMBER(S) NRL Report 6195 | | |
| b. PROJECT NO. Special Projects Task No. 72404 | 9 b. OTHER REPORT NO(S) (Any other numbers that may be assigned this report) | | |
| c. | | | |
| d. | | | |
| 10. AVAILABILITY/LIMITATION NOTICES Unlimited availability - Copies available at CFSTI - \$2.00 | | | |
| 11. SUPPLEMENTARY NOTES | | 12. SPONSORING MILITARY ACTIVITY Dept. of the Navy (Special Projects Office) | |
| 13. ABSTRACT <p>Current hypotheses were reviewed relative to the contribution of radiant energy to heat transfer in BeO. The problem of radiant energy transmission in BeO was explored by exposing simultaneously, two types of BeO sample materials heated from 1000° to 2000°C, to pulses of radiant energy of known intensity. The effects were monitored with potentiometer and oscilloscope instruments from emf signals obtained from thermocouple detectors.</p> <p>Translucent thin-walled BeO tube material, heated from 1000° to 2000°C, exhibited no sustained transmission of radiant energy when exposed to radiant energy pulses of high intensity. An initial effect from the applied incident radiant energy was detected, however, which was interpreted to be due to the exposed surface of the BeO reaching a high temperature so rapidly that, momentarily, little heat was generated in the mass of the material and no immediate temperature rise occurred in the heated BeO. It was postulated that during this short interval incident radiant energy was transferred in the BeO by a process involving simultaneous emission and absorption of radiant energy in depth. As soon as the BeO temperature began to rise, this process of radiant energy transfer appeared to be replaced by the normal process of radiant energy absorption, conversion to heat, and reradiation. A comparison was made of calculated temperature-time heating curves (based on the detected initial rates of temperature rise) with the experimental data. This comparison indicated that the temperature rise per unit of time, measured for the full duration of a pulse of radiant energy was actually less than that calculated, showing that the initial rate and therefore, the initial process of radiant energy transfer was not sustained. BeO heated above 1800°C exhibited no tendency toward an initial rapid transfer of radiant energy. The lack of initial temperature effects from incident radiant energy was attributed to insufficient intensity.</p> <p>The transfer of radiant energy in granular fused BeO was studied simultaneously with that of the BeO tube material. The temperature effects observed in the granular material were very minor. There were no detectable effects observed in this material from the brief initial transfer of radiant energy through the BeO tube. The temperature effects produced in the granular BeO were considered to result from heating the granular material by a process of absorption and reradiation of radiant energy emitted by the BeO tube and by conduction at contact points between grains.</p> <p>The overall results indicated that hot BeO did not become progressively diathermanous as its temperature increased but displayed a stronger opaque behavior toward radiant energy.</p> | | | |

REF ID: A66000

| 14. KEY WORDS | LINK A | | LINK B | | LINK C | |
|---|--------|----|--------|----|--------|----|
| | ROLE | WT | ROLE | WT | ROLE | WT |
| Beryllia Radiant energy transport Phonon conduction Photon conduction Exciton conduction Thermal conductivity of BeO Vapor pressure of BeO Emissivity of BeO | | | | | | |

INSTRUCTIONS

1. **ORIGINATING ACTIVITY:** Enter the name and address of the contractor, subcontractor, grantee, Department of Defense activity or other organization (*corporate author*) issuing the report.
- 2a. **REPORT SECURITY CLASSIFICATION:** Enter the overall security classification of the report. Indicate whether "Restricted Data" is included. Marking is to be in accordance with appropriate security regulations.
- 2b. **GROUP:** Automatic downgrading is specified in DoD Directive 5200.10 and Armed Forces Industrial Manual. Enter the group number. Also, when applicable, show that optional markings have been used for Group 3 and Group 4 as authorized.
3. **REPORT TITLE:** Enter the complete report title in all capital letters. Titles in all cases should be unclassified. If a meaningful title cannot be selected without classification, show title classification in all capitals in parenthesis immediately following the title.
4. **DESCRIPTIVE NOTES:** If appropriate, enter the type of report, e.g., interim, progress, summary, annual, or final. Give the inclusive dates when a specific reporting period is covered.
5. **AUTHOR(S):** Enter the name(s) of author(s) as shown on or in the report. Enter last name, first name, middle initial. If military, show rank and branch of service. The name of the principal author is an absolute minimum requirement.
6. **REPORT DATE:** Enter the date of the report as day, month, year; or month, year. If more than one date appears on the report, use date of publication.
- 7a. **TOTAL NUMBER OF PAGES:** The total page count should follow normal pagination procedures, i.e., enter the number of pages containing information.
- 7b. **NUMBER OF REFERENCES:** Enter the total number of references cited in the report.
- 8a. **CONTRACT OR GRANT NUMBER:** If appropriate, enter the applicable number of the contract or grant under which the report was written.
- 8b, 8c, & 8d. **PROJECT NUMBER:** Enter the appropriate military department identification, such as project number, subproject number, system numbers, task number, etc.
- 9a. **ORIGINATOR'S REPORT NUMBER(S):** Enter the official report number by which the document will be identified and controlled by the originating activity. This number must be unique to this report.
- 9b. **OTHER REPORT NUMBER(S):** If the report has been assigned any other report numbers (*either by the originator or by the sponsor*), also enter this number(s).
10. **AVAILABILITY/LIMITATION NOTICES:** Enter any limitations on further dissemination of the report, other than those

imposed by security classification, using standard statements such as:

- (1) "Qualified requesters may obtain copies of this report from DDC."
- (2) "Foreign announcement and dissemination of this report by DDC is not authorized."
- (3) "U. S. Government agencies may obtain copies of this report directly from DDC. Other qualified DDC users shall request through _____."
- (4) "U. S. military agencies may obtain copies of this report directly from DDC. Other qualified users shall request through _____."
- (5) "All distribution of this report is controlled. Qualified DDC users shall request through _____."

If the report has been furnished to the Office of Technical Services, Department of Commerce, for sale to the public, indicate this fact and enter the price, if known.

11. **SUPPLEMENTARY NOTES:** Use for additional explanatory notes.
12. **SPONSORING MILITARY ACTIVITY:** Enter the name of the departmental project office or laboratory sponsoring (*paying for*) the research and development. Include address.
13. **ABSTRACT:** Enter an abstract giving a brief and factual summary of the document indicative of the report, even though it may also appear elsewhere in the body of the technical report. If additional space is required, a continuation sheet shall be attached.

It is highly desirable that the abstract of classified reports be unclassified. Each paragraph of the abstract shall end with an indication of the military security classification of the information in the paragraph, represented as (TS), (S), (C), or (U).

There is no limitation on the length of the abstract. However, the suggested length is from 150 to 225 words.
14. **KEY WORDS:** Key words are technically meaningful terms or short phrases that characterize a report and may be used as index entries for cataloging the report. Key words must be selected so that no security classification is required. Identifiers, such as equipment model designation, trade name, military project code name, geographic location, may be used as key words but will be followed by an indication of technical context. The assignment of links, roles, and weights is optional.